Development of Metalloenzyme Dioxygen Reduction Cathodes

Thesis by Peter Chukwudi Ifeanychukwu Agbo

In Partial Fulfillment for the Requirements

of the Degree of

Doctor of Philosophy

California Institute of Technology

Pasadena, CA

2015

(Defended August 1, 2014)

Table of Contents

Table of Figures

Chapter I

Chapter II

Chapter III

Chapter IV

Appendix

Tribute

"No man is an island, entire of itself; every man is a piece of the continent, a part of the main."
- John Donne

If anything in my life serves as a testament to this idea, it has been my time here at Caltech. My matriculation to this campus, the decision to switch from molecular biology into chemistry, scientific skills accrued during my graduate work and finally, the conception and completion of this very dissertation, are not solely my accomplishments. Instead, they are byproducts of being born into a loving family, having the good fortune to be surrounded by both friends and mentors of rare caliber, and a research experience in the Gray group which has fundamentally transformed me as a scientist over the last five years. While paying sufficient homage to all these positive influences in the brief span of a thesis acknowledgments section remains something of a fool's errand, I'll nevertheless try my best to do so. Note that when this section inevitably devolves into simple lists of the many people that have supported me, any failure to elaborate on them is not a commentary on their relative significance.

The origins of this dissertation lie with Jesse Frankel. Jesse was my closest companion in fourth grade at Teach Elementary and it was he who endowed me with my current appreciation for science. Despite his young age, Jesse had already resolved to become an entomologist, though as a devoted student of the sciences, could expound on a variety of scientific topics other than insects. I have yet to again encounter any nine year old who can boast a solid qualitative understanding of superconductivity; Jesse Frankel, however, was such an individual. With him, you had rare intellect coupled to a radiant persona (being talkative, surprisingly opinionated, and stubborn), and to witness somebody so remarkable place high premiums on acquiring scientific knowledge had the effect of making science look very, very cool. Aspiring to be cool myself, I followed Jesse's lead, and where I was eager to learn, he was eager to instruct. My conversations with him during lunchtime recess were enough to make me want to become a scientist as well, and I've met no pause in that conviction since. Jesse has since

passed away, but the profound effect he had on me then has persisted. Being a scientist now constitutes an integral part of my identity, making Jesse largely responsible for the person I am today and this thesis by extension. Thank you Jesse, for your friendship back then and your continuing influence now.

Patricia Jafar has been one of my dearest friends and supporters since we met in college. Her frequent, early-morning calls from Jakarta — generally made for the purpose of relating some ridiculous office anecdote, cheesy joke or simply to ask how I'm doing — have served to keep my morale high, even during some of the more dispiriting times in grad school.

To an excellent group of friends from high school who remain among my closest companions today — Chris Todd-Healey, Isaac Masicampo, Brian Jones, Paul Dier, Kayvan Chinichian, Jigger Patel, Robert Peters, Allen Kunde, Eric Lee, Josh Knox, Fred Gibson and Nick Inchausti — thanks for all you've done for me over the years and for making growing up enjoyable.

Mrs. Carrie Zinn was an influential teacher during my formative years. Despite some ungracious comments I made regarding her fondness for Luna Energy Bars during 10th grade history class, she has always been a great friend to me. Thanks Mrs. Zinn.

The Coates Environmental Microbiology Lab at UC Berkeley was where I got my first serious introduction to lab research. These people, who helped foster my interest in bench work and made my undergraduate lab experience so enjoyable, are definitely owed some accolades: John D. Coates, J. Cameron Thrash, Ian Van Trump, Saumyaditya Bose, Yvonne Sun, Steven Smith, Karrie Weber, Kamal Ghandi, Forest Kaiser, Dara Goodheart, Ana Peterson, Kathy Byrne-Bailey, Mark Heinnickel, Traci Knox, Thuy Nguyen, Justin Ishida, Caroline Chow, Lacey Westphal, Shaunt Oungoulian, Seema Madan, Sarir Ahmadi, Antinea Chair and Hannah Marcus. With respect to this group of people, my biggest thanks go out to Kelly Wrighton, who was my graduate student mentor and biggest advocate during my three year tenure in the Coates Lab.

Members of the Knox family, Jones family and also the hometown church (St. Stephen's) in which I was brought up have always been kind, making

inquiries into the progress of my research during holidays and vacations when I returned home. Thank you for your interest and support these past years.

The Gray group represents an exemplary collection of scientists and I count myself lucky to have worked alongside them. Harry has been an incredible adviser, granting me free rein in my work, while also providing advice, guidance and support when it was sought. It goes without saying that he is a great scientist whom I will always strive to emulate. Jay Winkler has served to maintain a high standard for scientific rigor in the Gray group. It is hard not to be impressed by the breadth of Jay's scientific prowess, a trait that makes him one of the best examples of a truly well-rounded scientist. As my career advances, I hope to mimic Jay in this aspect. Bruce Brunschwig has been another voice lending nuggets of experimental wisdom whenever it was needed.

Having Jack Richards and Frances Arnold on my thesis committee has been among the smarter decisions I've made while at Caltech; their tendency to ask probing questions during candidacy and props conditioned me to think deeper and more critically when critiquing my own work and I am a better researcher as a result.

The lab of James Heath has complemented my experience in the Gray group, helping to make for a research experience that was far more productive than it would have been otherwise. Jim has been a great provider, establishing a work environment where his researchers can conduct their studies unencumbered by the funding limitations that plague many graduate students. For this, I owe him many thanks. Others in his group, especially Samir Das, Habib Ahmad and Sheryl Mathis, are great individuals and I'm glad to have met them. I would also like to especially thank his lab administrator, Elyse Garlock, for her eagerness to always lend me a helping hand.

During my graduate study, the flux of staff, postdoctoral and graduate-level researchers through BILRC has been considerable, so I will simply list them here, adding that I am grateful to each of these individuals for their role in making my experience in the Gray group what

it was: Carl Blumenfeld, James Blakemore, Tania Darnton, Sarah Del Ceillo, Bryan Hunter, Yan Choi Lam, Michael Lichterman, Astrid Mueller, Chris Roske, Aaron Sattler, Wes Sattler, Oliver Shafaat, Kana Takematsu, Reneé Arias, Matthew Bierman, Morgan Cable, Jillian Dempsey, Alec Durrell, Matthew Hartings, Hemala Karunadasa, Kyle Lancaster, Paul Oblad, Michael Rose, Bryan Stubbert, Charlotte Whited, Heather Williamson, Melanie Pribisko, Keiko Yokoyama, Nicole Ford, Gretchen Keller, Jeffrey Warren, Mariah Ener, James McKone, Paul Bracher, Seiji Yamada, and Yuling Sheng.

I would also like to thank Rick Jackson and Catherine May, kind administrators who have often been of great help to me in grad school.

Thank you Steve Gould, Elisa Brink, Memo Correa, Arthur Larenas, Pat Anderson, Joe Drew and Ron Koen for all the work you do for CCE. I would also like to thank Agnes Tong for being a great administrator to the graduate students in the Chemistry Division.

Fan Liu, aside from being a very bright, young biophysicist from whom I expect great things, is simply a wonderful person, made of what may be truly unimpeachable character. Thank you for encouraging me when I did not see the value in my own work, for giving me feedback on my research, and being an outstanding moral example and friend. I will miss our Friday lunch rendezvouses.

Through my good friend Chinenye Idigo and our joint project attempting to crystallize laccase, I discovered what will surely be a lifelong disdain for protein crystallography. Thank you Chinny, for this important life lesson and giving up your time to indulge me in that failed venture. On a related note, let me also thank Jeff Lai for laughing at my jokes.

Paul Bracher is one of the most interesting personalities and talented chemists I met during my time at Caltech and it was a joy to have shared an office with him for two years. Nighttime sandwich runs to Gandolfos after group meeting will be remembered fondly. I wish him the best at St. Louis University.

To Joseph 'Rain Man' Varghese, the closest friend I made here, thank you for all you have done for me, from your probe microscopy tutorials, to

allowing me to assist on your MoS_2 project, to being a close confidant whom I can tell anything.

Ryan Henning, Alex Sutherland, Michael Grodick, Jacob Kanady, Paul Kelley, Guy Edouard, Andy Zhou, and Mary Louie have been great friends and great people to hang out with. Thank you for making Caltech a better experience for me.

I owe thanks to the friendly maintenance staff, especially those who have kept working conditions sanitary and humane in the Beckman Institute subbasement and Noyes third floor. Despite having thankless jobs, I have often witnessed Caltech custodians going far beyond what is required of them, particularly John Bennet, Ralph Crowder, Cecilia Tostado, Bonifacio Mazas, Sergio Meza, Jose Delgado and Patricia Estrada.

To Larry 'The Crystallographer' Henling — while you never solved any structures for me, you did provide plenty of comedic relief during my time here and introduce me to cumquats. To Pavle Nikolovski, Julie Hoy and Jens Kaiser, thank you for helping me when I worked on the Mosquito and home source.

I would also like to thank Professor Chris Kitts and his lab manager Alice Hamrick, who allowed me to work in their lab while I was a high school student. My neighbors, Scott Barker and Norma Sepulveda, have been good friends since I moved to Pasadena. I am also grateful to Jennifer Kim, who helped me proofread this thesis.

The bulk of my gratitude goes to my family. Thank you Mom and Dad, for how you have always provided for me, raised me to appreciate the value of education and encouraged me to excel in all my undertakings. My siblings — Chioma Boukai, Ngozi Agbo, Nwamaka Agbo-Balmer, Ogochukwu Agbo, and Joseph Agbo — are among the best that anyone could hope for and I love them very much. Thank you for all you have done and continue to do for me. Akram Boukai and Misha Balmer are wonderful brothers in law, though I prefer to simply call them brothers now — and I'm grateful for how they've encouraged me throughout this process.

Finally, to Alec Durrell: as you may gather from this thesis, I took your advice.

Research Brief

The prime thrust of this dissertation is to advance the development of fuel cell dioxygen reduction cathodes that employ some variant of multicopper oxidase enzymes as the catalyst. The low earth-abundance of platinum metal and its correspondingly high market cost has prompted a general search amongst chemists and materials scientists for reasonable alternatives to this metal for facilitating catalytic dioxygen reduction chemistry. The multicopper oxidases (MCOs), which constitute a class of enzyme that naturally catalyze the reaction $O_2 + 4H^+ + 4e^- \rightarrow 2H_2O$, provide a promising set of biochemical contenders for fuel cell cathode catalysts. In MCOs, a substrate reduces a copper atom at the type 1 site, where charge is then transferred to a trinuclear copper cluster consisting of a mononuclear type 2 or "normal copper" site and a binuclear type 3 copper site. Following the reduction of all four copper atoms in the enzyme, dioxygen is then reduced to water in two two-electron steps, upon binding to the trinuclear copper cluster. We identified an MCO, a laccase from the hyperthermophilic bacterium *Thermus thermophilus* strain HB27, as a promising candidate for cathodic fuel cell catalysis. This protein demonstrates resilience at high temperatures, exhibiting no denaturing transition at temperatures high as 95 ^oC, conditions relevant to typical polymer electrolyte fuel cell operation.

In Chapter I of this thesis, we discuss initial efforts to physically characterize the enzyme when operating as a heterogeneous cathode catalyst. Following this, in Chapter II we then outline the development of a model capable of describing the observed electrochemical behavior of this enzyme when operating on porous carbon electrodes. Developing a rigorous mathematical framework with which to describe this system had the potential to improve our understanding of MCO electrokinetics, while also providing a level of predictive power that might guide any future efforts to fabricate MCO cathodes with optimized electrochemical performance. In Chapter III we detail efforts to reduce electrode overpotentials through site-directed mutagenesis of the inner and outer-sphere ligands of the Cu sites in

laccase, using electrochemical methods and electronic spectroscopy to try and understand the resultant behavior of our mutant constructs. Finally, in Chapter IV, we examine future work concerning the fabrication of enhanced MCO cathodes, exploring the possibility of new cathode materials and advanced enzyme deposition techniques.

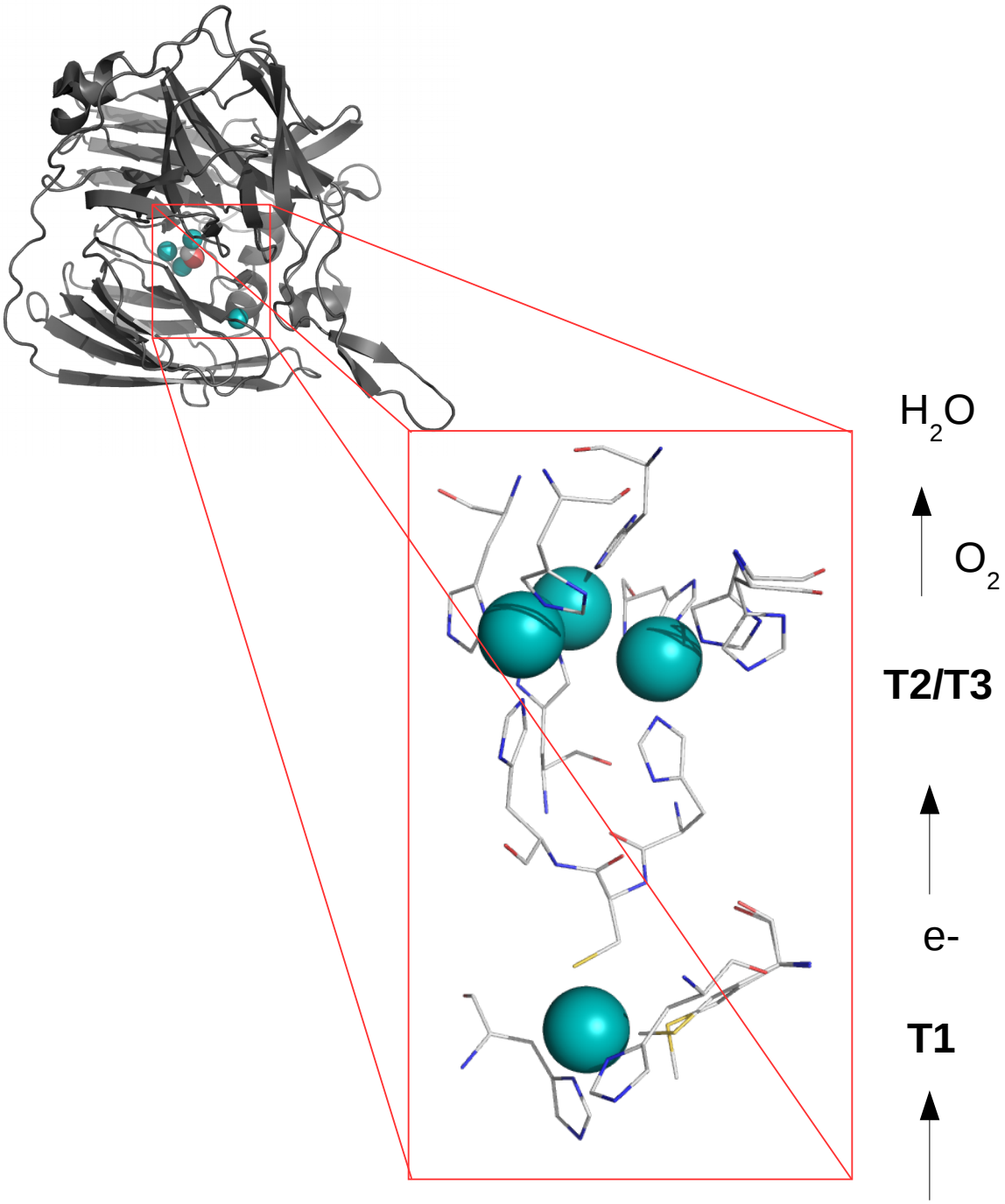

General MCO architecture. Copper atoms shown as cyan spheres.

I. Catalysis of Dioxygen Reduction by *Thermus thermophilus* strain HB27 Laccase on Ketjen Black Electrodes

Peter Agbo[1], James R. Heath[1], Harry B. Gray[1]*

[1] California Institute of Technology, Pasadena California

*Corresponding Author

Reproduced with permission from the

The Journal of Physical Chemistry B 2013, *117*, 527-534.

American Chemical Society

(Adapted)

Abstract

We present electrochemical analyses of the catalysis of dioxygen reduction by *Thermus thermophilus* strain HB27 laccase on ketjen black substrates. Our cathodes reliably produce 0.56 mA cm^{-2} at 0.0 V vs. Ag|AgCl reference at 30 °C in air-saturated buffer, under conditions of non-limiting O_2 flux. We report the electrochemical activity of this laccase as a function of temperature, pH, time, and the efficiency of its conversion of molecular dioxygen to water. We have measured the surface concentration of electrochemically active species, permitting the extraction of electron transfer rates at the enzyme-electrode interface: 1 s^{-1} for this process at zero driving force at 30 °C and a limiting rate of 23 s^{-1} at 240 mV overpotential at 50 °C.

Introduction

Fuel cells remain one of the most promising modes of utilizing hydrogen or methanol by coupling their oxidation at anodic surfaces to the four-electron reduction of dioxygen to water at the cathode. In general, the cathodic transformation of dioxygen to water proves limiting to current production (and therefore power output) in fuel cells.[1] While kinetic limitations may be overcome by employing platinum on carbon (Pt/C) catalysis at the cathode, this is not a viable, long-term solution as a consequence of the high cost of platinum.[2] In biochemical approaches to this problem, the multicopper oxidases (MCOs) have proven to be a good starting point. These enzymes, comprised of either two or three cupredoxin domains that ligate copper ions at type 1 and type 2/3 centers, have evolved as efficient dioxygen reductases, capable of coupling the oxidation of phenols and other organic substrates to the reduction of O_2 to form H_2O.[3] Electron flow through these proteins proceeds in a stepwise fashion, with a reduced substrate donating charge to the type 1 center, followed by long-range electron transfer to the type 2/3 trinuclear copper cluster where dioxygen reduction occurs.[3–6]

We are working with an MCO from *Thermus thermophilus* strain HB27, an isoform of the multicopper oxidase subset known as laccases. The reported thermostability of this MCO makes it a promising candidate for operation in fuel cells, with a half-life of 14 hours at 80 °C and a catalytic optimum at 95 °C in solution.[7] To date, characterization of *T. thermophilus* laccase has been limited to either biochemical assays of the enzyme's catalytic turnover of substrates in solution or homogeneous electrochemical measurements in the presence of the small-molecule mediator 2,2'-azino-bis(3-ethylbenzothiazoline-6-sulphonic) acid (ABTS).[7,8] As a complement to such work, we performed a comprehensive study of the electrochemical activity of *T. thermophilus* laccase with the enzyme functioning as a heterogenous catalyst without a redox mediator. Our choice of catalytic support was inspired by previous studies where other MCOs, such as copper

efflux oxidase (CueO), *Trametes versicolor* laccase and *Streptomyces coelicor* laccase, were found to catalyze dioxygen reduction when adsorbed on ketjen black, a carbon substrate that has a very high specific (BET) surface area due to its porosity (Figure 1-1) .[9–13]

While past work in protein electrochemistry has explored the utility of other electrode materials such as anthracene-modified gold and surfaces modified with self-assembled alkyl monolayers (SAMs), these electrodes are not realistic options for cathodes intended for practical fuel cell applications because of their lengthy fabrication times and relative fragility. Conductive carbon powders such as ketjen black represent cheap, robust surfaces that are readily processed into electrode assemblies for electrochemical testing. Perhaps the most compelling reason to employ these materials in protein electrochemistry derives from the existing precedent for the use of carbon blacks in fuel cell membrane-electrode assemblies (MEAs), making ketjen black supports a logical starting point for investigations of heterogenous catalysis by *Thermus thermophilus* strain HB27 laccase.

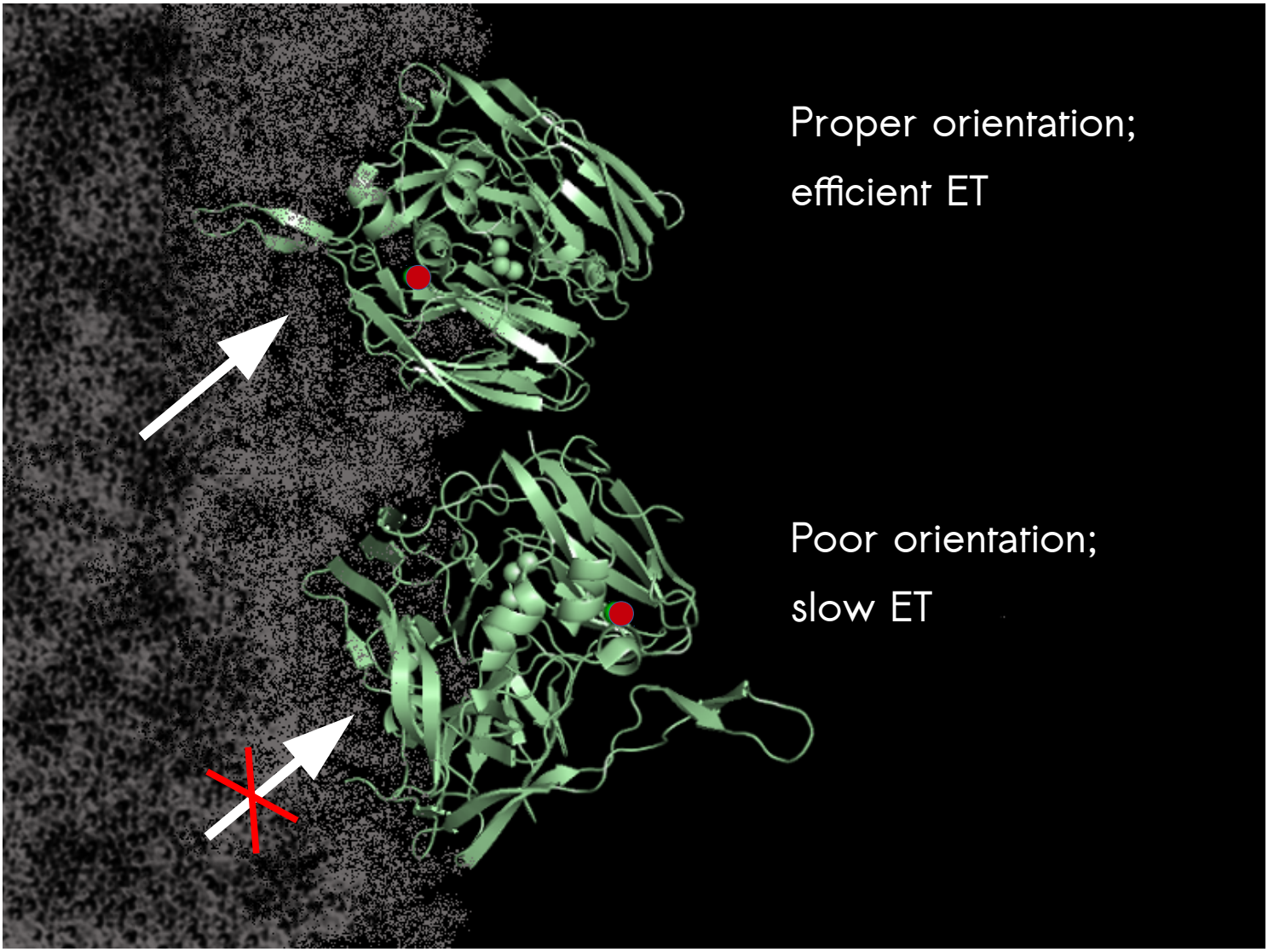

Figure 1-1

Orientations representing one of two possible extremes when laccase (PDB ID: 2XU9) is adsorbed onto a ketjen black substrate: (top) The protein is adsorbed with the type 1 copper center (shown in red) held near the electrode surface, allowing for rapid interfacial ET (bottom). Enzyme adsorption occurs such that the type 1 center is held opposite the electrode surface, inhibiting charge transfer.

Experimental

Cloning

The gene for wild type *T. thermophilus* laccase was amplified from a non-expression vector using the following primers: 5′-GATCCgcggaacgcccgaccctgccgattccggatctgc-3′ (Forward) and 5′-AATTCcacggtaaagcccagcatcatgccggtatcttcatg-3′ (Reverse). Capitalized regions in the primers denote restriction sites that were used for cloning into plasmids (BamH1, EcoR1). PCR amplification of the wild-type gene was performed using the Expand High Fidelity PCR system (Roche). Spurious nucleic acid amplicons were cleaned from the PCR reaction using the Qiagen PCR Purification Kit. The gene was ligated into the pET22b(+) expression vector by separately digesting both the plasmid and gene insert using BamH1 and EcoR1 restriction enzymes in a single reaction, yielding hanging end restriction cuts for both the laccase gene insert and the pET22b(+) vector. Removal of residual nucleic acid fragments from the restriction cutting was also performed using the Qiagen PCR Purification Kit. The purified, linear plasmid and gene insert were then mixed in 1:5 molar ratio and incubated in a reaction using T4 DNA ligase (Roche) at room temperature for 12 hours, to allow insertion of the WT laccase gene into the pET vector. Novablue Singles cells (EMD Millipore Chemicals) were then transformed with the ligation reactions and plated on agar plates with LB media (BD) inoculated with 0.1 mg/mL ampicillin (Sigma). Colonies to be screened were then picked and grown in 5 mL cultures in LB broth for 16 hours at 37 ˚C. A Qiagen miniprep kit was used to isolate plasmid DNA. Confirmation of successful cloning was performed both through diagnostic digests of plasmid DNA extracted from transformed cells, and also through sequencing (Laragen Sequencing) using T7 promoter and T7 terminator sequencing primers.

Expression

Plasmid DNA cloned with the gene for laccase was transformed into *E. coli* Rosetta 2 (DE3) cell lines (EMD Millipore Chemicals). Low

expression yields of laccase in standard BL21 (DE3) *E. coli*, caused by poor codon compatibility between our gene and typical *E. coli* tRNA expression profiles, mandated our use of Rosetta 2 (DE3) cell lines that overexpress tRNAs uncommon in *E. coli*. Transformed cells were grown in 6 L of autoclaved TB broth (47.6 g/L) amended with 0.1 mg/mL sodium ampicillin and 34 μg/mL chloramphenicol for 16 hours at 37 ˚C, and induced with 1 mM IPTG for an additional 5 hours. Cells were then harvested by centrifugation and equilibrated against 20% sucrose, 1 mM EDTA, 300 mM Tris, pH 8.1 for one hour. After equilibration, the cells were re-pelleted by centrifugation at 7000 rpm for 25 minutes. Following removal of the supernatant, the cells were resuspended in pH 6 20 mM sodium acetate, and then treated with lysozyme and DNAse for 30 minutes. Extracts were sonicated for 10 minutes, and then centrifuged for 1 hour at 14000 rpm. Following centrifugation, the supernatant was carefully decanted into a clean container and stored overnight in a cold room.

Metallation

Incorporation of copper into the laccase apoenzyme was achieved by dropwise addition of 10 mM $CuSO_4$ to the crude extracts. Addition continued until the extracts turned a dark green color. The metallated lysate was then stirred for at least an hour in a 4 ℃ cold room.

Chromatography

Following metallation, batch columns were run as initial purifications of the extracts. Crude lysates were loaded onto a CM Sepharose (cation exchange) column equilibrated with 3 column volumes of 100 mM sodium acetate, pH 6.0. Following the passage of non-binding proteins through the column, bound proteins were eluted using 100 mM sodium acetate + 500 mM NaCl. Bound fractions were collected, pooled, and concentrated to a 15 mL volume using an Amicon with a 30 kDa molecular weight cutoff (MWCO) membrane.

Buffer exchange of the extract was then performed using an FPLC desalting column (20 mL bed volume) equilibrated with 20 mM sodium acetate, pH 6.3. Immediately after desalting, cation exchange was performed using a HiTrap SP column equilibrated with pH 6.3, 20 mM sodium acetate and eluting in a 30% gradient of 1M NaCl over 40 minutes. A final chromatographic separation by size was done using a Superdex 75 gel filtration column equilibrated in pH 6.0, 20 mM sodium acetate. Expression yields were quantified using the type 1 copper absorption at 610 nm ($\varepsilon \sim 5000\ M^{-1}\ cm^{-1}$). Enzyme purity was verified using SDS-PAGE and Matrix Assisted Laser Desorption Ionization – Time of Flight (MALDI-TOF) mass spectrometry (Supporting Information).

Circular Dichroism Spectroscopy (CD)

CD wavelength scans and thermal denaturation characterization were performed by diluting protein samples so that absorbances at 280 nm were 0.2. Scans of protein samples were taken as a function of wavelength between 210 and 260 nm. To confirm that the purified enzyme was laccase and not wild-type CueO, an enzyme homologue (found in the *E. coli* genome) with a similar mass and virtually identical UV-vis spectrum to that of *Thermus thermophilus* laccase, titrations were performed by monitoring changes in ellipticity at 222 nm as a function of temperature between 18 and 95 °C (SI). CueO exhibits a sharp denaturing transition at 80°C, whereas wild-type *T. thermophilus* laccase retains its structure at temperatures beyond 95 °C. [7]

Electrode Fabrication

Ketjen black (AzkoNobel) was used as received. Ketjen black slurries were prepared by first modifiying the carbon blacks with 1-pyrenebutyric acid (Sigma). This modification had the effect of reducing the electrode background, making anaerobic voltammetry more feasible. A 4.7 mg/mL solution of 1-pyrenebutyric acid was prepared in a solvent mixture of 70%

acetone and 30% DMSO. Ketjen pellets were ground in a mortar. The ground ketjen black (60 mg) was then added to the 1-pyrene butyrate solution. The resulting colloid was vortexed briefly, then placed on a shaker in a cold room for 30 minutes to ensure saturation of the carbon black with the pyrene derivative. Adsorption isotherms generated by monitoring the 344 nm (pyrene) signature in the supernatant (ε = 41000 M^{-1} cm^{-1}) revealed an adsorption capacity of ca. 2.5 mg pyrene butyrate per mg ketjen black with the given solvent composition. The modified ketjen black was then collected by vacuum filtration. Electrode slurries using the modified carbon powders were made by adding 40 mg ketjen black and 10 mg polyvinylidene diflouride (PVDF, Sigma) to a scintillation vial with 5.0 mL N-methyl-2-pyrrolidone (Sigma). The slurry was mixed by pipette and then sonicated for at least two hours to homogenize. Eight μL of the slurry were pipetted onto the surfaces of highly oriented pyrolytic graphite (HOPG, K-TEK Nanotechnology) electrodes which had been lightly abraded using emery paper and cut to dimensions of 0.5 x 0.5 cm. The electrodes were then dried in an oven at 60-70 °C for at least 12 hours.

Polarization and RDE Experiments

Electrode polarization studies were performed in 20 mM sodium acetate, pH 5.0 in a 250 mL cell held at 30 °C. All potentials were referenced versus an Ag|AgCl electrode (CHI Instruments). The ketjen black assembly served as the working electrode while a platinum wire served as the counter electrode. Rotating disk electrode experiments were performed using a PINE Instruments rotator. Before these experiments, background scans were taken of each electrode at each speed examined in our tests. Following control scans, the electrode tips were immersed in 5 μM solutions of *T. thermophilus* laccase for two hours. During the immobilization process, electrodes were rotated at 100 rpm to mix. Following electrode functionalization with laccase, electrode surfaces were rinsed free of excess enzyme by brief immersion and gentle stirring in pH 5.0 20 mM sodium

acetate. Anaerobic control measurements were performed by sparging the cell buffer with argon for at least 30 minutes prior to voltammetry. Linear sweep voltammetry (LSV) was performed by scanning electrodes from 0.6 to 0.0 V vs Ag|AgCl at 10 mV s^{-1}. We employed rotating disk electrode (RDE) analysis to discern the dependence of electrode activity on rates of dioxygen mass transport and also to determine an upper limit for the cathodic current produced by these electrodes in the absence of mass transport limitations.

Tafel Analysis

Tafel data were collected by scanning the electrodes anodically in aerated pH 5.0 20 mM sodium acetate while rotating at 3000 rpm between 0.0 and 0.6 V vs. Ag|AgCl. Cathodic branches of the generated Tafel plots were used for fitting and extraction of the exchange current (i_0), charge transfer resistance (Ω_{ct}), Tafel slope, and transmission coefficient (α) of the system.[14] We fit these data to a low-overpotential limiting case of the Butler-Volmer equation, constraining the the quantity $d\eta/di$ with respect to the exchange current (eq. 1-1):[15]

$$d\eta/di = RTF^{-1}i_0^{-1} \qquad (1\text{-}1),$$

where R is the ideal gas constant (8.31 J mol^{-1} K^{-1}) and T is the cell temperature, 303 K. In practice, data fitting was achieved by comparing the Tafel linear fit to the value of $d\eta/di$ yielded by a corresponding linear sweep voltammogram of an electrode. If the correct regime in the Tafel plot (the range of η) is chosen for a linear fit, the resulting exchange current, when applied to (2), should yield a value for $d\eta/di$ equal to that observed in a linear sweep of the electrode in the same voltage region. This method provided a systematic way to determine the appropriate range of overpotentials that were required for correct Tafel fitting. Using this procedure, our fits reliably yielded a $d\eta/di$ within 6% of the ideal value

(for a given exchange current).

Faradaic Efficiency

Faradaic yields for O_2 conversion to H_2O by laccase were obtained by comparing the charge passed over the course of an experiment with the change in O_2 content of the cell. A five-port, 25 mL distillation flask filled with pH 5.0 20 mM sodium acetate served as the electrochemical cell. Prior to electrode operation, the reference electrode and FOXY O_2 sensor (Ocean Optics) were inserted into the ports of the distillation flask and secured with parafilm. The counter electrode was placed in a glass capillary with a fritted end that was filled with the cell buffer. The capillary was then mounted in a cell port and secured with parafilm. Two-point calibration using dissolved O_2 concentrations of 0% and 20.8% (atmospheric pO_2) was used to ready the probe before each experimental trial. A small, magnetic stir bar was placed in the cell to allow for even mixing of dissolved dioxygen during experimental runs. Following calibration, a ketjen black working electrode modified with laccase, as described earlier, was fitted to the cell. Rubber gaskets were fitted over the electrode assembly to ensure an airtight seal. A 5.0 mL syringe filled with the cell buffer was attached to the fifth port. Any remaining air pockets in the cell were easily removed by depressing the syringe and filling the cell to its maximum volume. Following apparatus assembly, the dioxygen levels in the cell were allowed to stabilize for at least one hour. Once the baseline was established, a 0.0 V potential (vs. Ag|AgCl) was applied to the working electrode and the resulting current and changes in O_2 concentration were monitored for two hours. With gentle stirring, we were able to maintain a current of 25-30 μA during data acquisition. At the end of the experiment, we quantified the faradaic yield using (eq. 1-2):

$$E = nF\nu\frac{\Delta[O_2]}{\int_0^t i(t)dt} \qquad (1\text{-}2),$$

where E is the faradaic efficiency, n = 4, for dioxygen reduction to water, v is the cell volume, $\Delta[O_2]$ is the change in the concentration of dioxygen during the experiment, F is Faraday's constant and i is the current.

Temperature and pH Dependence

Titrations of laccase electrodes were conducted in pH 5.0 20 mM sodium acetate between 20 and 80 °C while rotating at 3200 rpm. Following cell equilibration at each temperature, the electrodes were inserted into the cell and voltammograms were recorded at 10 mV s^{-1} between 0.0 and 0.6 V vs. Ag|AgCl. Electrodes were immediately removed from the cell following completion of a scan to help minimize reduced electrode activity caused by any overexposure of the protein films to high temperatures. Studies of pH dependence were done at 18 °C in 20 mM sodium acetate at pH 2.90, 5.05, 6.04, 6.98, 8.06, and 9.16. Investigations of the pH dependence of the type 1 copper reduction potential were conducted at pH 4.00, 4.50, 5.00, 5.46, and 6.01.

Surface Concentration Measurements

Concentrations of active enzymes adsorbed to ketjen black were measured by cyclic voltammetry. Electrodes were functionalized with laccase as described before and then fitted to an airtight cell. The cell was placed in a copper mesh Faraday cage, with the working electrode grounded to the base of the cage. The cell buffer (pH 4.76 50 mM sodium phosphate + 250 mM sodium sulfate) was purged of dioxygen by vigorous sparging of the media with argon for one hour. To reduce the risk of any O_2 leakage into the cell, argon was pumped into the cell during the entire course of the

experiment. After establishing an anoxic atmosphere, amperometric scans of the electrodes were performed to ensure all enzyme centers were oxidized. This was done by poising the electrodes at 0.6 V vs. Ag|AgCl reference and monitoring the transient current decay for two hours. Cyclic voltammograms were then initiated by scanning cathodically from 0.4 to 0.2 V at a rate of 10 μV s^{-1}. Enzymes were quantified by integrating the cathodic peak in the

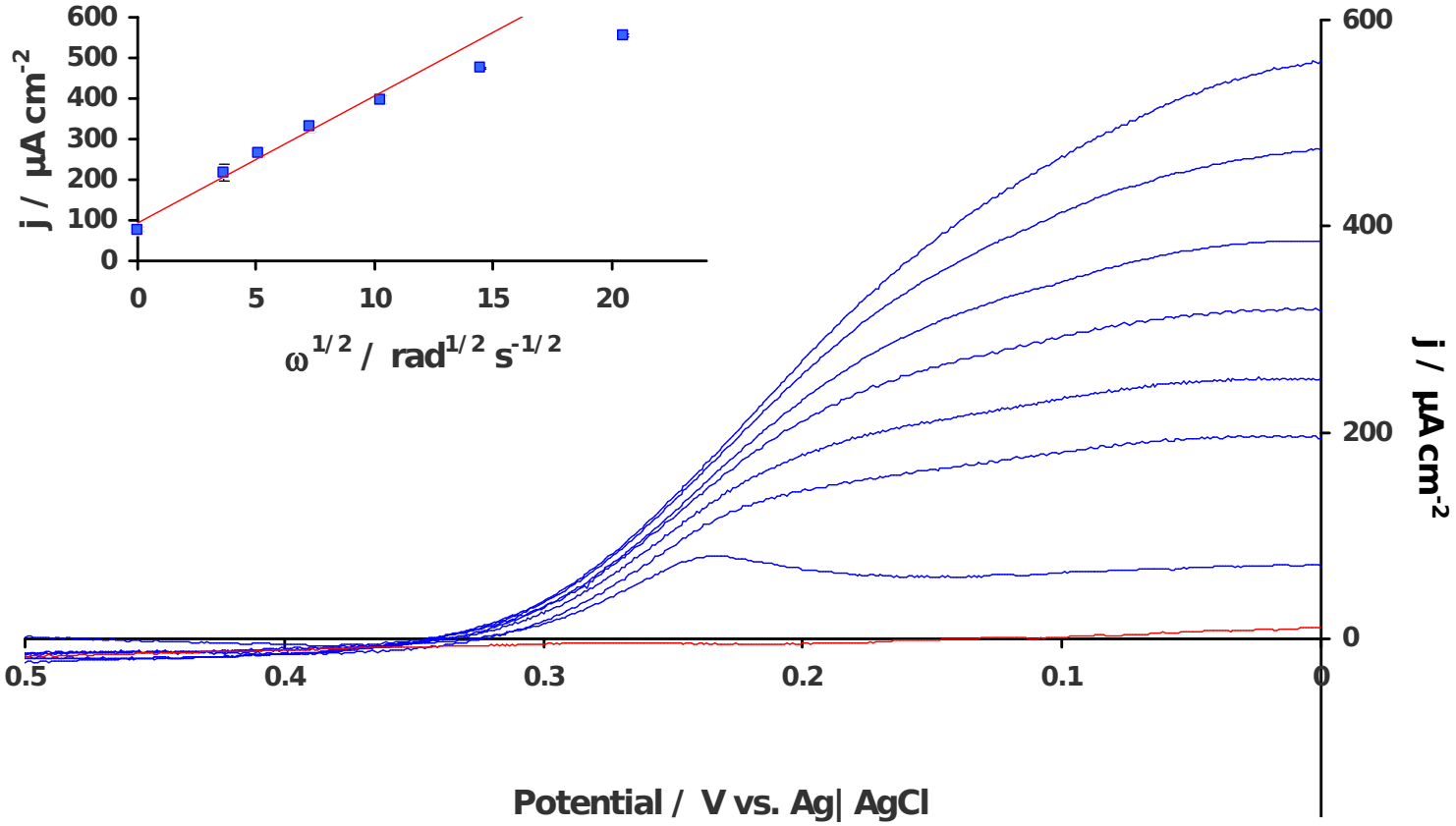

Figure 1-2

Cathodic polarization of electrodes comprised of laccase adsorbed onto modified ketjen black in pH 5.0, 20 mM sodium acetate buffer. Current onset is observed around 340 mV vs. Ag|AgCl. Linear sweep voltammagrams of the electrodes demonstrate monotonic increases in the current as a function of rotation rate from 0 to 4000 rpm (blue traces). Electrodes show no activity in the absence of O_2 (red curve, Argon sparged media). Inset: peak current density as a function of rotation rate. Loss of the linear relationship between current density and $\omega^{1/2}$ begins around 2000 rpm as O_2 flux stops being rate limiting. Error bars are in black.

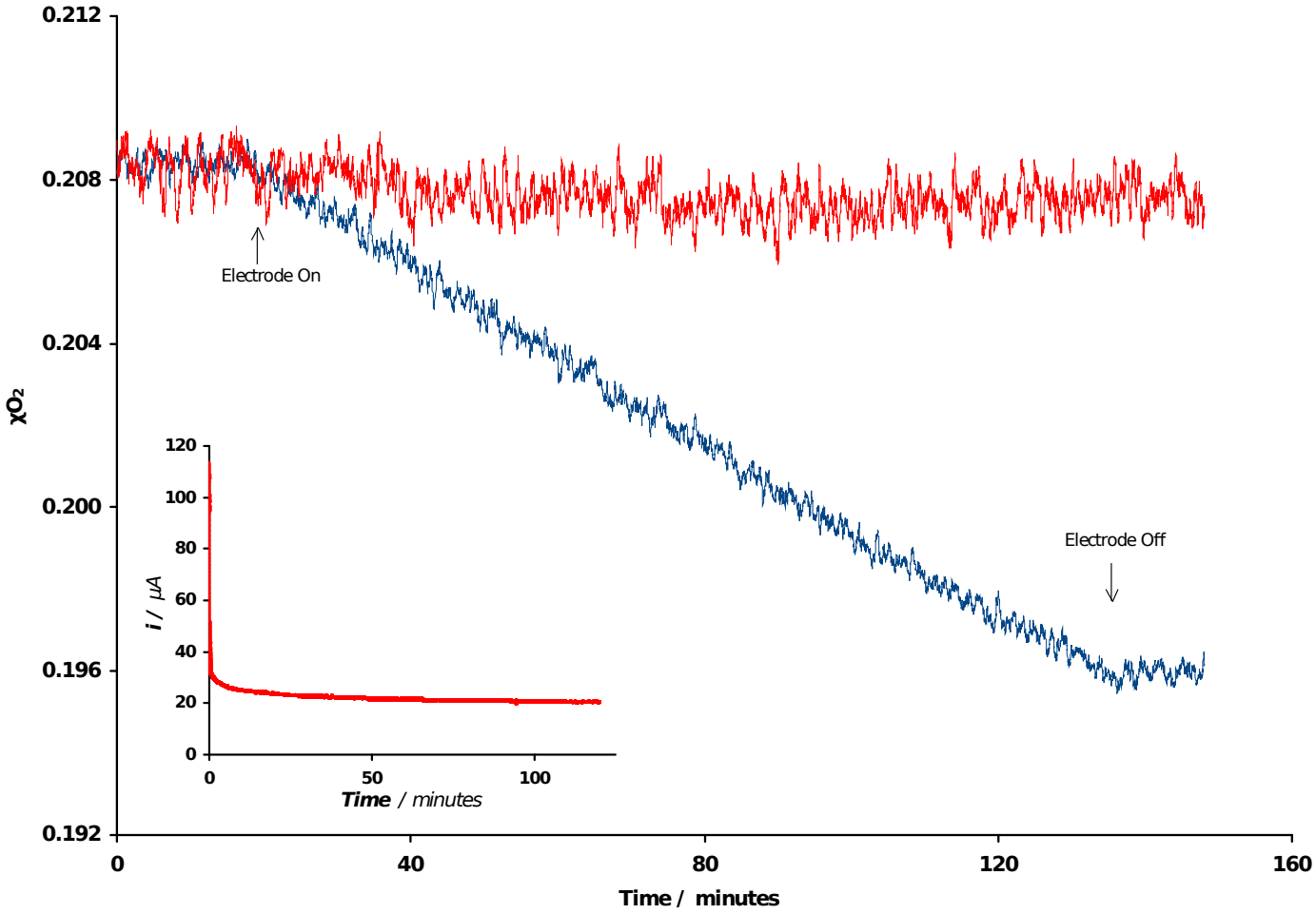

Figure 1-3a

Faradaic yields for laccase electrocatalysis. Electrodes were poised at 0.0 V vs. Ag|AgCl for two hours with concomitant monitoring of O_2 consumption. Dioxygen concentration of a cell operating with an enzyme-functionalized electrode is depicted in blue. Control electrodes (no enzyme) show no decrease in O_2 content over time (red trace). Inset: An amperometric trace of electrode current during the experiment.

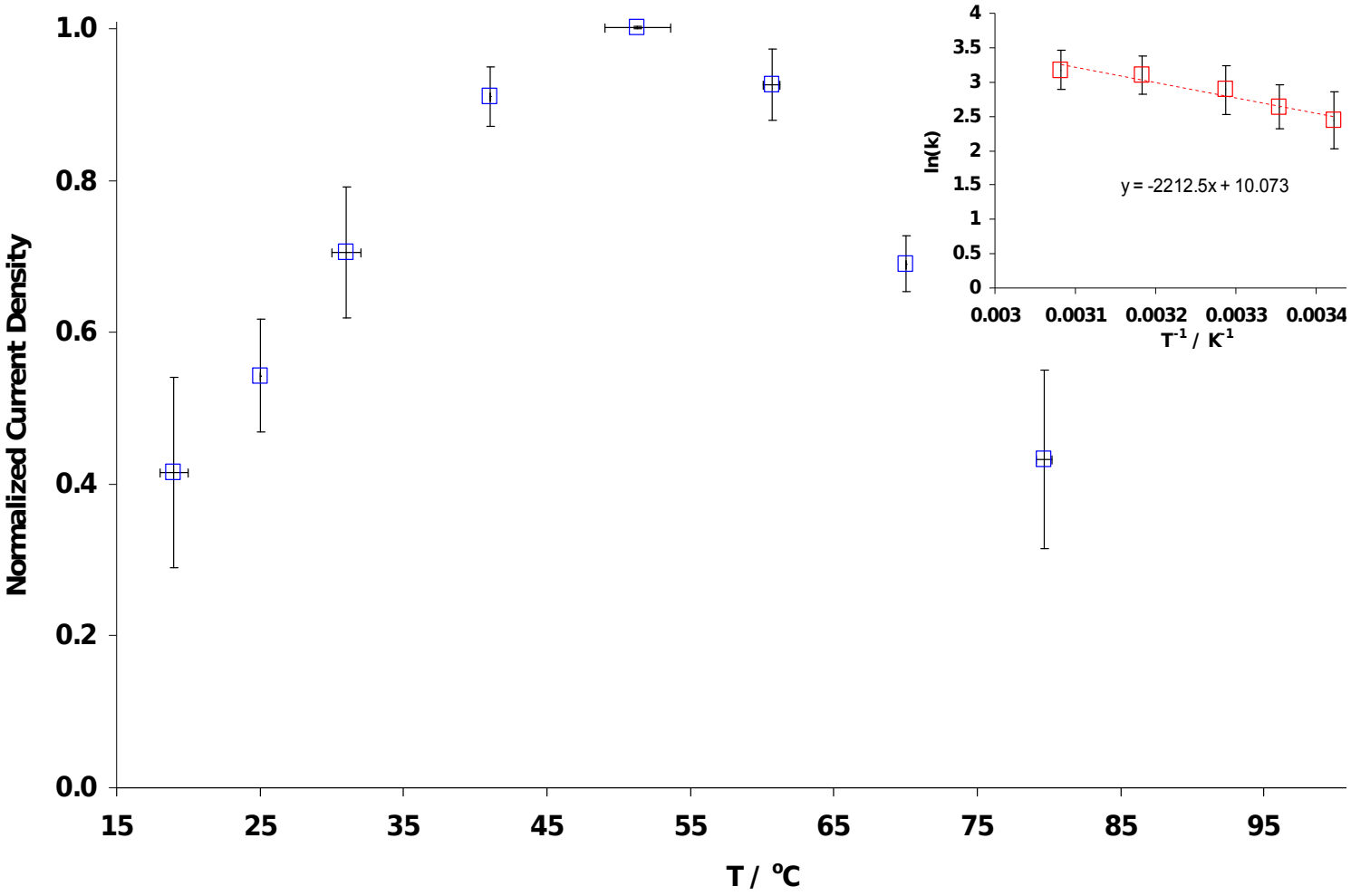

Figure 1-3b

Temperature dependence of laccase activity in pH 5.0, 20 mM sodium acetate with electrode rotation at 3200 rpm. Inset: Eyring analysis reveals an activation energy of 18.4±2.2 kJ mol^{-1} for heterogenous electrochemical O_2 reduction by *T. thermophilus* laccase. (fitting equation: y = -2212.5x + 10.073; R^2 = 0.93)

.

CV. The resulting charge, Q, was converted to surface concentration by assuming four reducing equivalents per enzyme (for type 1, 2, and 3 copper centers in laccase) under anaerobic conditions.

Results

Cathodic polarization of laccase-adsorbed ketjen black electrodes was performed between 0.6 and 0.0 V in pH 5.0 acetate buffer. Under these conditions, the onset of a catalytic current was observed at ca. 340 mV vs. Ag|AgCl, with a limiting current observed by 0.0 V. Dependence of this catalytic wave on the presence of dioxygen was confirmed through experiments carried out under anaerobic conditions, which resulted in the disappearance of the wave (Figure 1-2, red curve). To establish an upper limit of the current that could be drawn from this system, studies of the current dependence on electrode rotation were conducted using an RDE setup. At lower speeds we observe a linear variance of the cathodic current density (j_L) by the square root of the rotation rate ($\omega^{1/2}$), as predicted by the Levich equation (eq. 1-3):[14]

$$j_L = 0.62nFD^{2/3}\omega^{1/2}\nu^{-1/6}C \quad (1\text{-}3).$$

Higher angular velocities result in a loss of the linear relationship between current and rotation rates, as dioxygen flux to the cathodic surface stops being rate-limiting above 4000 rpm (Figure 1-2, inset). At this rotation speed, the catalytic current trends toward a plateau around 0.56 mA cm^{-2} under the stated conditions.

Quantitative evidence for the complete electrochemical transformation of O_2 to H_2O by *T. thermophilus* laccase was obtained by measuring the steady-state O_2 consumption of laccase under a constant applied potential (Figure 1-3a). By comparing the total amount of dioxygen consumed over a period of two hours to the total amount of charged passed through the system during the same time interval, we calculated a faradaic yield of

0.947±0.023, indicating that approximately 95% of the dioxygen turned over by the enzyme results in water production. This outcome serves as a testament to the high catalytic specificity of this laccase variant, even when operating as a heterogenous catalyst.

Despite a catalytic optimum of 95 °C reported for *T. thermophilus* laccase when acting upon organic substrates in solution, our studies revealed a catalytic optimum of only 55 °C for this enzyme when adsorbed onto modified ketjen black. By 80 °C, the electrode had lost most of its activity (Figure 1-3b). Laccase cathodes displayed reasonably good temporal stability during potentiostatic trials, retaining over 98% of their initial activity over the course of an hour at 30 °C when poised at a high (340 mV) overpotential. Eyring analysis of *T. thermophilus* laccase thermal dependence reveals an activation enthalpy of 18.4±2.2 kJ mol^{-1}, substantially lower than those reported for *Myrothecium verrucaria* (28.2 kJ mol^{-1}) and *Trachyderma tsunodae* (34.3 kJ mol^{-1}) laccases employed in similar electrode systems (Figure 1-3b, inset).[16] The optimal catalytic activity was observed at pH 5.0, with the enzyme exhibiting a linear dependence on proton concentration in the range pH 4.0 — 6.0, with a slope of 57±1 mV $decade^{-1}$, a value close to the ideal slope of 59 mV for the pH dependence of a Nernstian, one-electron process (SI).[15]

Investigations of interfacial electron transfer processes were aided by Tafel analysis, which allowed for the determination of the equilibrium exchange current density (j_0), charge transfer resistance (Ω_{ct}) and the transmission frequency (α) of electron transfer between the type 1 copper site in laccase and the cathode surface. We find j_0 = 27.2±3.7 μA cm^{-2} at 303 K and a corresponding Ω_{ct} of 3890±518 ohms (Figure 1-4).

Our system exhibits an α of 0.48±0.05, which is highly suggestive of a symmetric Marcus coordinate, the situation expected for electron flow between a donor and acceptor in the zero-overpotential limit. The moderate Tafel slope of 128±13.8 mV $decade^{-1}$ is typical of this class of electrode and within error of the expected slope (~118 mV) of an ideal, one-electron

transfer at ambient temperature, where $\alpha = 0.5$.[15] Furthermore, this Tafel slope agrees well with the reported value of 145 mV decade^{-1} for *Trametes versicolor* laccase – modified gold cathodes and also bilirubin oxidase cathodes (120 mV decade^{-1}).[16,17]

Using voltammetry performed under strictly anaerobic atmospheres, we were able to quantify the amount of electrochemically active enzymes incorporated into our ketjen black electrodes through observation of peaks due to sacrificial reduction of the type 1 copper site in *Thermus*

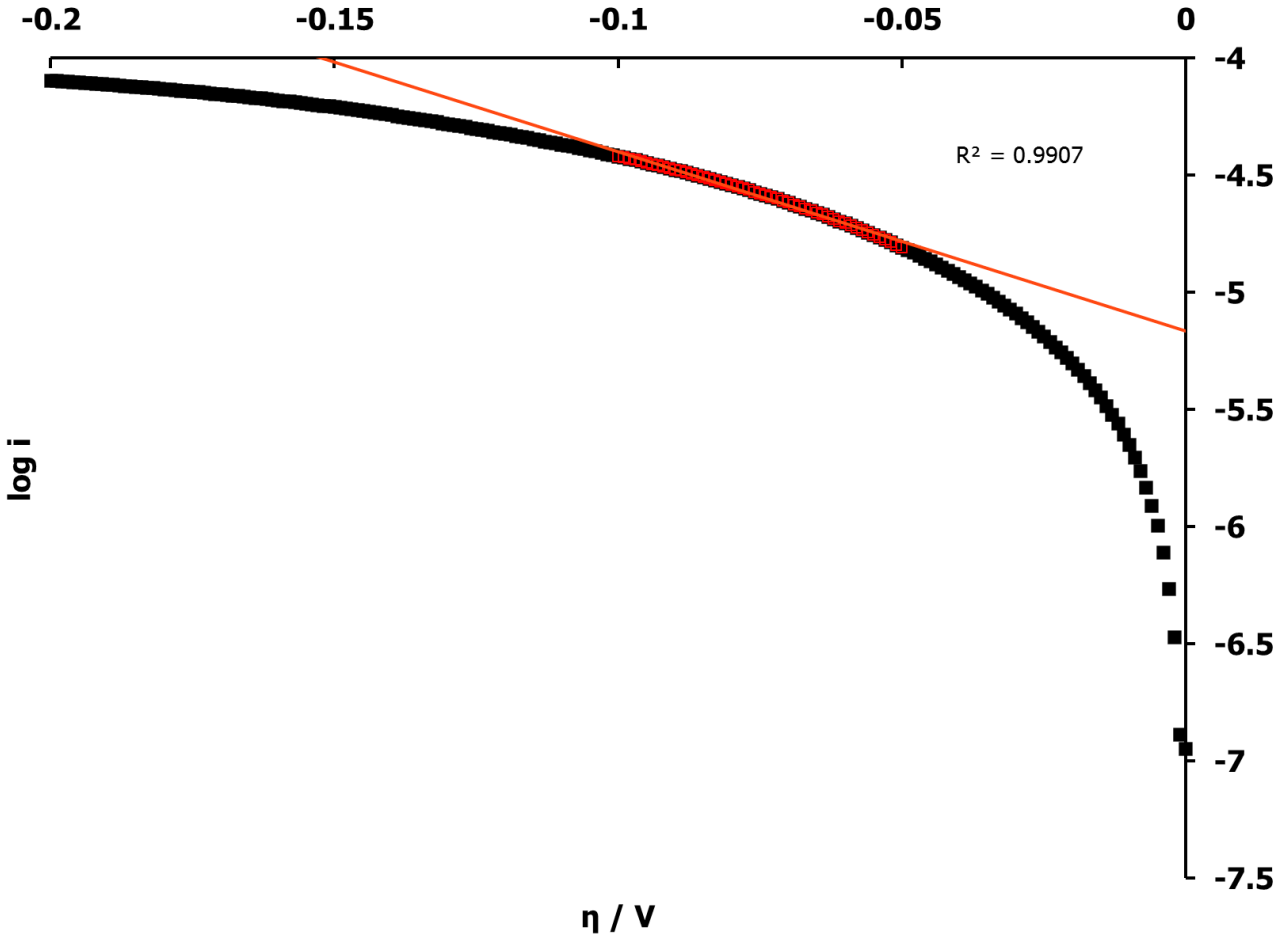

Figure 1-4

A typical cathodic Tafel branch of a laccase electrode scanned anodically in pH 5.0, 20 mM sodium acetate at 3000 rpm. Our fitting methodology predicts the 50-100 mV overpotential regime as the most appropriate region for conducting the linear analysis. Using this fit, extrapolation of the linear region to the point of zero driving force reveals an exchange current density of 27.2 μA cm^{-2}.

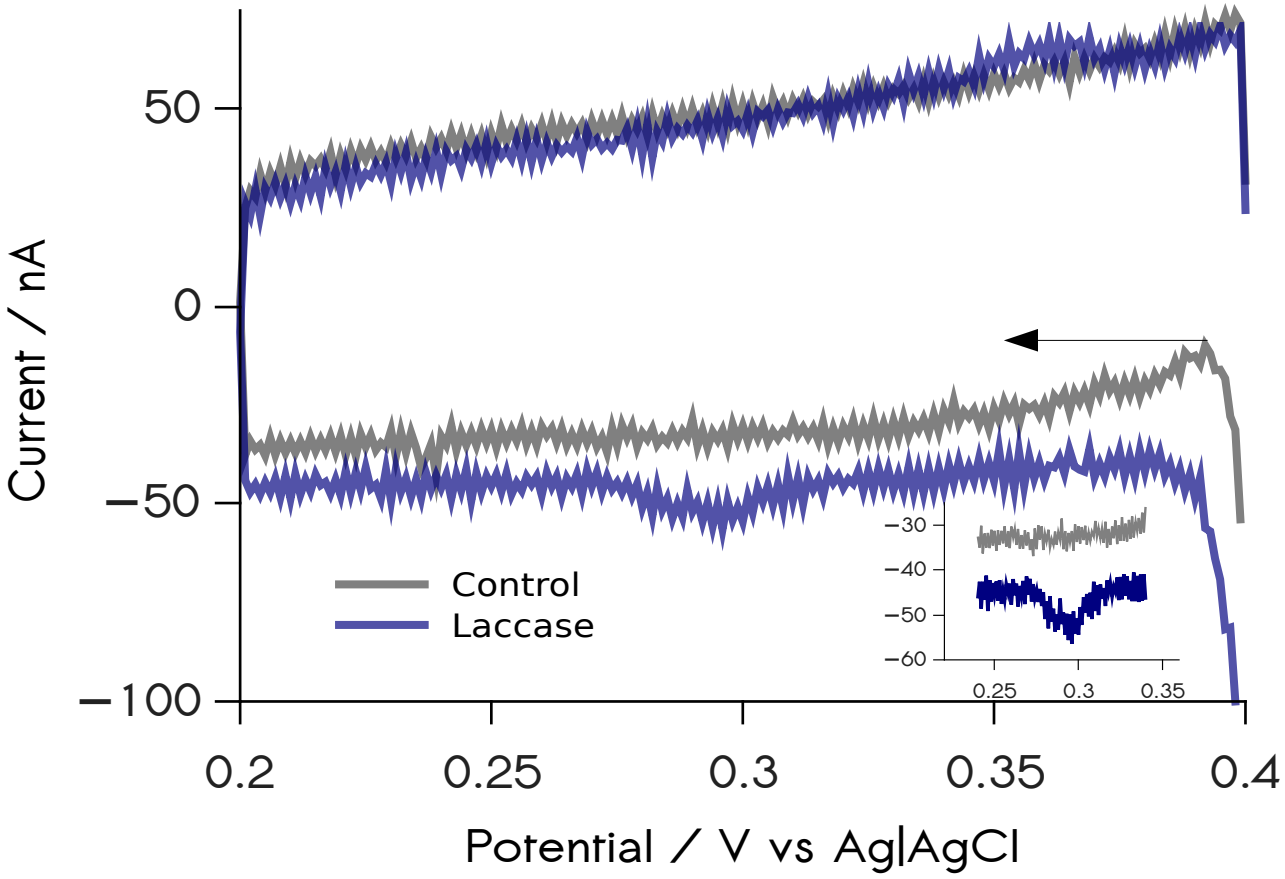

Figure 1-5

Cyclic voltammgram of a laccase-modified electrode under anaerobic conditions (blue trace) scanned from 0.4 to 0.2 V vs Ag|AgCl at 10 μV s^{-1} in pH 4.6 50 mM phosphate + 250 mM sulfate buffer. Peaks occur at 300 and 360 mV for the cathodic and anodic processes, respectively and are assigned to sacrificial reduction and oxidation of the Type I copper site in laccase. Peak integration provides a value of 25 μC, corresponding to 3.9×10^{13} electrochemically active enzymes on the ketjen substrate. Negative (no enzyme) controls show no peaks in the c.v. (gray trace) under identical conditions. The black arrow signifies the start of the scan (cathodic direction).

thermophilus laccase. Prior to running CVs, amperometric sweeps were run at 0.6 V under argon until the current decayed to zero, ensuring that at least the type 1 Cu sites in all electrochemically active enzyme centers were fully oxidized. CVs were then run starting in the cathodic direction at a rate of 10 μV s^{-1}. Peaks assigned to the reduction and oxidation of the type 1 active site occurred at 0.30 V and 0.36 V, respectively (Figure 1-5). Integration under the cathodic peak yielded 25±7 μC. Our use of amperometric oxidation prior to voltammetry prompted the assumption of a four-electron-per-enzyme stoichiometry when calculating the size of the electrochemically active enzyme population from the cathodic integral. This yields 3.9±1.1 $x10^{13}$ functioning enzyme centers. We emphasize that the cathodic peak is far more ideal for this calculation than the anodic signal, since knowledge that the resting form of an MCO has all metal sites in the cupric state guarantees that during an anaerobic, cathodic scan, four equivalents of charge are taken up by the enzyme.[18]

The ability to probe both the surface concentration of electrochemically competent enzymes and the value of the equilibrium exchange current enabled us to calculate a k_{ET} value of 1.0±0.3 s^{-1} for electron transport across the enzyme-electrode interface at zero driving force at 30 °C. Using values for the peak current achieved during temperature dependence studies (3200 rpm rotation), we estimate a k_{ET} of 16.2±7.5 s^{-1} at 30 °C and a maximum rate constant of 22.7±8.6 s^{-1} at 50 °C under an applied 240 mV overpotential during catalytic electrode operation.

Discussion

We assign the current onset at ca. 340 mV vs Ag|AgCl to the reduction potential of the type 1 copper center of *T. thermophilus* laccase. This type 1 potential is considerably depressed relative to those of other high-potential laccase homologues and is far from the thermodynamic potential for the reduction of dioxygen to water, possibly owing to the short Cu-(S)Met axial bond in this enzyme, an interaction known to be critical for

tuning type 1 copper reduction potentials.[16,18,19] A primary challenge posed by the cathodes designed for this study is that their peak current of 0.56 mA cm^{-2} is not only low compared to targets for fuel cells aimed at mobile applications (~100 mA cm^{-2}), but is also associated with a high (~ 240 mV) overpotential.[20] Furthermore, the longevity of these cathodes still needs to be improved for continuous use in devices running for several weeks or months.

The successful determination of faradaic yields for this electrochemical process indicate that *T. thermophilus* laccase is incredibly efficient at using dioxygen as an electron sink, with hardly any O_2 reduction intermediates resulting from catalytic turnover. Our result is consistent with findings for other MCOs, where high coulombic efficiencies have been inferred from studies employing methods such as rotating ring disk analysis to probe for O_2 reduction intermediates resulting from enzymatic turnover.[38, 39]

The extracted interfacial rate constant of $1 s^{-1}$ represents an average rate for all centers in electrical contact with the electrode surface, as our passive adsorption method results in an ensemble of immobilized proteins of non-uniform orientation. For electron tunneling from a conductive surface through a peptide to a redox cofactor, this rate implies a relatively large average distance between the type 1 site and the electrode surface.[21–26] Estimating a reorganization energy between 0.3 and 1.0 eV for the type 1 site, a range encompassing reorganization in most type 1 centers,[27,28] places the average value of the electronic coupling (H_{ab}) between the type 1 copper and the electrode surface between 0.0002 and 0.008 cm^{-1}, respectively. Such poor coupling explains the reason for slow electron transfer in this system, which falls far below the interfacial rate constant that has been measured for an oriented enzyme electrode.[29]

The very slow scan rates employed during anaerobic voltammetry made it possible for us to resolve the non-catalytic peaks due to reduction of the type 1 copper sites in *T. thermophilus* laccase. We note that among the

many studies conducted on MCOs functioning on ketjen black, and, more generally, substrates where enzymes are randomly oriented on high surface area materials, measurements of the interfacial ET rates are seldom reported. This recurring omission derives from the difficulty in determining the surface concentrations of electrochemically active enzymes adsorbed to electrode surfaces in these systems. This problem seems also to extend to other types of proteins passively adsorbed on electrode substrates, prompting rough quantification by non-electrochemical methods such as atomic-force microscopy, transmission electron microscopy, or using very generalized approximations derived from catalytic polarization curves.[16,30,31] Some groups have suggested that the number of active enzyme centers on these electrodes is too small to probe with standard voltammetric techniques.[16] Although likely a contributing factor to the difficulty of surface measurement, rough estimations in the literature for surface concentrations of these enzymes on surfaces (10^{12}-10^{13} centers cm^{-2}), coupled with the knowledge of the exchange current densities in these systems, allowed for our preliminary estimates of a k_{ET} between 0.1 and 10 s^{-1} .[16,30] These approximations suggested that performing voltammetry under scan rates traditionally used in protein electrochemistry (10 - 200 mV s^{-1}) may be too high to probe such slow electron transfer processes, prompting our work at much lower scan rates. We suggest that voltammetric sweeps at 10 μVs^{-1} are best suited for determining surface concentrations of electrochemically active species in a ketjen-MCO electrode assembly. We also note that while such slow sweep rates are unusual, they are not without precedent[14] and, in fact, agree with the general rule that sweep rates should be limited according to eq. 1-4:

$$C_{DL}dv/dt \leq j_F \qquad (1\text{-}4),$$

where C_{DL} is the dual-layer capacitance of a system of interest, the differential is the sweep rate, and j_F is the current density of the

faradaic process of interest.[15] Our anaerobic scans reveal peak currents in the nanoampere regime; assuming prototypical dual-layer capacitances of 50 - 100 μF cm^{-2}, this relation predicts sweep rates of 10 - 20 μVs^{-1} as a prerequisite for their resolution from the background noise resulting from capacitive charging.[15] We regard this final point as additional validation of the methodology presented here.

Electron transfer between the electrode and the type 1 active site is the rate-limiting step in laccase electrocatalysis. In catalysis requiring charge transfer between sequential redox centers, only electron acceptors within electrical contact of the electrode should exhibit any sensitivity to the surface potential. In MCOs the type 1 site is such an acceptor. This view is corroborated both by the observations in MCO literature that the type 2/3 centers in these enzymes are too insulated to interact with either electrodes or small molecule redox mediators in solution chemistry and the higher rates of intramolecular ET that have been measured in laccase homologues using spectroscopic methods.[32–35]

Conclusion

The laccase homologue from the bacterium *Thermus thermophilus* strain HB27 is capable of catalyzing dioxygen reduction to water in a heterogeneous system with high faradaic yield. The system has a number of drawbacks, namely the low potentials where electrocatalysis is maximal and also the relatively small peak currents. However, we emphasize that many of these shortcomings can be addressed, either through improvements to the enzyme itself or the techniques used to fabricate the electrode assemblies. In particular, many studies have demonstrated the tunability of the type 1 copper center in a variety of blue copper proteins, yielding higher potential variants; most notable in this field is the large body of work that has been done on *Pseudomonas aeruginosa* azurin and CueO from *E. coli*.[19,28,36,37] We are currently seeking to enhance the electronic coupling by establishing enzyme monolayers of homogenous orientation, with

the type 1 center held proximal to the electrode surface. Assuming catalyst coverages reported here, the results of this study suggest that achieving H_{ab} values between ~ 0.002 and 0.08 cm^{-1} would allow for realization of currents in the 60 mA cm^{-2} regime.

We report explicit quantification of the surface concentration of *active* laccase species on ketjen black using voltammetry, allowing for determination of the number of enzymes coupled to the electrode following adsorption to this high-surface area material. This, in turn, provided a rare opportunity to calculate the value of the heterogenous rate constant for electron transfer between the electrode surface and an MCO active site on ketjen black. The small value of k_{ET} reported here indicates that interfacial charge transfer is rate-limiting in these systems and that its optimization should be the primary focus of any future attempts to increase the current densities of biological cathodes.

Acknowledgements

We thank James McKone, Alec Durrell and Bryan Stubbert for helpful discussions regarding electrochemistry and Kyle Lancaster for discussions regarding biochemistry. This research was funded by GCEP (Stanford) and CSER (The Gordon and Betty Moore Foundation). Additional support was provided by a partial fellowship from the Institute for Collaborative Biotechnologies through grant W911NF-09-0001 from the U.S. Army Research Office, and the Department of Energy, Basic Energy Sciences (DE-FG03-01ER46175)(JRH PI).

References

(1) Soukharev, V.; Mano, N.; Heller, A. *J. Am. Chem. Soc.* **2004**, *126*, 8368–8369.

(2) Carver, C. T.; Matson, B. D.; Mayer, J. M. *J. Am. Chem. Soc.* **2012**, 134, 5444–5447.

(3) Roberts, S. A.; Weichsel, A.; Grass, G.; Thakali, K.; Hazzard, J. T.; Tollin, G.; Rensing, C.; Montfort, W. R. *Proc. Natl. Acad. Sci. U.S.A.* **2002**, *99*, 2766–2771.

(4) Komori, H.; Sugiyama, R.; Kataoka, K.; Higuchi, Y.; Sakurai, T. *Angewandte Chemie International Edition* **2012**, *51*, 1861–1864.

(5) Blanford, C. F.; Heath, R. S.; Armstrong, F. A. *Chem. Commun.* **2007**, 1710–1712.

(6) Miura, Y.; Tsujimura, S.; Kurose, S.; Kamitaka, Y.; Kataoka, K.; Sakurai, T.; Kano, K. *Fuel Cells* **2009**, *9*, 70–78.

(7) Miyazaki, K. *Extremophiles* **2005**, *9*, 415–425.

(8) Liu, X.; Gillespie, M.; Ozel, A. D.; Dikici, E.; Daunert, S.; Bachas, L. G. *Anal. Bioanal. Chem.* **2011**, *399*, 361–366.

(9) Tsujimura, S. *Electrochim. Acta* **2008**, *53*, 5716.

(10) Blanford, C. F.; Foster, C. E.; Heath, R. S.; Armstrong, F. A. *Faraday Discuss.* **2008**, *140*, 319–335.

(11) Kataoka, K.; Hirota, S.; Maeda, Y.; Kogi, H.; Shinohara, N.; Sekimoto, M.; Sakurai, T. *Biochemistry* **2011**, *50*, 558–565.

(12) Cracknell, J. A.; Vincent, K. A.; Armstrong, F. A. *Chem. Rev.* **2008**, *108*, 2439–2461.

(13) Gallaway, J.; Wheeldon, I.; Rincon, R.; Atanassov, P.; Banta, S.; Barton, S. C. *Biosens. Bioelectron.* **2008**, *23*, 1229–1235.

(14) Bard, A. J.; Faulkner, L. R. *Electrochemical Methods: Fundamentals and Applications*; Wiley, 2001.

(15) Bockris, J. O.; Reddy, A. K. N.; Gamboa-Aldeco, M. *Modern Electrochemistry*; Springer, 2000.

(16) Thorum, M. S.; Anderson, C. A.; Hatch, J. J.; Campbell, A. S.; Marshall, N. M.; Zimmerman, S. C.; Lu, Y.; Gewirth, A. A. *J. Phys. Chem. Lett.* **2010**, *1*, 2251–2254.

(17) Mano, N.; Fernandez, J. L.; Kim, Y.; Shin, W.; Bard, A. J.; Heller, A. *J. Am. Chem. Soc.* **2003**, *125*, 15290–15291.

(18) Solomon, E. I.; Sundaram, U. M.; Machonkin, T. E. *Chem. Rev.* **1996**, *96*, 2563–2606.

(19) Lancaster, K. M.; George, S. D.; Yokoyama, K.; Richards, J. H.; Gray, H. B. *Nature Chem.* **2009**, *1*, 711–715.

(20) Thomas, S. C.; Ren, X.; Gottesfeld 2, S.; Zelenay, P. *Electrochim. Acta* **2002**, *47*, 3741–3748.

(21) Gray, H. B.; Winkler, J. R. *Chem. Phys. Lett.* **2009**, *483*, 1–9.

(22) Gray, H. B.; Winkler, J. R. *Proc. Natl. Acad. Sci. USA* **2005**, *102*, 3534–3539.

(23) Gray, H. B.; Winkler, J. R. *Quart. Rev. Biophys.* **2003**, *36*, 341–372.

(24) Gray, H. B.; Winkler, J. R. *Biochim. Biophys. Acta - Bioenergetics* **2010**, *1797*, 1563–1572.

(25) Edwards, P. P.; Gray, H. B.; Lodge, M. T. J.; Williams, R. J. P. *Angew. Chem. Int. Ed. Engl.* **2008**, *47*, 6758–6765.

(26) Onuchic, J. N.; Beratan, D. N.; Winkler, J. R.; Gray, H. B. *Annu. Rev. Biophys. Biomol. Struct.* **1992**, *21*, 349–377.

(27) Lancaster, K. M.; Farver, O.; Wherland, S.; Crane, E. J.; Richards, J. H.; Pecht, I.; Gray, H. B. *J. Am. Chem. Soc.* **2011**, *133*, 4865–4873.

(28) Hong, G.; Ivnitski, D. M.; Johnson, G. R.; Atanassov, P.; Pachter, R. *J. Am. Chem. Soc.* **2011**, *133*, 4802–4809.

(29) Udit, A. K.; Hill, M. G.; Bittner, V. G.; Arnold, F. H.; Gray, H. B. *J. Am. Chem. Soc.* **2004**, *126*, 10218–10219.

(30) Tamaki, T.; Hiraide, A.; Asmat, F. B.; Ohashi, H.; Ito, T.; Yamaguchi, T. *Ind. Eng. Chem. Res.* **2010**, *49*, 6394–6398.

(31) Kato, M.; Cardona, T.; Rutherford, A. W.; Reisner, E. *J. Am. Chem.*

Soc. **2012,** *134* (20), 8332-8335

(32) Farver, O.; Pecht, I. *Proc*. *Natl*. *Acad*. *Sci*. **1992**, *89*, 8283–8287.

(33) Farver, O.; Wherland, S.; Koroleva, O.; Loginov, D. S.; Pecht, I. *FEBS J*. **2011**, *278*, 3463–3471.

(34) Farver, O.; Wherland, S.; Pecht, I. *J*. *Biol*. *Chem*. **1994**, *269*, 22933–22936.

(35) Simaan, A. J.; Mekmouche, Y.; Herrero, C.; Moreno, P.; Aukauloo, A.; Delaire, J. A.; Réglier, M.; Tron, T. *Chemistry - A European Journal* **2011**, *17*, 11743–11746.

(36) Sakurai, T.; Kataoka, K. *Cell*. *Mol*. *Life Sci*. **2007**, *64*, 2642–2656.

(37) Sheng, Y.; Wang, W.; Chen, P. *J*. *Mol*. *Struct*. **2011**, *995*, 142–147.

(38) Tonda-Mikiela, P.; Habrioux, A.; Boland, S.; Servat, K.; Tingry, S.; Kavanagh, P.; Napporn, T. W.; Leech, D.; Kokoh, K. B. *Electrocatalysis* **2011**, *2*, 268–272.

(39) Scodeller, P.; Carballo, R.; Szamocki, R.; Levin, L.; Forchiassin, F.; Calvo, E. J. *J*. *Am*. *Chem*. *Soc*. **2010**, *132*, 11132–11140.

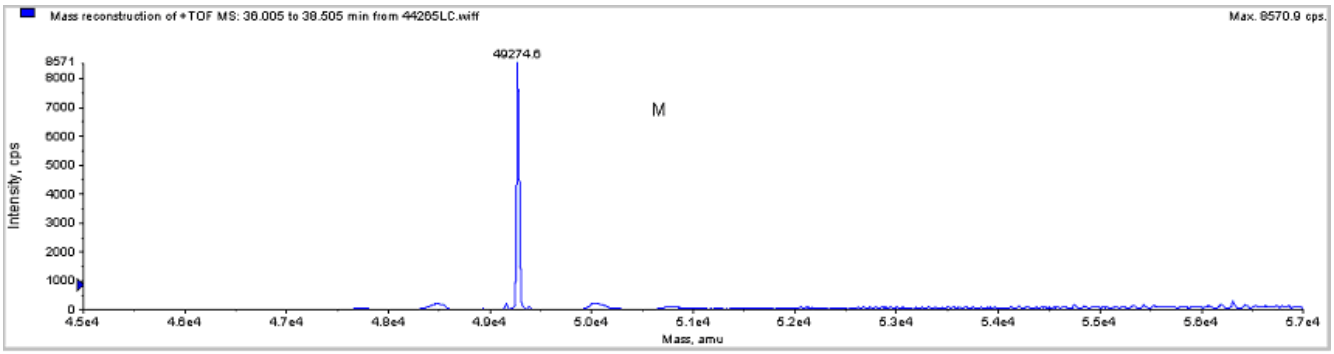

S.1

The reconstructed mass spectrum of *Thermus thermophilus* laccase. The observed mass represents a mature form of the enzyme, residues 19-462. Expected mass: 49267.2 da

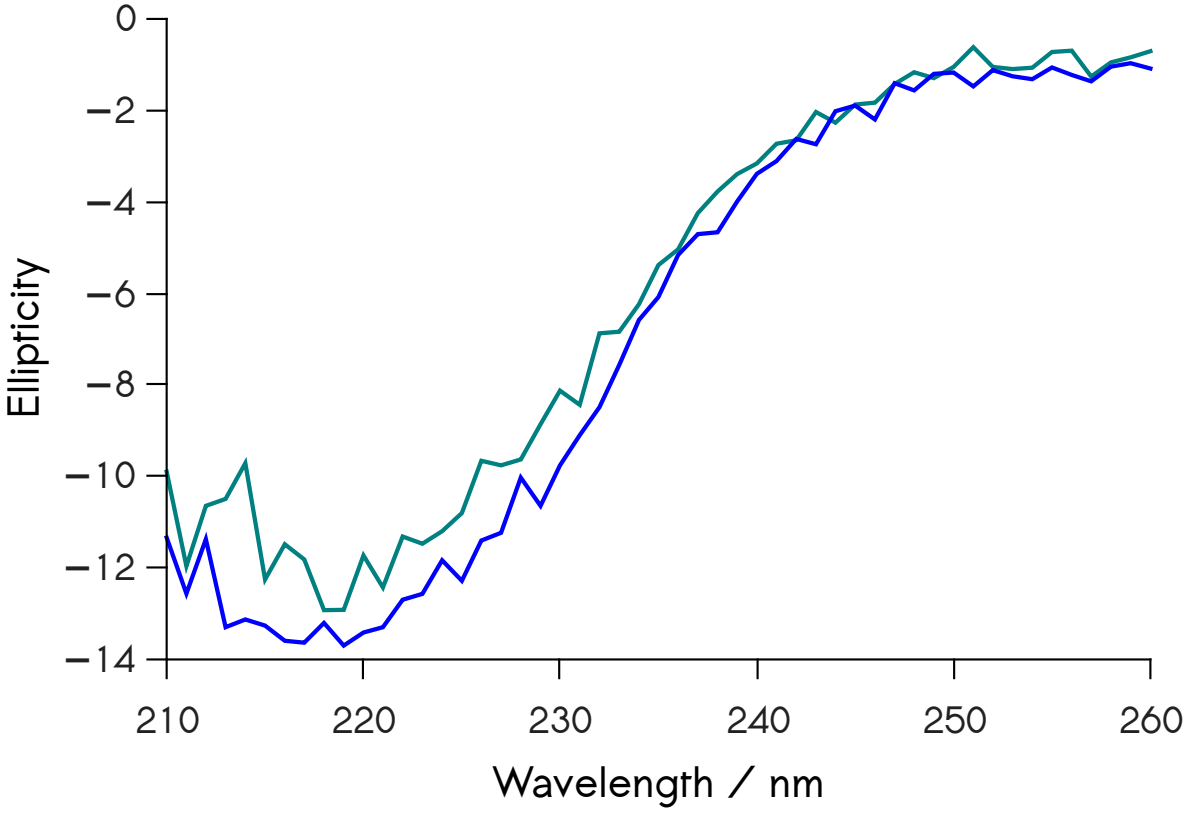

S.2

CD scans of laccase taken before (blue) and after (green) titrations between 10 and 95 °C reveal that the enzyme retains most of its secondary structure even after incubation at high temperatures.

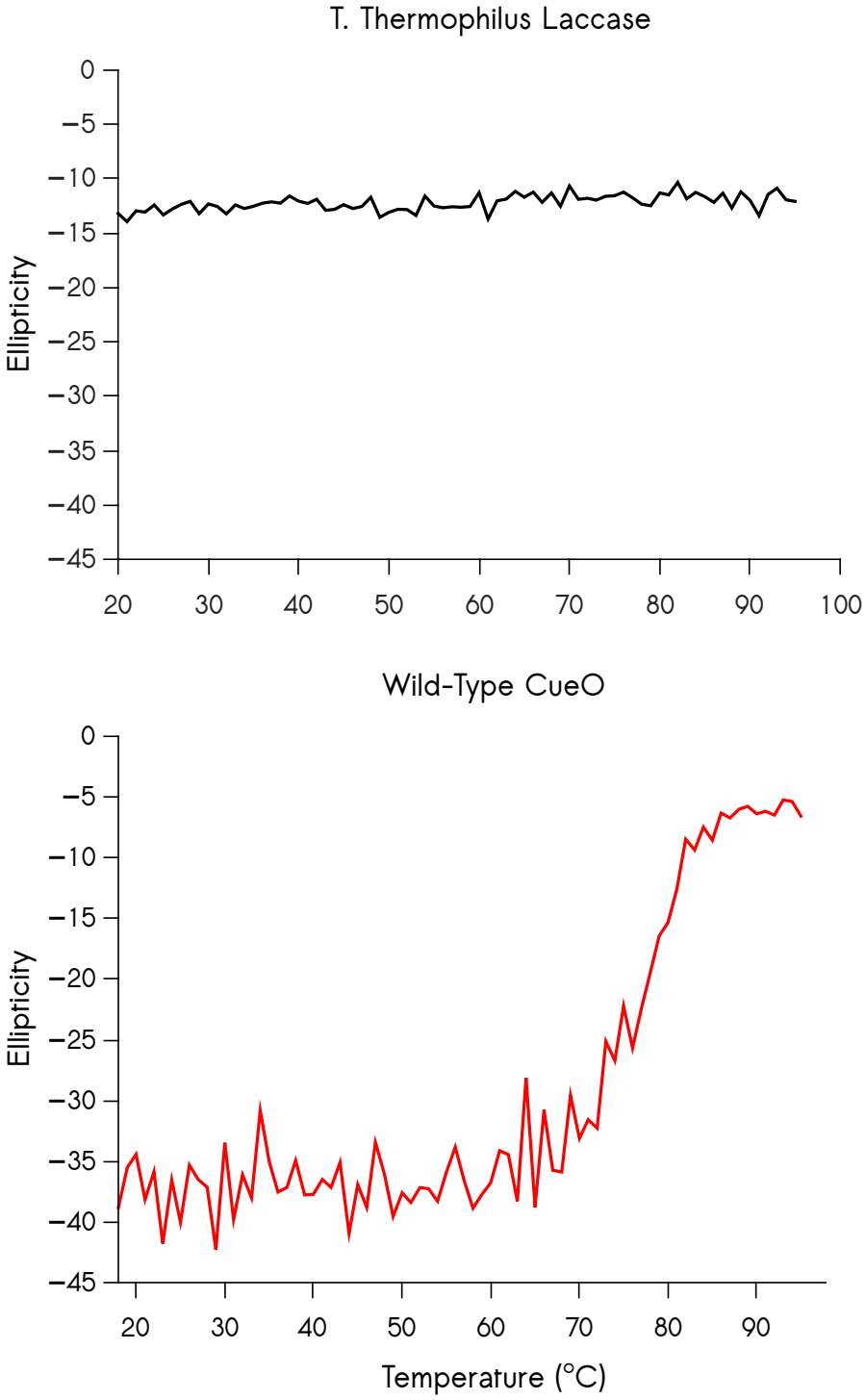

S.3

Temperature dependence of ellipticity at 220 nm. *Thermus thermophilus* laccase (black plot) shows no denaturation transition between 18 and 95 C. The denaturation profile for wild-type CueO (red plot) is shown for reference.

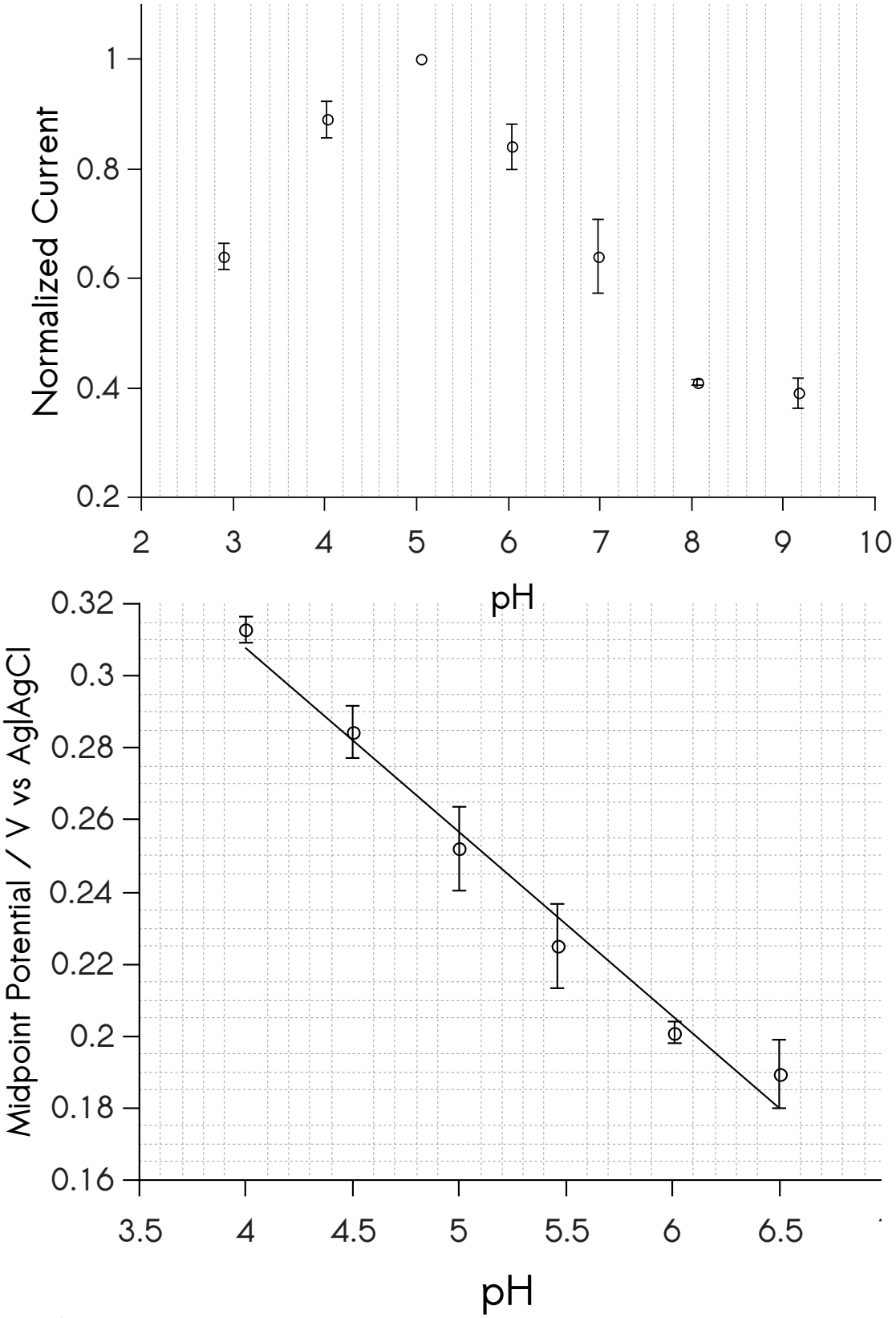

S.4

Top: Cathodic current as a function of pH. Bottom: The pH-dependent shifts of the catalytic wave at approximately half-maximum current ($E^{\circ}_{1/2}$). The regime examined represents the linear region of the enzyme's pH dependence and exhibits a slope of 57 mV decade^{-1}. Linear fit: y=-0.0568x+0.535; R^2=0.995

II. Modeling Dioxygen Reduction at Multicopper Oxidase Cathodes

Peter Agbo[1], James R. Heath[1], Harry B. Gray[1]*

[1] California Institute of Technology, Pasadena California

*Corresponding Author

Reproduced with permission from the

Journal of the American Chemical Society (DOI: 10.1021/ja5077519) 2014.

American Chemical Society

(Adapted)

Abstract

We report a general kinetics model for catalytic dioxygen reduction on multicopper oxidase (MCO) cathodes. Our rate equation combines Butler-Volmer (BV) electrode kinetics and the Michaelis-Menten (MM) formalism for enzymatic catalysis, with the BV model accounting for interfacial electron transfer (ET) between the electrode surface and the MCO type 1 copper site. Extending the principles of MM kinetics to this system produced an analytical expression incorporating the effects of subsequent intramolecular ET and dioxygen binding to the trinuclear copper cluster into the cumulative model. We employed experimental electrochemical data on *Thermus thermophilus* laccase as benchmarks to validate our model, which we suggest will aid in the design of more efficient MCO cathodes. In addition, we demonstrate the model's utility in determining estimates for both the electronic coupling and average distance between the laccase type-1 active site and the cathode substrate.

Introduction

Multicopper oxidases (MCOs) have shown great promise as cathode catalysts in bioinorganic fuel cells.[1–7] It is known that dioxygen reduction in these enzymes proceeds through initial electron transfer to all metal ions in the resting enzyme, resulting in an all-cuprous (reduced) state (Figure 2-1, A → B). In the reaction mechanism, diffusion of O_2 into the reduced enzyme, followed by two-electron reduction of the adduct, results in formation of a peroxy intermediate (Figure 2-1, B → C). Reduction of this adduct by two more electrons affords the "native intermediate" (Figure 2-1, C → D), which is converted back to the all-cuprous state to close the catalytic cycle. Return to the resting enzyme has been found not to be relevant to the catalytic cycle under steady-state conditions (Figure 2-1, D → A).[8–12]

In the MCO reaction cycle, outer-sphere oxidation of a donor species by the type 1 site is the rate-limiting step.[8,13] In systems where these proteins have a soluble reductant replaced with a cathodic surface, kinetics are dictated by interfacial charge transfer at lower overpotentials and by O_2 availability at higher driving forces.[1,5,14–20] Despite an extensive body of work on MCO chemistry delineating both the electrochemical behavior of various laccase isoforms and the overall kinetics scheme common to this enzyme family, a rigorous rate law accounting for the electrokinetics of MCOs when functioning as heterogeneous catalysts has yet to be reported. Kamitaka employed a generalized rate equation to fit bilirubin oxidase electrode kinetics, expressed simply as $r = k_{cat} / (1 + k_{cat} / k_f + k_b / k_f)$, where k_{cat} is the limiting rate constant, k_f is the forward interfacial ET rate constant, and k_b is the reverse interfacial ET rate constant.[18] However, this description, while capable of generating voltammetric curves similar to experimental ones, is insufficient because it omits all other rate constants inherent to the MCO reaction scheme from the rate equation.

We have developed a complete model of MCO electrode kinetics that sheds light on enzyme behavior when operating as a catalytic cathode. The generally accepted catalytic scheme of MCOs includes four intermediate

states, with the possibility of eight rate constants being used to express a corresponding rate law; the general equation used by Kamitaka includes only three.

In our model, interfacial charge transfer is expressed using a Butler-Volmer (BV) approach, where the current is scaled by an exponential dependence on overpotential.[21,22] We have further generalized the model by expressing the BV-dependent terms in our rate equation as a function of semi-classical ET theory parameters. We have tested our expression describing MCO cathode kinetics using experimental data from extensive investigations of the electrochemistry of *Thermus thermophilus* laccase.

Experimental Methods

All modeling was done using the Python programming language with *Numpy*, *Matplotlib* and *Xlrd* libraries. Laccase purification and electrode assembly were performed as previously described.[23] Thermal titrations employed electrode rotation at 4000 rpm in pH 5.0 20 mM sodium acetate. Electrodes with geometric surface areas of 0.25 cm^2 were used. A scan rate of 10 mV s^{-1} between 600 and 200 mV vs Ag|AgCl using a BAS 100 potentiostat was chosen for measurements. Current at 250 mV vs Ag|AgCl was used for back-calculation of the rates for Eyring analysis that allowed estimation of the type 1 Cu reorganization energy. Overpotentials are referenced relative to the type 1 redox potential of laccase (~340 mV vs Ag|AgCl), determined via pH-adjusted values of redox titrations measurements for this protein (appendix).

Results

Starting with the kinetics scheme common to laccases (Figure 2-1), we write the overall rate law for dioxygen reduction by *Thermus thermophilus* laccase, where O_2 binding (k_2, k_2') is the limiting step:

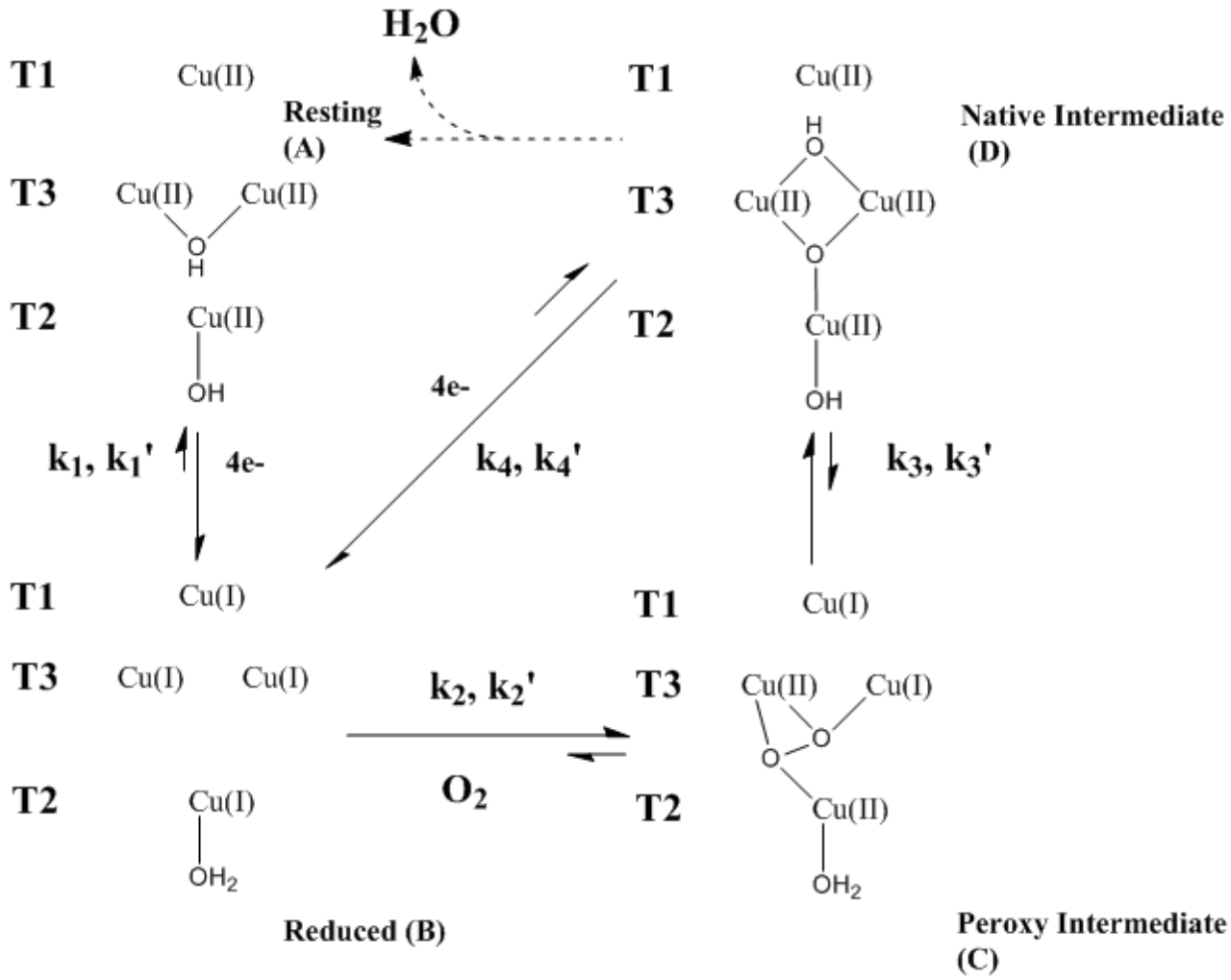

Figure 2-1

Catalytic cycling of dioxygen reduction to water by a multicopper oxidase. Forward rate constants are denoted k_n, reverse rate constants are of the form k_n'.

$$r = k_2[B][O_2] - k_2'[C] \qquad \text{(eq. 2-1).}$$

A system of differential equations expressing the changing concentrations of all four intermediates is then assembled, allowing us to express the unknown intermediate concentrations in terms of total enzyme surface concentration, N_T (S.I.). Explicit solution for the concentration of all intermediates gives a cathodic rate equation, which, when expressed as a cathodic current density (j), yields:

$$j(\eta) = -\frac{eFk_1 N_T\left(k_2[O_2] - k_2 f\right)}{N_A G\left(1 + \frac{k_1}{G}\left(1 + f + \frac{k_3 f + k_4'}{k_3' + k_4}\right)\right)} \qquad \text{(eq. 2-2),}$$

where

$$f = \frac{k_2[O_2]\left(k_3' + k_4\right)}{\left(k_3' + k_4\right)\left(k_2' + k_3\right) - k_3 k_3'} \qquad \text{(eq. 2-3)}$$

and

$$G = k_4' + k_1' + k_2[O_2] - k_2 f - \frac{k_4\left(k_3 f + k_4'\right)}{k_3' + k_4} \qquad \text{(eq. 2-4).}$$

Dependence of j on the overpotential, η, arises from the rates k_1, k_1', k_4 and k_4'. Terms k_1 and k_4 represent the forward rate constants for interfacial charge transfer, which can be expressed by substituting the exchange rate term of the BV model for the semiclassical (Marcus) equation when ΔG = 0 (S.I.):

$$k_1 = k_4 = \frac{4\pi^2}{h\sqrt{4\pi\lambda k_B T}} H_{AB}^2 \exp\left(\frac{-\lambda}{4k_B T}\right) \exp\left(\frac{-\alpha n F \eta}{RT}\right) \qquad \text{(eq. 2-5).}$$

An analogous description for the reverse interfacial rate constants (k_1' and k_4') then follows:

$$k_1' = k_4' = \frac{4\pi^2}{h\sqrt{4\pi\lambda k_B T}} H_{AB}^2 \exp\left(\frac{-\lambda}{4k_B T}\right)\exp\left(\frac{(1-\alpha)nF\eta}{RT}\right) \qquad \text{(eq. 2-6).}$$

In the high overpotential limit, the current density transforms to a function independent of η, reducing eq. (2-2) to:

$$j = -\frac{eFN_T k_2[O_2]\left(1-\frac{k_2'}{k_3}\right)}{N_A\left(1+\frac{k_2[O_2]}{k_3}\right)} \qquad \text{(eq. 2-7).}$$

Values used as modeling parameters were taken from studies of laccase on ketjen black electrodes: N_T = 1.56x10^{14} cm^{-2}, F is Faraday's constant (96485 C mol^{-1}), e is the total number of electrons transferred during a single catalytic turnover (4), n is the number of electrons transferred during a single interfacial charge transfer event (1), λ is the type 1 site reorganization energy, T is temperature (303 K), H_{AB} is the electronic coupling between the type 1 site and electrode surface, η is the overpotential and α is the symmetry factor (0.48).[23] Rate constants (k_n, k_n') are defined in Figure 2-1.

The reorganization energy for the type 1 center on these electrodes was estimated from the temperature dependence of current production in the low overpotential range, where kinetics are dominated by interfacial electron transfer to the type 1 copper site. From the values of current between 20 and 50 °C at η = -90 mV, we find $\Delta G^{\neq}$ =15 kJ mol^{-1} for reduction of type 1 Cu (S.2-3). The type 1 reorganization energy can then be estimated from eq. (2-8):[24]

$$\Delta G^{\neq} = (\Delta G + \lambda)^2 / 4\lambda \qquad \text{(eq. 2-8),}$$

where ΔG is calculated using the relation ΔG = -nFη. Here, analysis of thermal titration data yielded λ = 0.4 eV. Besides falling within the range

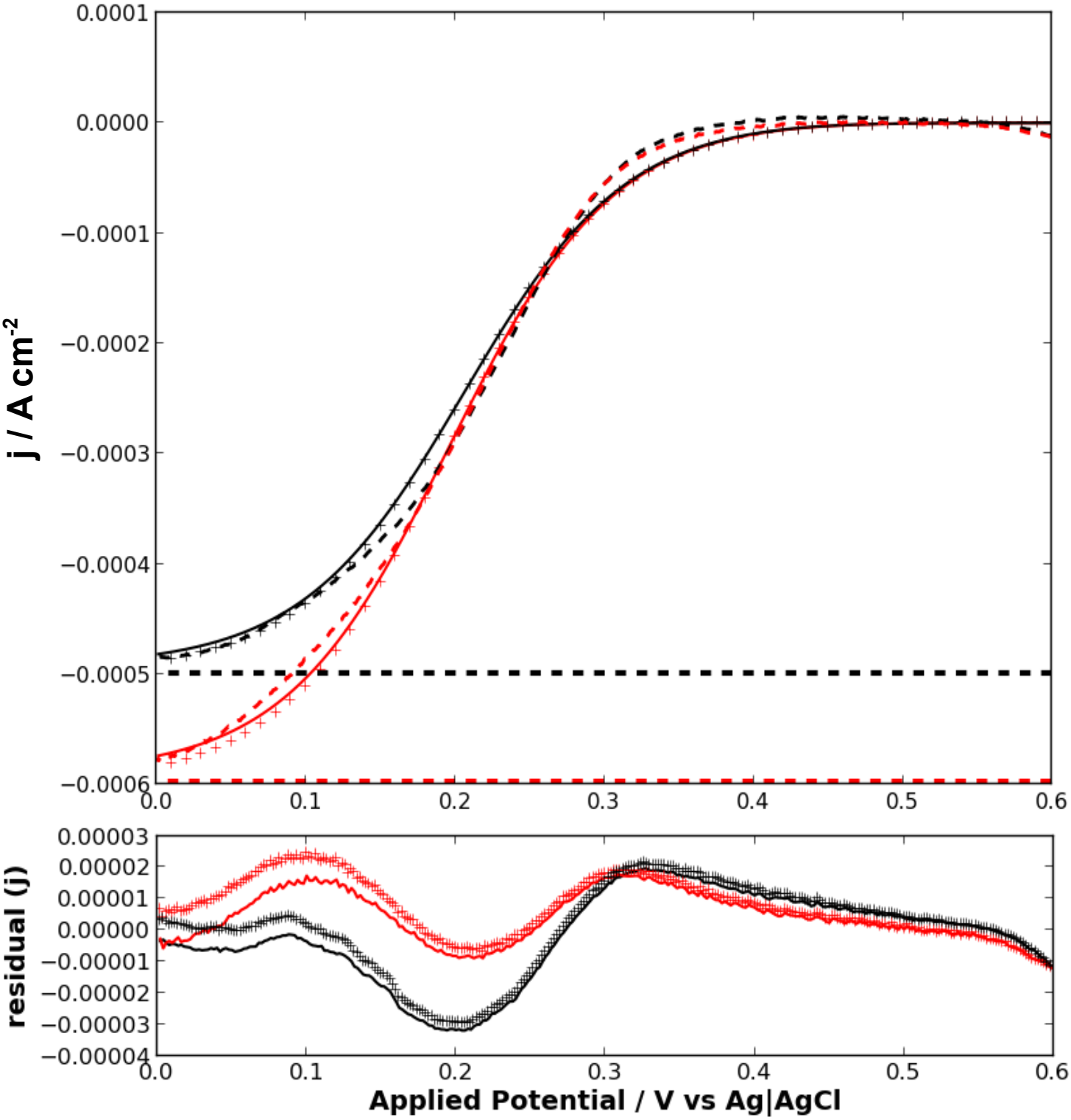

Figure 2-2a

J / V behavior for *Thermus thermophilus* strain HB27 laccase cathodes (black = 2000 rpm, red = 4000 rpm). Calculated voltammograms (solid lines) agree well with experimental data (--).[23] (+) markers denote the predictions of the rate law used by Kamitaka et al. The flat dotted lines represent the maximum current density for such electrodes as predicted by the high-overpotential limiting case of our MCO model (equation 7). The residual subplot indicates the difference between experimentally determined and modeled LSVs using our model (lines) and the rate law employed by Kamitaka (+).

of literature values for type 1 copper reorganization energies, this estimate is close to that reported for azurin hydrophobically adsorbed to Au-alkane thiol electrodes (0.33 eV).[25] These lower values for type 1 reorganization should be expected for physisorbed blue-copper systems, as hydrophobic binding of the protein will result in exclusion of water at the electrode surface (desolvation will reduce the outer-sphere contribution to the total reorganization energy of the type 1 copper site). With these parameters in hand, we calculate a coupling (H_{AB}) of 6.6×10^{-27} J (330 μcm^{-1}) per enzyme (eqs. 2-5 or 2-6).

The reported dependence of the catalytic current on dissolved O_2 concentration indicates that the step B ↔ C controls electrokinetics at limiting values of the current, as the conversion of the reduced enzyme to the peroxy intermediate is the rate-limiting step (the net rate of reaction is as described by eq. 2-1). We have determined the overall rate, *r*, to be 5 and 6 s^{-1} from experimental data acquired at 2000 and 4000 rpm, respectively. These values represent the peak current measured at 2000 or 4000 rpm normalized to each molecule of O_2 converted to water on a per-enzyme basis.[23] In our modeling procedures, we equated the quantity $k_2[O_2]$ to that of the net rate, an assignment that was supported by the observation that the k_2' term in the numerator of eq. 2-2 is weighted by a factor of *f*, resulting in a current density that scales almost entirely as a function of $k_2[O_2]$. As a result, the approximation $j \propto (k_2[O_2] - k_2' f) \approx k_2[O_2]$ holds under conditions relevant to catalysis. A value of 350 s^{-1} was assigned to k_3 based on previous measurements of formation of the native intermediate in laccases.[26] We set k_2' and k_3' to zero, as, to our knowledge, there exist no reports for the back-conversion of the peroxy intermediate to form the reduced enzyme, nor the native intermediate to the peroxy intermediate.

Using these values as inputs to the model gave a calculated LSV that agreed well with experimental data, accounting for properties of the electrochemical waves in both the low-overpotential (BV) and high-overpotential (O_2 diffusion-controlled) limits (Figure 2-2a). Overpotentials are referenced relative to the type 1 redox potential of

laccase (~340 mV vs Ag|AgCl). Allowing for a small variance in the calculated H_{AB} value (H_{AB} = 3.7x10^{-27} J, 190 μcm^{-1}), our model reproduced experimental data with minimized residuals. The switching point between the two catalytic regimes was evidenced by the change in concavity of the voltammogram between 0 and -250 mV overpotential. The point at which

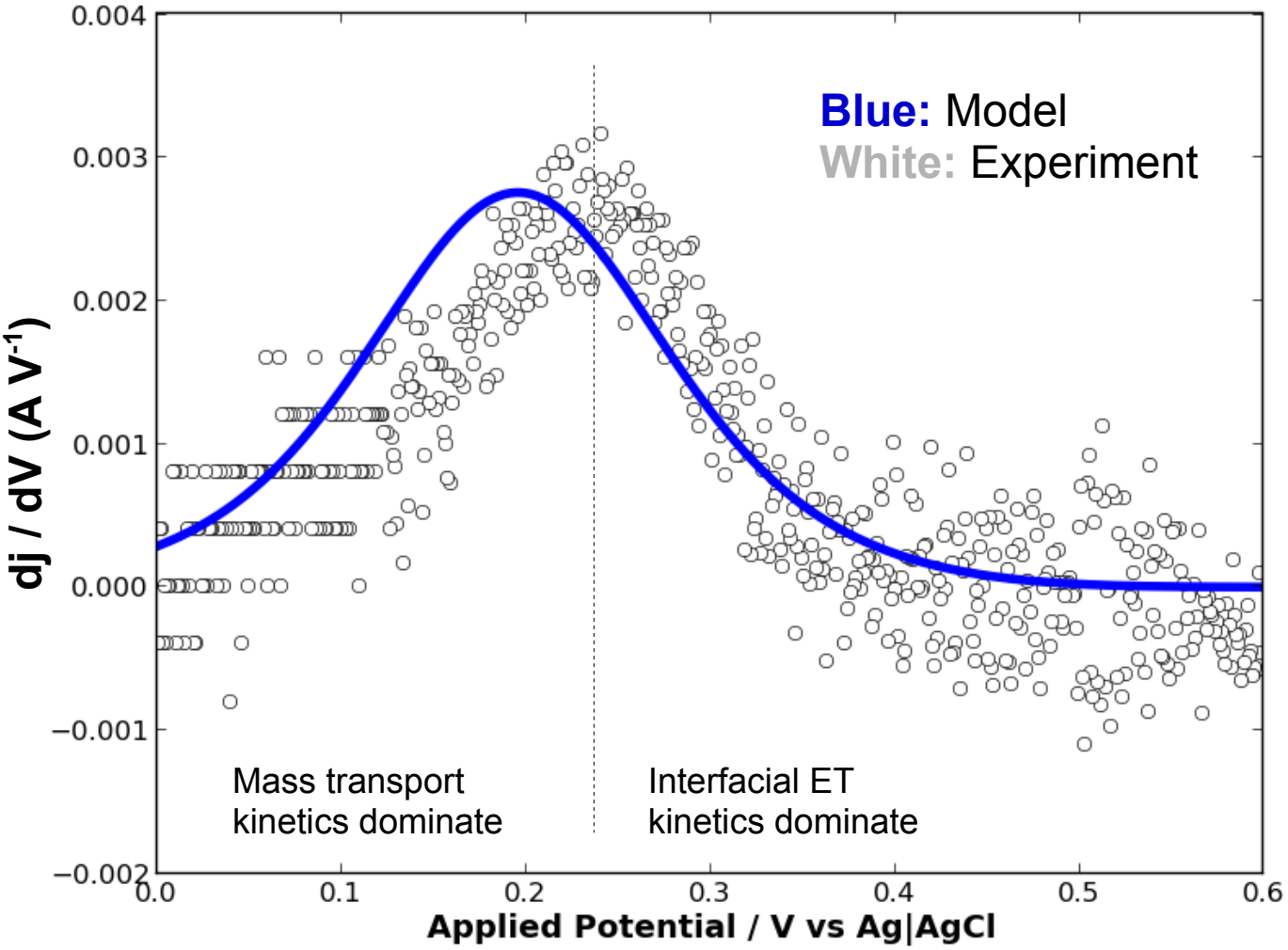

Figure 2-2b

Numerical differentiation of eq. (2) yields a modeled differential voltammogram (blue line) that agrees well with experimental derivative LSV data (white dots). Conditions of electrode rotation at 2000 rpm ($k_2[O_2]$= 5 s^{-1}) shown here. The derivative peaks highlight the region where current output is primarily controlled by interfacial kinetics (> 230 mV vs. Ag|AgCl) and mass transport of O_2 (< 230 mV).

current goes from being controlled primarily by interfacial ET vs. O_2 diffusion was therefore most apparent in the CV's derivative plot (Figure 2-2b). In this study, the quantity dj / dV took on a maximum value at about 110 mV overpotential, indicating catalysis was primarily controlled by interfacial kinetics below (and O_2 diffusion above) this value.
Tafel plots generated using the model also gave promising results. The linear region of the modeled tafel trace extends for a much longer range of overpotentials than the linear region of the experimental data. However, the small overpotential region previously used for fitting tafel data had a slope (128 mV decade^{-1}) similar to that of the entire linear region of the modeled data (132 mV decade^{-1}), and the modeled exchange current (30.0 μA cm^{-2}) was close to the experimentally determined value (27.2 μA cm^{-2}).[23] The close agreement gave us confidence in the novel fitting methodology we employed previously, as it allowed for the identification of the proper region for conducting linear tafel analysis, despite the low-overpotential curvature that often obscures tafel fitting of data obtained from measurements on porous carbon MCO cathodes (Figure 2-3).[27]

Discussion

Interfacial charge transfer rates

It is generally accepted in the field of protein electrochemistry that enzymes adsorb randomly onto porous carbon substrates, adopting configurations that position the active site at variable distances from the electrode.[4,19,28,29] As a result, experimental measurements of interfacial electron transfer rates and electronic couplings represent values averaged over the broad range of surface orientations.

As we have determined the mean value of interfacial electronic coupling (H_{AB}) in laccase cathodes, we can estimate the average distance between the type 1 site and the electrode surface. Using the canonical driving-force optimized ($-\Delta G^0 = \lambda$) rate of 10^{13} s^{-1} for a donor-acceptor separation at closest contact (r_0),[30] we can express H_{AB}^0 as follows:

$$H_{AB}^{0}=\frac{1}{2\pi}10^{6.5}h^{0.5}\left(4\pi\lambda k_{B}T\right)^{0.25}$$ (eq. 2-9).

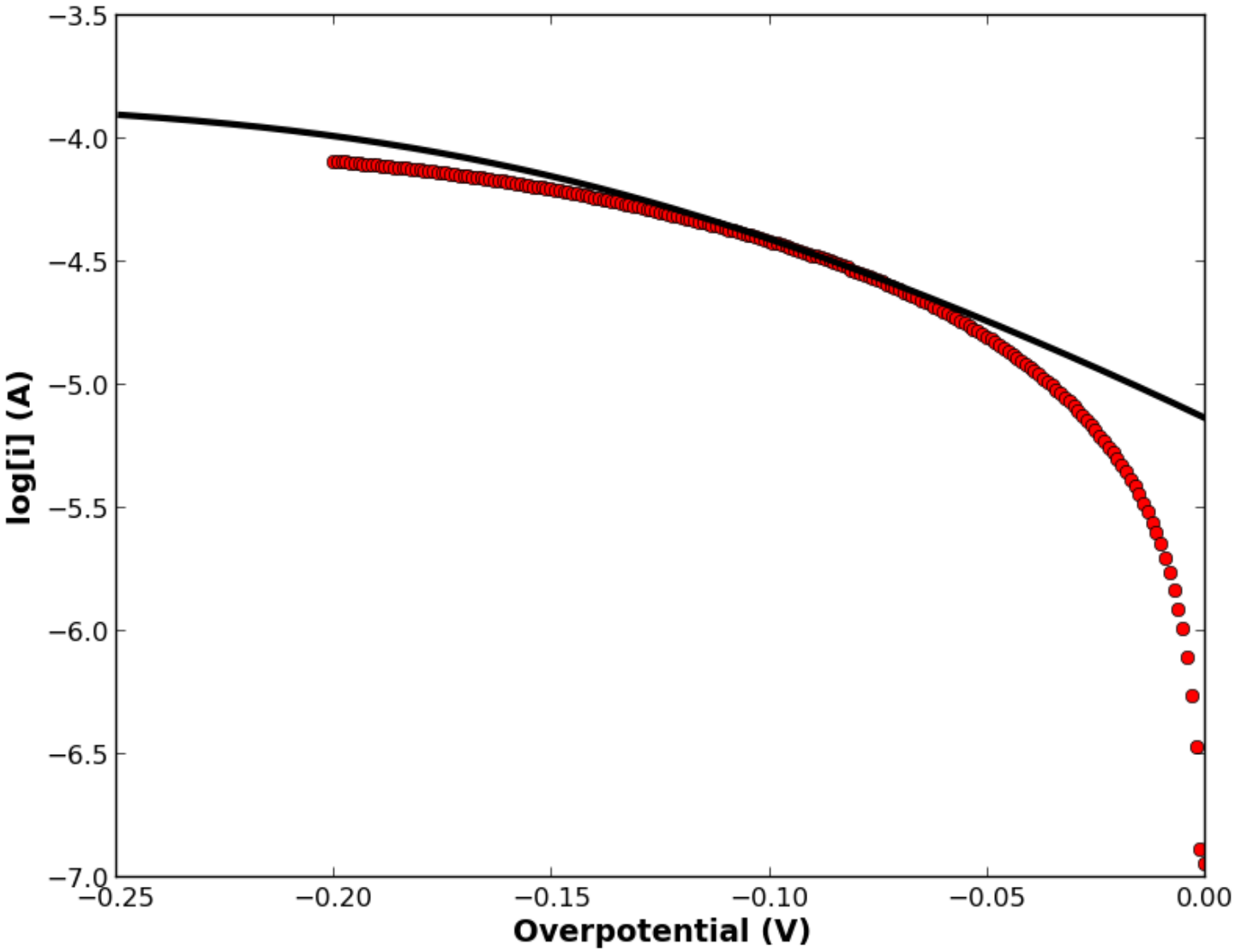

Figure 2-3

Tafel overlays of experimental[23] (red, circles) and modeled (black line) data. The 50-100 mV overpotential region previously used for fitting the data yielded a Tafel slope and exchange current that are similar to those obtained from the model.

The average cathode-type 1 distance is then obtained from eq. 2-10:

$$r = r_0 - \frac{2}{\beta} \ln \frac{H_{AB}(r)}{H_{AB}^0} \qquad \text{(eq. 2-10)},$$

where β is the distance-decay constant. For the system under study, we find a value of 3.0×10^{-21} J (150 cm^{-1}) for the coupling at r_0 (3 Å). The average cathode-type 1 site separation falls in the range of 24-28 Å, assuming established β values of 1.3 and 1.1 A^{-1} for electron tunneling through alpha-helices and beta-sheets.

Our finding of a 24-28 Å range for the average cathode-type 1 distance is also consistent with the work of Armstrong and coworkers, who demonstrated the utility of a uniform probability distribution function in accounting for rate dispersion in the interfacial charge transfer kinetics of NiFe hydrogenase proton reduction cathodes.[29] In this approach, we may approximate the average distance between a type 1 acceptor and the electrode surface by using the expectation value of r:

$$\langle r \rangle = \int r P(r)\, dr \qquad \text{(eq. 2-11)},$$

for a uniform distribution,

$$P(r) = \frac{1}{r_{max} - r_{min}} \qquad \text{(eq. 2-12)}.$$

It follows from eq. (2-11) that the expectation value for a uniform distribution is simply the average of two distances:

$$\langle r \rangle = \frac{1}{2}(r_{max} + r_{min}) \qquad \text{(eq. 2-13)}.$$

Inspection of the laccase crystal structure (PDB: 2XU9) suggests that the closest distance between the type 1 site and the protein surface is

approximately 10 Å, while the longest path is about 50 Å. From eq. (2-13), we then obtain an average value of ca. 30 Å for the cathode-type 1 distance for randomly oriented enzymes. This result lies in close agreement with our value for the mean distance found using the value for H_{AB} derived from our kinetics model. Furthermore, the observed correspondence between these two methods for estimating the average donor-acceptor distance supports the long-held view that enzymes hydrophobically adsorbed on porous carbon substrates exhibit random surface orientations.

Adjusting our previously measured value of the interfacial electron transfer rate (1.0 s^{-1} measured at $\Delta G^0 = 0$)[23] to its driving-force-optimized value of 16 s^{-1} enables direct comparison of the enzyme's electrochemical performance with known ET-distance relationships. We find that 16 s^{-1} electron tunneling over a distance of 25-30 Å places our system in a distance-decay region characteristic of beta-sheet proteins such as *Pseudomonas aeruginosa* azurin.[31] This result demonstrates a correlation between charge transport and protein secondary structure that conforms to known trends in macromolecular electron tunneling, despite the marked heterogeneity of the protein-electrode interface in these cathodes. As expected, these results also suggest an independence of tunneling behavior from the method used to determine ET rates, with our electrochemical data providing similar results to the photochemical methods that have been used to validate distance-decay relationships.[30,32–35]

Model limitations and features

We did not explicitly incorporate the complex problem of dioxygen flux through bulk solution in our model. As a result, the model is best suited for describing electrochemical behavior under conditions of non-limiting dioxygen diffusion. It should be noted that experimental data used for model validation were acquired at 2000 rpm or higher, angular velocities where the rotational dependence of the catalytic current had essentially ceased.

We assumed that direct, interfacial charge transfer to the trinuclear cluster did not occur. This model of MCO catalysis, where the type 1 site

acts as the initial point of reduction and relays charge to a trinuclear cluster that is heavily insulated from outer-sphere electron transfers by the peptide matrix, is generally accepted.[8,18,19,36–39]

While in the derivation we allowed for reversibility in the transformation of the native intermediate in order to keep the model as general as possible ($k_4' \neq 0$), convincing arguments can be made for assigning this reverse interfacial rate constant a value near zero. A non-zero value for k_4' suggests that anodic ET, in concert with the rebinding of water at the MCO active site, is non-negligible, allowing for some degree of water oxidation at the trinuclear cluster. While such activity has been reported for *Trametes hirsuta* laccase,[40] the observed water oxidation occurred at potentials far more positive than those used in our modeling. As there is no evidence that these enzymes are capable of any oxidative chemistry at the low potentials we employed here, it is reasonable to assign k_4' a rate of 0 s^{-1}. In any case, these electrodes can only be operated cathodically, bracketing the maximum value of the anodic current to that of the exchange current, an already small value that quickly decays to zero as a cathodic bias is applied. As a result, modeling with k_4' set to zero gives similar output to that with k_4' made equal to the anodic term of the BV equation, with differences only becoming apparent at higher values of electronic coupling (S.4).

As expected, enhanced electronic couplings between MCO type 1 sites and electrode surfaces are manifested by shallower tafel slopes and higher exchange current densities. However, the model suggests that for heterogeneous MCO cathodes fabricated with porous carbon substrates, increasing the electronic coupling beyond 10 H_{AB} (>3.7×10^{-26} J) will not result in appreciable reductions in the activation overpotential (S.3). Furthermore, the optimization of peak catalytic currents by improving O_2 delivery also will suffer from the problem of successive enhancements becoming more difficult as a result of an expanding $k_2[O_2]$ term in the denominator of the rate expression.

Conclusions

We have developed a quantitative model for the electrochemical behavior of multicopper oxidases when functioning as heterogenous catalysts. Notably, the model accounts for experimental data obtained from studies on *Thermus thermophilus* laccase cathodes. We demonstrated that the predictive power of our model allowed for determination of cathode-type 1 electronic couplings and distance dispersions in laccase-surface interactions. Our work represents an advancement in understanding biological charge transport in heterogeneous electrochemical systems that should aid in the design of more efficient MCO cathodes.

Acknowledgements

We thank Fan Liu, Joseph Varghese and Jay Winkler for helpful discussions and the Beckman Institute Molecular Materials Research Center for access to equipment. This research was funded by the NSF CCI Solar Fuels Program (CHE-1305124) and a Perkins Grant (JRH.PERKINS3-1-GRANT.PERKINS3).

Supplemental Information

Includes an annotated derivation of the rate law presented in this manuscript, additional figures demonstrating model predictions and thermal voltammetric data used for determination of type 1 copper reorganization energies.

References

(1) Miura, Y.; Tsujimura, S.; Kurose, S.; Kamitaka, Y.; Kataoka, K.; Sakurai, T.; Kano, K. *Fuel Cells* **2009**, *9*, 70–78.

(2) Liu, X.; Gillespie, M.; Ozel, A. D.; Dikici, E.; Daunert, S.; Bachas, L. G. *Anal. Bioanal. Chem.* **2011**, *399*, 361–366.

(3) Tsujimura, S. *Electrochimica Acta* **2008**, *53*, 5716.

(4) Cracknell, J. A.; Vincent, K. A.; Armstrong, F. A. *Chem. Rev.* **2008**, *108*, 2439–2461.

(5) Blanford, C. F.; Heath, R. S.; Armstrong, F. A. *Chem. Commun.* **2007**, 1710–1712.

(6) Lee, S.-K.; George, S. D.; Antholine, W. E.; Hedman, B.; Hodgson, K. O.; Solomon, E. I. *J. Am. Chem. Soc.* **2002**, *124*, 6180–6193.

(7) Lau, C.; Adkins, E. R.; Ramasamy, R. P.; Luckarift, H. R.; Johnson, G. R.; Atanassov, P. *Adv. Energy Mater.* **2012**, *2*, 162–168.

(8) Solomon, E. I.; Sundaram, U. M.; Machonkin, T. E. *Chem. Rev.* **1996**, *96*, 2563–2606.

(9) Sakurai, T.; Kataoka, K. *Chem. Rec.* **2007**, *7*, 220–229.

(10) Palmer, A. E.; Lee, S. K.; Solomon, E. I. *J. Am. Chem. Soc.* **2001**, *123*, 6591–6599.

(11) Sakurai, T.; Kataoka, K. *Cell. Mol. Life Sci. CMLS* **2007**, *64*, 2642–2656.

(12) Augustine, A. J.; Kjaergaard, C.; Qayyum, M.; Ziegler, L.; Kosman, D. J.; Hodgson, K. O.; Hedman, B.; Solomon, E. I. *J. Am. Chem. Soc.* **2010**, *132*, 6057–6067.

(13) Roberts, S. A.; Weichsel, A.; Grass, G.; Thakali, K.; Hazzard, J. T.; Tollin, G.; Rensing, C.; Montfort, W. R. *Proc. Natl. Acad. Sci. U. S. A.* **2002**, *99*, 2766–2771.

(14) Soukharev, V.; Mano, N.; Heller, A. *J Am Chem Soc* **2004**, *126*, 8368–8369.

(15) Miura, Y.; Tsujimura, S.; Kamitaka, Y.; Kurose, S.; Kataoka, K.; Sakurai, T.; Kano, K. *Chem. Lett.* **2007**, *36*, 132–133.

(16) Hong, G.; Ivnitski, D. M.; Johnson, G. R.; Atanassov, P.; Pachter, R. *J Am Chem Soc* **2011**, *133*, 4802–4809.

(17) Shleev, S.; Wang, Y.; Gorbacheva, M.; Christenson, A.; Haltrich, D.; Ludwig, R.; Ruzgas, T.; Gorton, L. *Electroanalysis* **2008**, *20*, 963–969.

(18) Kamitaka, Y.; Tsujimura, S.; Kataoka, K.; Sakurai, T.; Ikeda, T.; Kano, K. *J. Electroanal. Chem.* **2007**, *601*, 119–124.

(19) Blanford, C. F.; Foster, C. E.; Heath, R. S.; Armstrong, F. A. *Faraday Discuss.* **2008**, *140*, 319–335.

(20) Scodeller, P.; Carballo, R.; Szamocki, R.; Levin, L.; Forchiassin, F.; Calvo, E. J. *J. Am. Chem. Soc.* **2010**, *132*, 11132–11140.

(21) Bard, A. J.; Faulkner, L. R. *Electrochemical Methods: Fundamentals and Applications*; Wiley, 2001.

(22) Bockris, J. O.; Reddy, A. K. N.; Gamboa-Aldeco, M. *Modern Electrochemistry*; Springer, 2000.

(23) Agbo, P.; Heath, J. R.; Gray, H. B. *J. Phys. Chem. B* **2013**, *117*, 527–534.

(24) Marcus, R. A.; Sutin, N. *Biochim. Biophys. Acta BBA - Rev. Bioenerg.* **1985**, *811*, 265–322.

(25) Khoshtariya, D. E.; Dolidze, T. D.; Shushanyan, M.; Davis, K. L.; Waldeck, D. H.; Eldik, R. van. *Proc. Natl. Acad. Sci.* **2010**, *107*, 2757–2762.

(26) Solomon, E. I.; Augustine, A. J.; Yoon, J. *Dalton Trans.* **2008**, 3921–3932.

(27) Thorum, M. S.; Anderson, C. A.; Hatch, J. J.; Campbell, A. S.; Marshall, N. M.; Zimmerman, S. C.; Lu, Y.; Gewirth, A. A. *J Phys Chem Lett* **2010**, *1*, 2251–2254.

(28) Armstrong, F. A.; Hill, H. A. O.; Oliver, B. N.; Walton, N. J. *J Am Chem Soc* **1984**, *106*, 921–923.

(29) Léger, C.; Jones, A. K.; Albracht, S. P. J.; Armstrong, F. A. *J. Phys. Chem. B* **2002**, *106*, 13058–13063.

(30) Gray, H. B.; Winkler, J. R. *Proc. Natl. Acad. Sci. U. S. A.* **2005**, *102*, 3534–3539.

(31) Gray, H. B.; Winkler, J. R. *Q. Rev. Biophys.* **2003**, *36*, 341–372.

(32) Lancaster, K. M.; Farver, O.; Wherland, S.; Crane, E. J.; Richards, J. H.; Pecht, I.; Gray, H. B. *J Am Chem Soc* **2011**, *133*, 4865–4873.

(33) Crane, B. R.; Di Bilio, A. J.; Winkler, J. R.; Gray, H. B. *J. Am. Chem. Soc.* **2001**, *123*, 11623–11631.

(34) Shih, C.; Museth, A. K.; Abrahamsson, M.; Blanco-Rodriguez, A. M.; Bilio, A. J. D.; Sudhamsu, J.; Crane, B. R.; Ronayne, K. L.; Towrie, M.; Vlček, A.; Richards, J. H.; Winkler, J. R.; Gray, H. B. *Science* **2008**, *320*, 1760–1762.

(35) Gray, H. B.; Winkler, J. R. *Biochim. Biophys. Acta BBA - Bioenerg.* **2010**, *1797*, 1563–1572.

(36) Djoko, K. Y.; Chong, L. X.; Wedd, A. G.; Xiao, Z. *J. Am. Chem. Soc.* **2010**, *132*, 2005–2015.

(37) Kataoka, K.; Hirota, S.; Maeda, Y.; Kogi, H.; Shinohara, N.; Sekimoto, M.; Sakurai, T. *Biochemistry (Mosc.)* **2011**, *50*, 558–565.

(38) Santos, L. dos; Climent, V.; Blanford, C. F.; Armstrong, F. A. *Phys. Chem. Chem. Phys.* **2010**, *12*, 13962–13974.

(39) Roberts, S. A.; Wildner, G. F.; Grass, G.; Weichsel, A.; Ambrus, A.; Rensing, C.; Montfort, W. R. *J. Biol. Chem.* **2003**, *278*, 31958–31963.

(40) Pita, M.; Mate, D. M.; Gonzalez-Perez, D.; Shleev, S.; Fernandez, V. M.; Alcalde, M.; De Lacey, A. L. *J. Am. Chem. Soc.* **2014**.

Supplemental Information

Figure S.1

Eyring analysis of low-overpotential voltammetry (current measured at V = 250 mV vs Ag|AgCl reference) gave an activation energy of 15.0 kJ mol^{-1} and corresponding reorganization energy of 0.4 eV for redox cycling of the type 1 copper center.

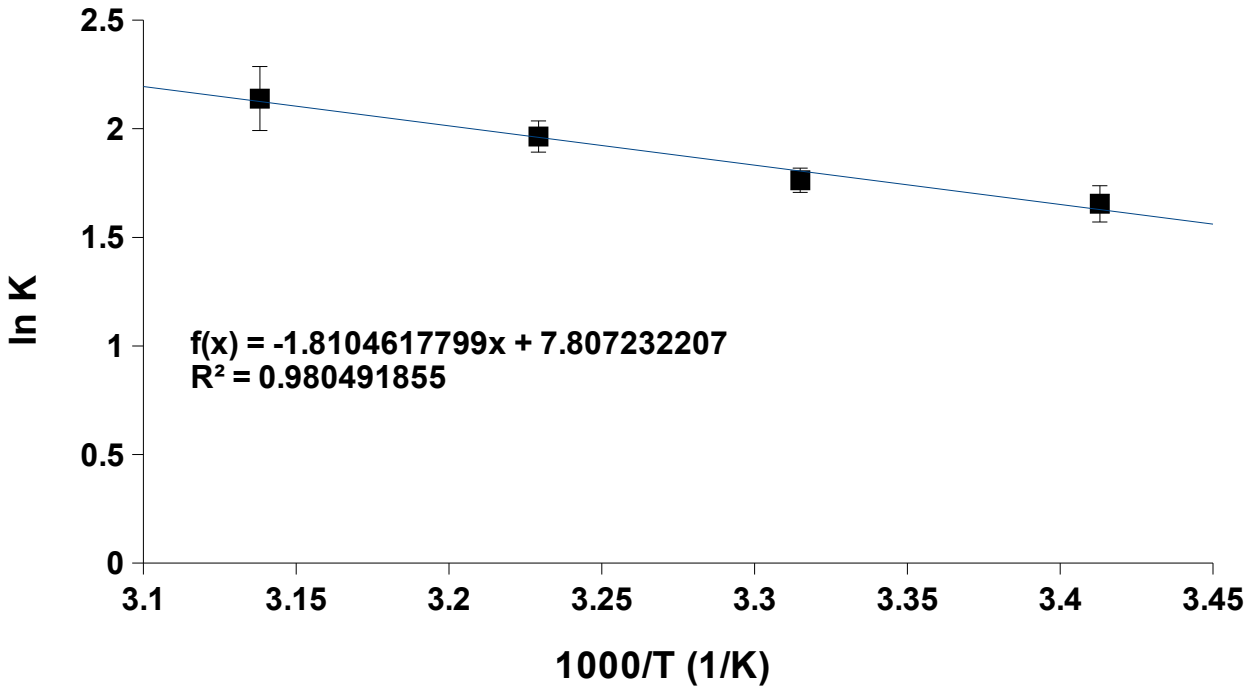

Figure S.2

Representative (low-overpotential) linear sweep voltammagrams of WT *Thermus thermophilus* laccase in pH 5.0 20 mM sodium acetate, 10 mV s^{-1} at 4000 rpm.

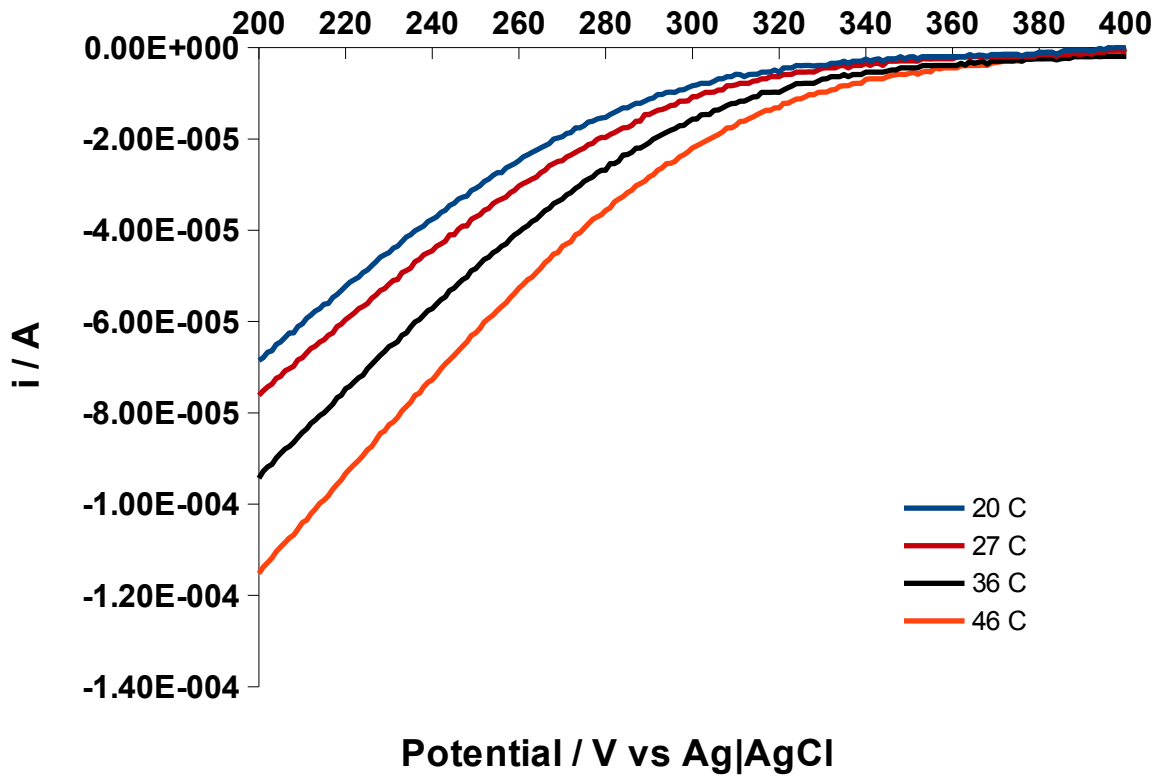

Figure S.3

Dotted Black: Experimental data. Blue: Modeled LSVs using parameters as defined in main paper. LSVs of increasing multiples of H_{AB} (1-10) are shown in blue, with coupling increasing in the direction indicated.

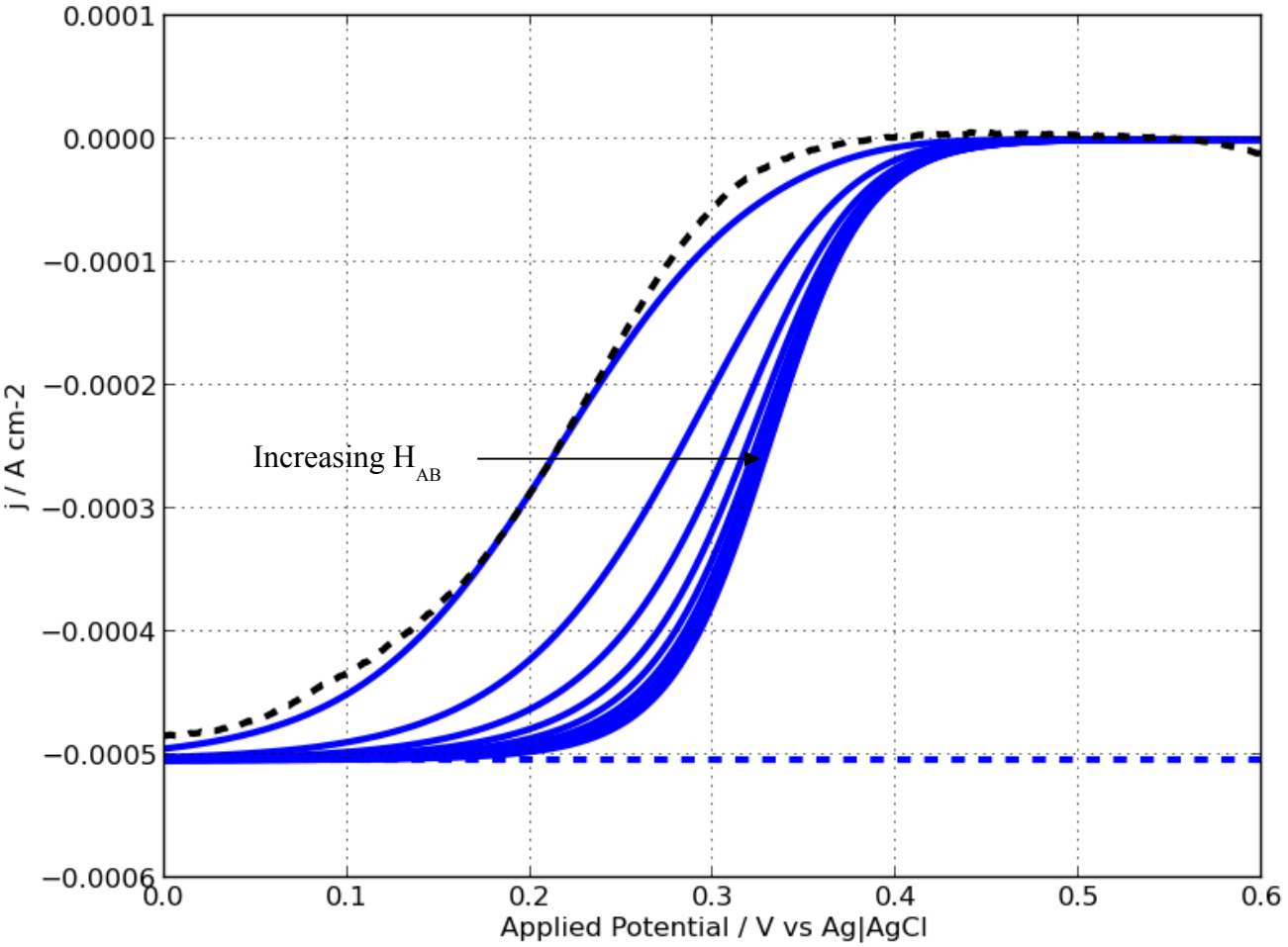

Figure S.4

Top: Modeling gave similar results when k_4' = 0 and when k_4' equaled the anodic term of the BV equation. Bottom: Differences between the two cases only became apparent at high coupling values ($10H_{AB}$ shown). Red curve: k_4' = 0; Blue curve: k_4' given by anodic BV term.

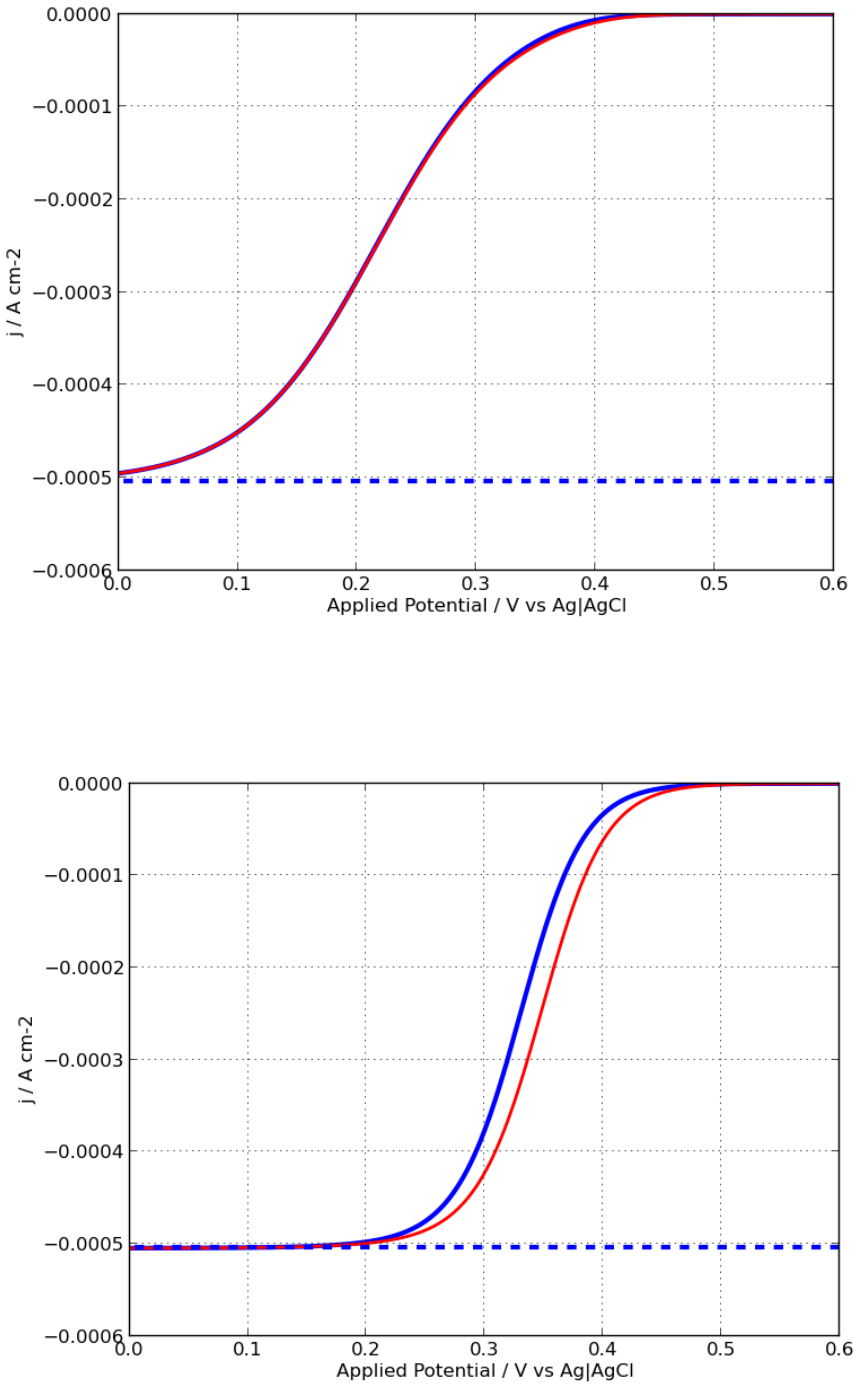

Figure S.5

Predictions of our MCO model vs. the rate law used by Kamitaka et al. Our model predicts that successive improvement of catalytic current densities by improving dioxygen delivery will become a challenge as the oxygen concentration increases, as a result of an increasing $k_2[O_2]$ term in the denominator of the limiting form of the model. The generic rate equation used by Kamitaka predicts no such effect, with catalytic current infinitely increasing as a linear function of $k_2[O_2]$. Conditions of $k_2[O_2]$ = 6-194 s^{-1}, H_{AB} = 3.7×10^{-27} J ($10H_{AB}$) shown.

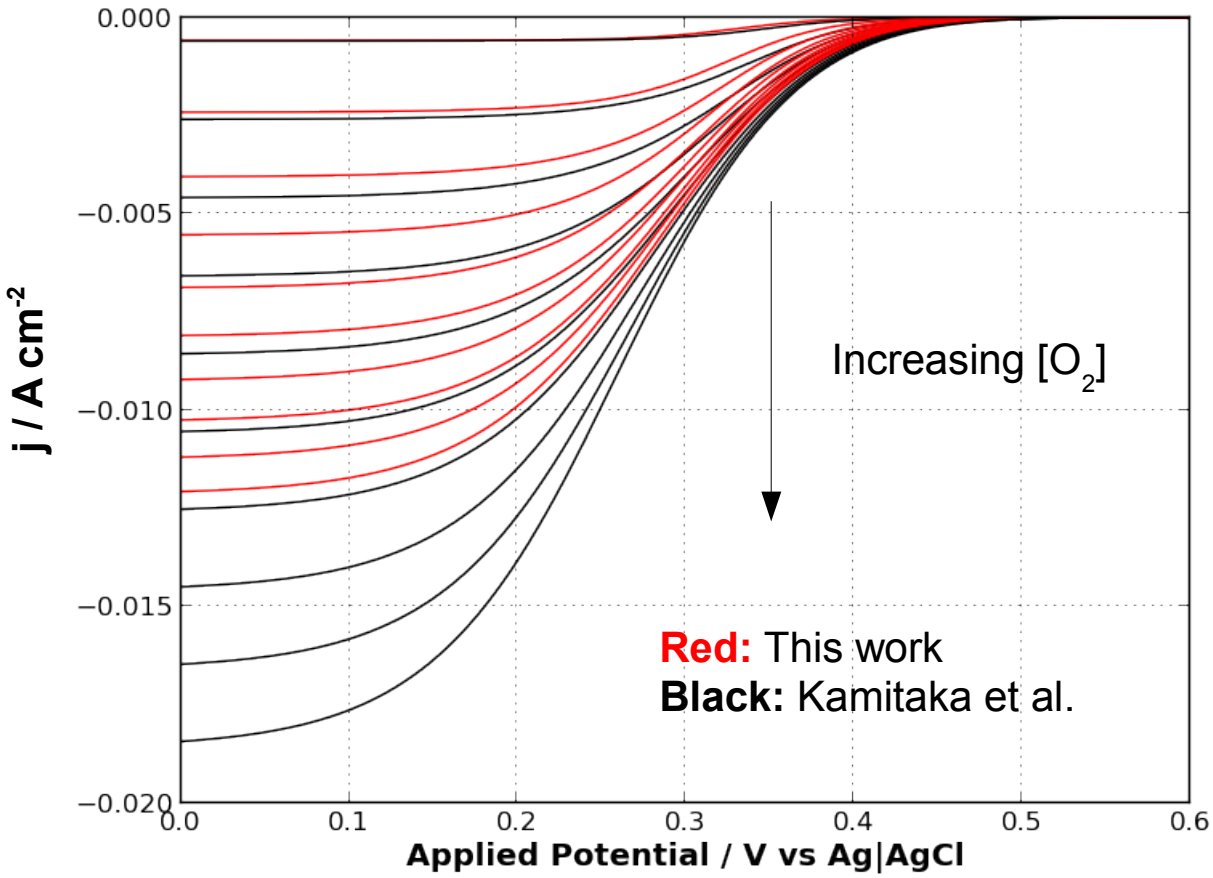

A Python Script for generating simulated LSVs, differential LSVs, and Tafel plots using MCO model.

```
#Global Constants
pi = 3.4159267
h = 6.626*10**-34 # Js
Na = 6.022*10**23 # mol-1
F = 96485.3415 #C mol-1
kb = 1.38*10**-23 #J K-1
Ncat = 4

# global intramolecular rate constants
k3 = 1000
k3p = 0
k2 = 6 #k2 for 4000 rpm data
k2p = 0.06 #k2' for 4000 rpm data
k22 = 5 #k2 for 2000 rpm data
k2p2 = 0.06 #k2' for 2000 rpm data

#Libraries
import matplotlib.pyplot as mt
import numpy as np
import xlrd

#calling data from a spreadsheet
data = xlrd.open_workbook('LSV.xls')
#choosing the correct sheet
sheet = data.sheet_by_index(4)
#parse a column, put data into a list format
column1 = sheet.col_values(0)
column2 = sheet.col_values(1)
column3 = sheet.col_values(2)

#used for calculating interfacial rate constants.
def ket(lamb, Hab, alpha, neta, n, T):
    ko = (4*(pi**2)/h)*(Hab**2)*(1/(4*pi*lamb*kb*T)**0.5)*np.exp(-lamb/(4*kb*T))
    kcathode = ko*(np.exp((-n*F*neta*alpha)/(Na*kb*T)))
    kanode = ko*np.exp(n*F*neta*(1-alpha)/(Na*kb*T))
    knet = kcathode - kanode
    return [kcathode, kanode, ko, knet]
```

```
#the MCO model
def Michaelis(lamb, Hab, alpha, neta, n, T, k2, k2p): # k4' =/= 0 (= k1p)
    i = ket(lamb, Hab, alpha, neta, n, T)
    k1 = i[0]
    k4 = k1
    k1p = i[1]
    k4p = k1p
    f = k2*(k3p + k4) / ((k3p + k4)*(k2p + k3) - k3p*k3)
    g = k4p + k1p + k2 - (k4*(k3*f + k4p) / (k3p + k4)) - k2p*f
    return (k2 - k2p*f) / ( g*(1 + k1/g*(1 + f + (k3*f + k4p)/(k3p + k4))) )

def Butler_Volmer(N, lamb, Hab, alpha, neta, n, T, forward, backrate):
    i = ket(lamb, Hab, alpha, neta, n, T)
    k1 = i[0]
    return -k1*Michaelis(lamb, Hab, alpha, neta, n, T, forward, backrate)*(Ncat*N*F/Na)
    # Michaelis() gives Michaelis-Menten contributions to total kinetics;
    # ket() gives interfacial electrode kinetics contribution.

def ev(energy): #converts from eV to joules
    return energy*(1.602e-19)

def derivative(xlist, ylist):
    z = 1
    dxlist = []
    dydxlist = []
    while z < len(xlist):
        dx = xlist[z] - xlist[z - 1]
        xbar = 0.5*(xlist[z] + xlist[z -1])
        dy = ylist[z] - ylist[z - 1]
        diff = dy / dx
        dxlist.append(xbar)
        dydxlist.append(diff)
        z += 1
    return dxlist, dydxlist
```

```
def hab(io, T, N, start, end):
#io = exchange current, lamb = reorganization energy, T = temp, N = # of catalysts
    Hab_list = []
    while start <= end:
        lamb = ev(start)
        num = h*Na*io*(4*pi*lamb*kb*T)**0.5
        den = (N*F*4*pi**2)*np.exp(-lamb/(4*kb*T))
        Hab_list.append((start, (num/den)**0.5))
        start += 0.01
    return Hab_list

#generates J/V curves using the model.
#a value of 0.35 V is used to adjust neta for referencing applied potential vs Ag|AgCl.
def LSV(N, lamb, Hab, alpha, n, T):
          neta = np.arange(0.25, -0.35, -0.001)
        #plot net current (modeling data)
          mt.plot(neta + 0.350, Butler_Volmer(N, lamb, Hab, alpha, neta, n, T, k2, k2p), 'b', linewidth = 3.0) # 4000
rpm
        mt.plot(neta + 0.350, Butler_Volmer(N, lamb, Hab, alpha, neta, n, T, k22, k2p2), 'b', linewidth = 3.0) #
2000 rpm
        #plot net current (experimental data)
        mt.plot(column1, column2, 'k--', linewidth = 3.0) # 2000 rpm
        mt.plot(column1, column3, 'k--', linewidth = 3.0) # 4000 rpm
        mt.plot(neta + .350, -k2*(Ncat*N*F/Na)*(1 - k2p/k3)/(1 + k2/k3) + neta*0, 'b--', linewidth = 5.0)
#theoretical limiting current @ 4000 rpm
        mt.plot(neta + .350, -k22*(Ncat*N*F/Na)*(1 - k2p2/k3)/(1 + k22/k3) + neta*0, 'b--', linewidth = 3.0)
#theoretical limiting current @ 2000 rpm
        mt.grid(False)
          mt.xlabel('Applied Potential / V vs Ag|AgCl ', fontsize=14, style='normal', fontweight='bold')
          mt.ylabel('j / A cm-$^2$', fontsize=14, style='normal', fontweight='bold')
          mt.show()
```

```
#show the effects of coupling for multiples of Hab (defined in the range parameter, a 1 x n array).
#k2f = k2, k2b = k2'
def coupling_dependence(N, lamb, Hab, alpha, n, T, k2f, k2b, range):
    neta = np.arange(0.25, -0.35, -0.001)
    z = range[0]
    while z <= range[1]:
        #plot net current (modeling data)
        mt.plot(neta + 0.350, Butler_Volmer(N, lamb, z*Hab, alpha, neta, n, T, k2f, k2b), 'b', linewidth = 1.5) #
4000 rpm
        z += 1
    mt.grid(False)
    mt.xlabel('Applied Potential / V vs Ag|AgCl ', fontsize=14, style='normal', fontweight='bold')
    mt.ylabel('j / A cm-$^2$', fontsize=14, style='normal', fontweight='bold')
    mt.show()

#calculates residues between modelled and experimental J/V data.
def LSV_residual(N, lamb, Hab, alpha, n, T):
    residualx4k = []
    residualy4k = []
    residualx2k = []
    residualy2k = []
    neta = 0.250
    counter = 0
    while neta >= -0.350:
        #4000 rpm residual
        model4k = Butler_Volmer(N, lamb, Hab, alpha, neta, n, T, k2, k2p)
        residualx4k.append(neta + 0.350)
        residualy4k.append(column3[counter] - model4k)
        #2000 rpm residual
        model2k = Butler_Volmer(N, lamb, Hab, alpha, neta, n, T, k22, k2p2)
        residualx2k.append(neta + 0.350)
        residualy2k.append(column2[counter] - model2k)
        neta -= .001
        counter += 1
    mt.plot(residualx2k, residualy2k, 'r-', linewidth = 1.5)
    mt.plot(residualx4k, residualy4k, 'b-', linewidth = 1.5)
    mt.grid(False)
    mt.xlabel('Applied Potential / V vs Ag|AgCl', fontsize=14, style='normal', fontweight='bold')
    mt.ylabel('residual (j)', fontsize=14, style='normal', fontweight='bold')
    mt.show()
```

```
#subprocedure for numerical differentiation of the model and experimental J/V data.
def di(N, lamb, Hab, alpha, n, T):
    x_list = []
    y_list = []
    neta3 = 0.25
    while neta3 >= -0.35:
        x_list.append(neta3 + .350)
        y_list.append(Butler_Volmer(N, lamb, Hab, alpha, neta3, n, T, k2, k2p)) #2000 rpm
        neta3 -= 0.001
    return [x_list, y_list]

#generates plot of a differential J/V curves.
def difigure(N, lamb, Hab, alpha, n, T):
    exp_listx = column1
    exp_listy = column2
    model_listx = di(N, lamb, Hab, alpha, n, T)[0]
    model_listy = di(N, lamb, Hab, alpha, n, T)[1]
    mt.plot( derivative(exp_listx, exp_listy)[0], derivative(exp_listx, exp_listy)[1], 'wo')
    mt.plot(derivative(model_listx, model_listy)[0], derivative(model_listx, model_listy)[1], 'b-', linewidth = 4.0)
    mt.ylabel('di / dv ( A V-$^1$)', fontsize=14, style='normal', fontweight='bold')
    mt.xlabel('Applied Potential / V vs Ag|AgCl', fontsize=14, style='normal', fontweight='bold')
    mt.grid(False)
    mt.show()

#Tafel simulation
def Tafel(N, lamb, Hab, alpha, n, T):
    #calling data from a spreadsheet
    data = xlrd.open_workbook('Tafel.xls')
    #choosing the correct sheet
    sheet = data.sheet_by_index(0)
    #parse a column, put data into a list format
    col1 = sheet.col_values(0)
    col2 = sheet.col_values(1)
    eta = np.arange(0.0, -0.25, -0.001)
    mt.plot(col1, col2, 'ro') # experimental tafel data
    mt.plot(eta, np.log10(abs(Butler_Volmer(N, lamb, Hab, alpha, eta, n, T, k2, k2p))), 'b-', linewidth = 3.0)
    mt.grid(False)
    mt.xlabel('Overpotential (V)', fontsize=14, style='normal', fontweight='bold')
    mt.ylabel('log[i] (A)', fontsize=14, style='normal', fontweight='bold')
    mt.show()
```

III. Perturbation of MCO Cu Sites Via Ligand Mutagenesis

Abstract

In this study, we present the results of efforts to increase the onset for catalytic dioxygen reduction of laccase cathodes. With the type 1 site in laccase serving as the initial electron acceptor of charge originating at the cathode surface, we first introduced inner and outer-sphere mutations to the type 1 site. Mutations M455L and M455F represented changes from the native type 1 methionine axial ligand to non-coordinating leucine and phenylalanine residues. Attempts to modify the type 1 outer-sphere are represented by the E352A mutation, which removes a glutamate residue involved in hydrogen bonding to the H393 type 1 Cu ligand. Inner-sphere mutation to laccase inhibits catalysis, while outer-sphere mutation slightly increases the catalytic onset potential, while reducing catalytic activity by about half. We ascribe the observed activity loss in M455F and M455L laccases to an over-increase of the type 1 potential relative to the type 2/type 3 trinuclear cluster (TNC) potential, which would make intramolecular ET from the type 1 center to the TNC thermodynamically disfavored. In response to these findings, we also studied mutations to the type 2/type 3 trinuclear copper cluster (TNC) to determine the possibility of introducing compensating high-potential mutations at the TNC in order to restore catalytic activity in laccases containing type 1 mutations.

Introduction

The architecture of the electron transfer system in multicopper oxidases (MCOs), consisting of a type 1 site serving as a terminal electron acceptor that relays charge equivalents to a trinuclear cluster where O_2 is reduced, makes any attempt to raise type 1 potentials in these proteins, while retaining catalytic activity, a complex problem (Figures 3-1,2)[1,2]. In most bioinorganic systems, such as single-heme cytochromes, where the metal site acts as both a terminal acceptor / donor and catalytic center, the effects of ligand mutation on a distal coordination sphere are not a concern. In response to the characterizations and modeling performed on laccase electrodes presented in earlier sections of this work, we now sought to enhance cathode performance by attempting to increase the onset potential for electrochemical dioxygen reduction. As electrochemical reduction of this enzyme proceeds through initial ET to the type 1 site, it is this copper center which determines the onset potential for electrocatalysis in heterogeneous laccase cathodes.[3–14] Consequently, any efforts to raise the observed onset potential for dioxygen reduction electrocatalysis requires tuning of the type 1 copper site. This site is characterized by an intense LMCT at 610 nm (ε ~ 5000 M^{-1} cm^{-1}), while transitions at the trinuclear cluster give rise to a broad shoulder featuring a maximum at 330 nm (ε ~ 4000 M^{-1} cm^{-1}).[1]

We have measured a type 1 (solution) potential of 227 ± 6.4 mV vs Ag|AgCl reference at pH 6.5 (427 mV vs. NHE; Figure 3-3) for laccase. Accounting for changes in pH, this differs only by about 25 mV from the value measured on ketjen black electrodes (~ 340 mV vs Ag|AgCl at pH 5.0). Deviations between solution and surface-bound redox potentials in metalloproteins are well documented in the literature,[15,16] and are presumably caused by distortion of the ligand coordination sphere upon surface adsorption of the protein. In the case of laccase, such surface adsorption must lead to a small net increase in bond lengths between the Cu atom and donor ligands in the type 1 active site. In either of these cases, the type 1 potential falls far below the potential for the reaction $O_2 + 4H^+$

$+4e^- \rightarrow 2H_2O$ (~940 mV vs. NHE at pH 5.0) catalyzed by the trinuclear copper cluster. From this, it becomes clear that there exists vast room for improving cathode performance by increasing the type 1 reduction potential.

A considerable body of work on site-directed mutagenesis of type 1 copper sites exists in bioinorganic literature, primarily as studies on *Pseudomonas aeruginosa* azurin.[17–20] This blue-copper protein is a distant relative of the MCO family, featuring a single copper ion resting in a 2His 1Met 1Cys coordination sphere, as with *Thermus thermophilus* laccase.[21] Studies on this protein have shown that the type 1 site potential in azurin can be raised by mutation of the weak methionine axial ligand to non-coordinating residues such as leucine, isoleucine and phenylalanine.[17,21] In addition, it has been found that some high-potential MCOs, particularly fungal laccases, contain no axial ligand or non-coordinating leucine or phenylalanine residues as the weak axial ligand.[1,22,23]

In this chapter, we present our attempts to engineer improved laccases for electrochemical dioxygen reduction by increasing the type 1 center redox potential. Mutations M455F and M455L are first explored, representing conversions of the type 1 methionine to non-coordinating phenylalanine (F) and leucine (L) residues, with the expectation that the introduction of non-binding amino acid side chains will reduce the net electron density at the type 1 copper ion, increasing its redox potential. We also explore the possibility of modifying outer-sphere interactions with the E352A mutant, which removes a glutamate (E) residue involved in hydrogen bonding to the H393 type 1 ligand of the native protein. In response to our findings with the M455F/L variants, we also constructed the following trinuclear copper cluster mutants: H135M, H398M, and H135M/H398M. Our initial motivation for making these mutants was to try raising the TNC redox potential in an attempt to restore activity in the M455F and M455L mutants, which as we show in our results have marginal catalytic activity. Insights into perturbations at the copper sites are gleaned from electrochemistry, absorption spectroscopy and electron paramagnetic resonance (EPR) spectroscopy. In addition, we outline a novel copper detection method for effectively counting the number of copper atoms per enzyme in order to support conclusions made from spectroscopic analyses.

In the case of the three TNC mutants made here, residues H135 and H398M were chosen for mutation because among the three possible T3 ligands at each Cu site, histidines at these positions showed the fewest number of polar contacts in the laccase crystal structure (either to active site waters or other residues) than the other T3 ligands. Furthermore, residues H135 and H398 are not part of the highly conserved HCH motif which occurs

Figure 3-1

A depiction of the arrangement of copper atoms (teal) in *Thermus thermophilus* laccase (PDB: 2XU9). Towards the surface of the protein is the lone type 1 copper ion, while the trinuclear cluster is embedded in the protein core. The μ2-hydroxide bridge of the type 3 copper ions can be seen in red (O) and white (H).

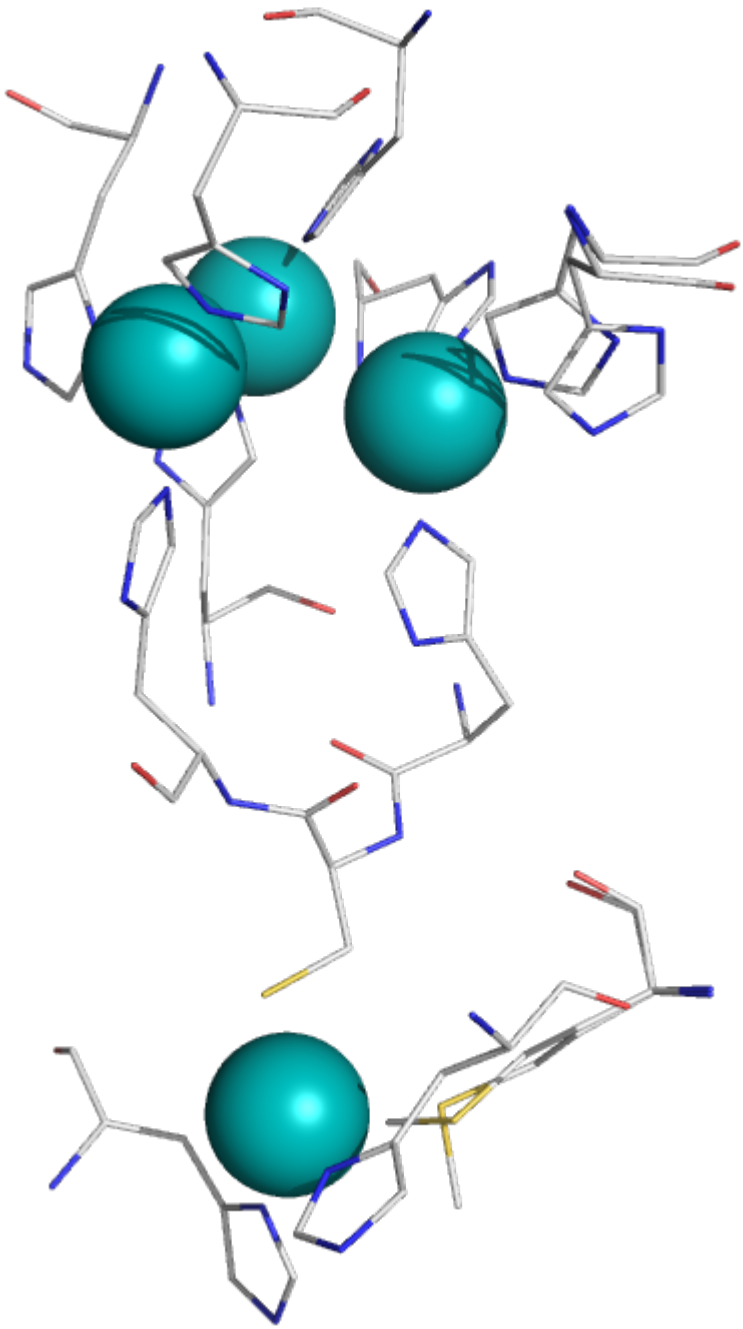

Figure 3-2

The primary ligand coordination spheres of copper ions in *Thermus thermophilus* laccase.

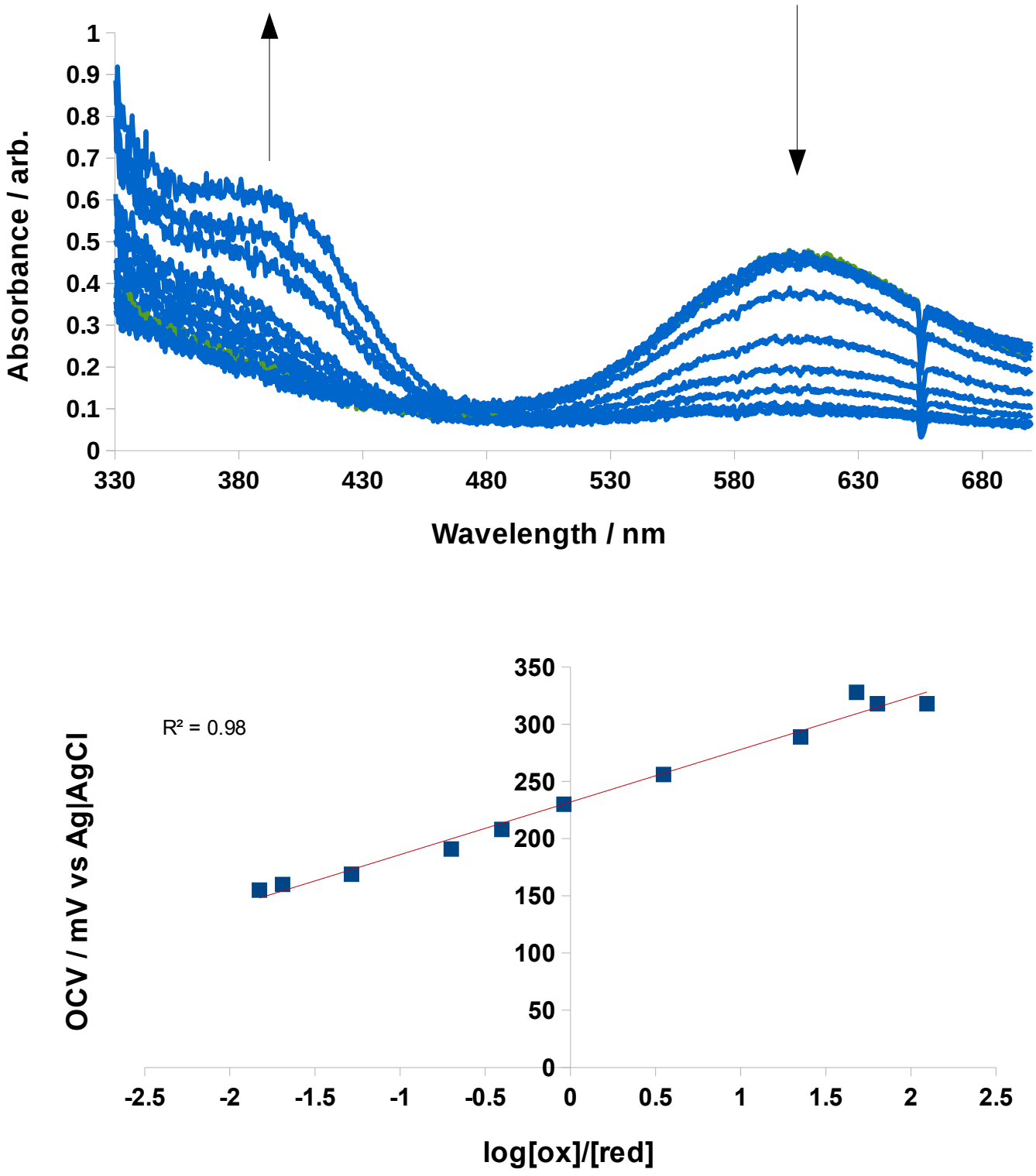

Figure 3-3

Redox titration of WT *Thermus thermophilus* laccase using $Ru(NH_3)_5Py$ mediator. A linearlized Nernst plot of titration data yields an intercept at 231 mV vs Ag|AgCl reference.

in all MCOs and serves as the wiring pathway funneling charge between the type 1 site and trinuclear cluster. As a result, we felt that these mutants would have the best chance at minimally perturbing protein function, while possibly raising the TNC reduction potential.

Materials and Methods

Mutagenesis

Mutants of *Thermus thermophilus* laccase were constructed using mutant PCR primers (primer sets for all mutants made here are presented in the appendix). Primers were ordered from Operon and used in PCR reactions with the appropriate DNA template. In general, primer:template molar ratios of ~ 420:1 were used to successfully induce mutation. Due to the high-GC content of the template DNA samples, additions of 2.5% DMSO to PCR samples were found to be essential for observing successful mutation of the laccase gene.

Protein Expression

All proteins were expressed according to the protocol outlined in the appendix.

Absorption Spectroscopy

UV-vis spectra of all mutants were acquired following protein expression and purification. Protein spectra were generally collected in pH 6.5 20-100 mM sodium acetate on an Agilent 8453 UV-Vis spectrometer. Protein concentrations of ~ 70 μM were typical. Serial dilutions of each protein were made and measured via UV-vis in order to measure the molar absorptivities of the mutant laccases at wavelengths between 300 and 800 nm.

Electrochemistry

Linear sweep and cyclic voltammograms of all mutants on ketjen black electrodes were collected according to protocols described in Chapter I (Materials & Methods, *Electrochemistry* section).

EPR Spectroscopy

For EPR, proteins were concentrated in Amicons (centrifugation at 5000 rpm) to final concentrations of 60-200 μM. Glycerol was added to a final concentration of 20% w/v to each protein sample used in EPR experiments. Total sample volumes of 120-200 μl were inserted into EPR tubes, placed on ice, and taken to the EPR spectrometer (Bruker, X-Band) for measurement. Prior to data acquisition, samples were glassed and stored in liquid N_2. Spectra were acquired using either liquid He (20 K) or liquid N_2 (77 K) to cool the instrument. Smoothened spectra were achieved by averaging 4 scans. Typical microwave power was 2 mW during spectral collection.

Copper Detection & Quantification

To quantify the degree of copper incorporation in the laccases investigated here, the commercial Pierce BCA protein assay for protein detection was adapted for the detection of Cu. In the reworked assay, Cu is now the reagent limiting formation of the purple $Cu^{I}(BCA)_2$ complex, rather than the amide nitrogens of peptide backbones as in the case of the commercial assay.

Reagents for the BCA assay were purchased from Thermo Scientific. Cu standards (100-500 μM) were made in milliQ water using $CuSO_4$ purchased from (EM Science). Due to the requirement for protein denaturation in order to release bound Cu, standards were made up in 6M Guanidine?HCl (Gu?HCl) at pH 13 (Sigma-Aldrich). The standard curve was made by incubating the standards made up in Eppendorf tubes at 37 °C with mixing (230 rpm) followed by 1 hour of cooling to room temperature (~ 18-20 °C). Tubes were centrifuged to remove precipitates generated during the incubation step. Aliquots of the standards were then added to a 96 well plate along with a Gu?HCl blank before measuring sample concentrations at 562 nm on a FlexStation 3 (Molecular Devices) plate reader (Figure 3-5).

Protein samples were prepared by first concentrating laccase to concentrations of at least 200 μM. 5 μl of protein was then added to 35 μl of pH 13, 6M Gu·HCl. The protein was then allowed to incubate at 37 °C for

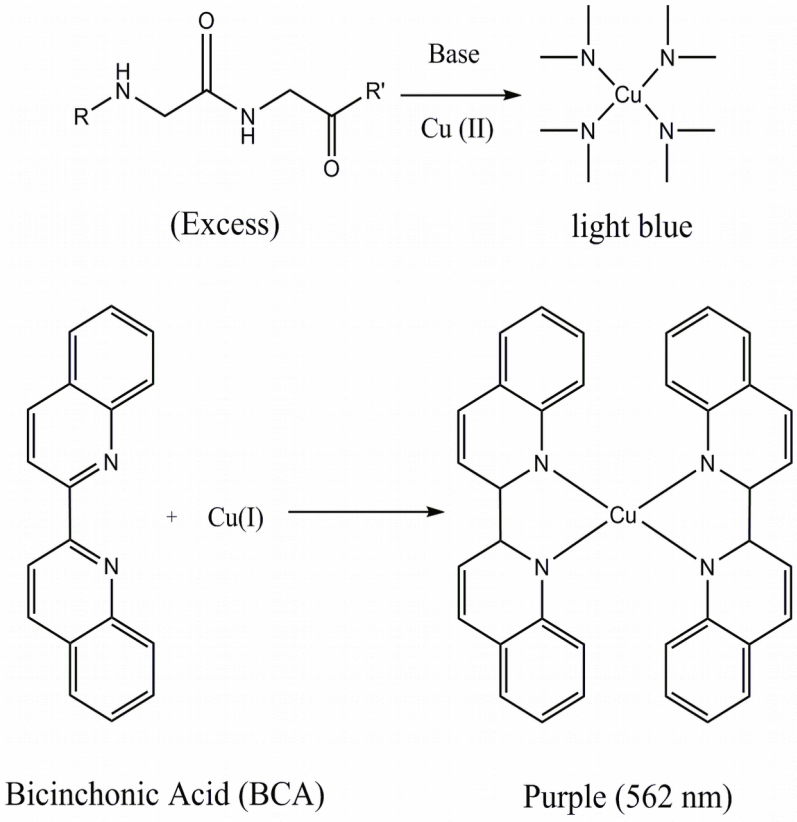

Figure 3-4
The BCA assay for Cu detection.

1 hour with mixing in order to denature. Following the denaturing step to release bound copper, the samples were prepped for the detection method. A "working reaction" consisting of a 1:25 mixture of 2 mg / ml albumin (Thermo BCA kit) and Reagent A (Thermo BCA kit) was prepared fresh for each run of the assay. Reagent A supplies the BCA ligand in a sodium bicarbonate buffer, while albumin, present in large excess relative to Cu, supplies the amide functionalites needed for the initial chelation of Cu^{II}. 200 μl of the working reaction and 25 μl of denatured protein sample were dispensed into Eppendorf tubes. Samples to serve as spectral blanks were prepared by substituting 25 μl of the Gu·HCl stock for protein in the Eppendorf tubes. Tubes were then incubated at 37 °C for 3 hours with shaking at 150 rpm to prompt development of the purple $Cu(BCA)_2$ complex. Following this step, tubes were removed from the incubator and allowed to cool to room temperature for 1 hour. Samples were then centrifuged at 15000 rpm for 20

minutes to remove precipitates. 200 μl of the supernatants were then added to a 96 well plate and absorption at 562 nm was measured for all samples. To account for minor variations between individual reads of the spectrometer, each sample run was measured 4-6 times, with subsequent averaging of these values to improve accuracy of the assay. For each protein sample run, copper quantification was performed in triplicate unless otherwise stated.

Results

Absorption Spectroscopy

Electronic absorption spectra were measured for all mutant constructs (Figure 3-6). The inner-sphere, type 1 mutants (M455F and M455L) showed some perturbation in their absorption spectra, with the type 1 site absorption showing a slight red shift of about 10 nm in their absorption maxima (these mutants take on a blue-green hue, rather than the deep blue

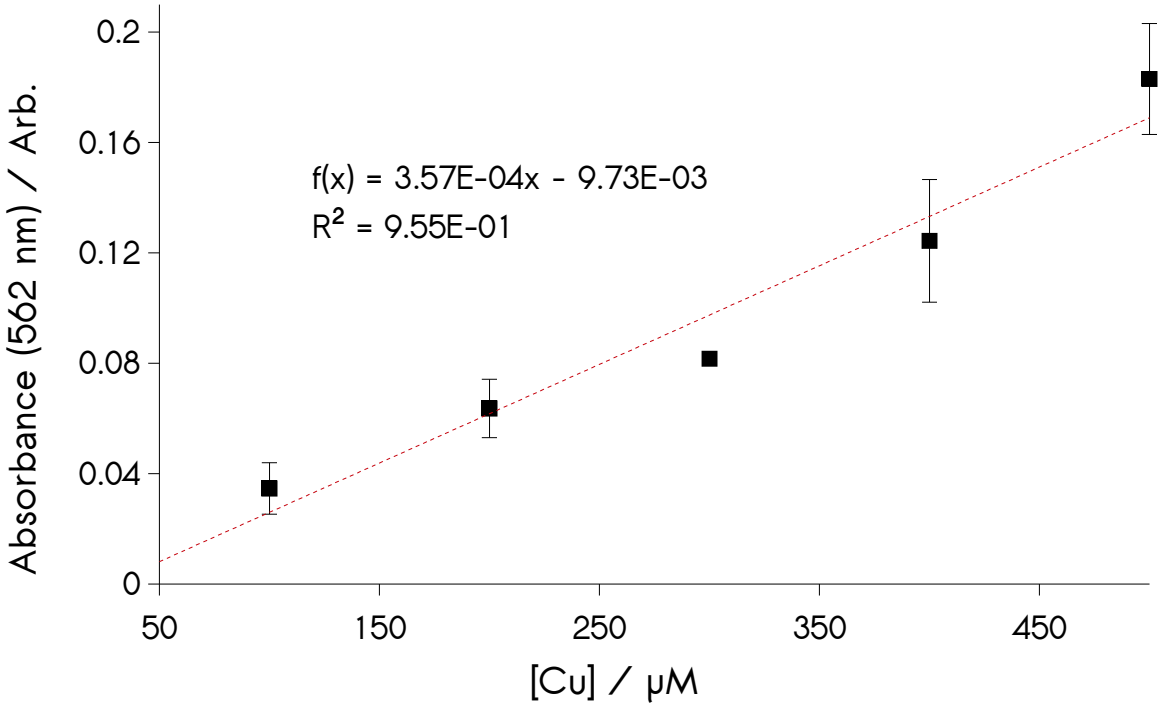

Figure 3-5

Standard curve for Cu detection. R^2 = 0.955. Equation of best fit: y=(3.57e-4)x - 9.73e-3.

color of WT laccase). In addition, the type 1 site in these mutants are weaker absorbers, with molar absorptivities at 610 nm decreasing to about 3700 and 2800 M^{-1} cm^{-1} for the M455L and M455F mutants, respectively. These constitute notable drops from an ε_{610} of 5000 M^{-1} cm^{-1} for the type 1 active site in the native laccase. The possibility of long-range structural and/or electronic perturbations at the trinuclear copper cluster are suggested by significant attenuation in the absorptivity of the shoulder at 330 nm for the M455F mutant (~ 2000 M^{-1} cm^{-1}). The M455L mutant, however, shows a TNC absorption profile resembling that of the wild type enzyme (~ 4000 M^{-1} cm^{-1}). As might be expected, mutation to the secondary sphere of the type 1 center results in less dramatic changes to the absorption spectrum of *Thermus thermophilus* laccase. Mutant E352A results in only minor reduction in the ε_{610} (4500 M^{-1} cm^{-1}), with little discernible change in absorption by the trinuclear cluster, suggesting only minor perturbative effects from mutation at this position.

Mutation at the trinuclear cluster was shown to induce significant changes to laccase's UV-vis footprint. The asymmetric TNC mutants, H135M and H398M, which each mutate one of the ligands of the two type 3 copper ligands, significantly reduce the ε_{330} (1400 and 900 M^{-1} cm^{-1} for H135M and H398M, respectively), suggesting that there are appreciable electronic and/or structural changes to the TNC resulting from these mutations. The H398M mutant demonstrates long-range effects which result in significant changes to the absorption at the type 1 active site, which drops to ε_{610} to 3600 M^{-1} cm^{-1} in this mutant. Electronic absorption of the symmetric TNC mutant (H135M / H398M) yields counterintuitive results, with the spectrum of this mutant not merely being an additive convolution of H135M and H398M spectral profiles. The drop in ε_{610} seen in the H398M mutant is not observed in the double mutant, which retains the ε_{610} of the native enzyme. However, attenuation in the ε_{330} (1500 M^{-1} cm^{-1}) resembles that of the H135M construct.

Electrochemistry

Mutant laccases were tested on ketjen black PTFE electrodes to check for the effects of mutation on dioxygen reduction activity (Figure 3-7). The inner-sphere type 1 mutants M455F and M455L showed very little

detectable electrochemical activity. Our E352A construct did demonstrate some successful increase in the onset potential for catalytic dioxygen reduction (ca. 50 mV). However, the peak current observed by 0 V vs. Ag|AgCl was far lower than that observed with the wild-type enzyme. Furthermore, both peak current and the onset potential for catalysis dropped off rapidly with successive cycling of the electrode for the E352A mutant (Figure 3-8). For each of the trinuclear cluster mutants (constructs H135M, H398M and H135M/H398M) electrochemical activity is completely arrested at low overpotentials; only H398M begins to exhibit some current response at ca. 100 mV vs Ag|AgCl.

EPR Spectroscopy

Generally, native multicopper oxidases exist in a resting state where type 1 and type 2 coppers give rise to resonances in EPR. The binuclear type 3 (T3) sites in these systems, despite having cupric resting forms, are not EPR visible, the consequence of a μ2-hydroxide bridge which facilitates antiferromagnetic coupling between the formally S = 1/2 T3 copper ions to give an effective S = 0 system for this site. The wild-type

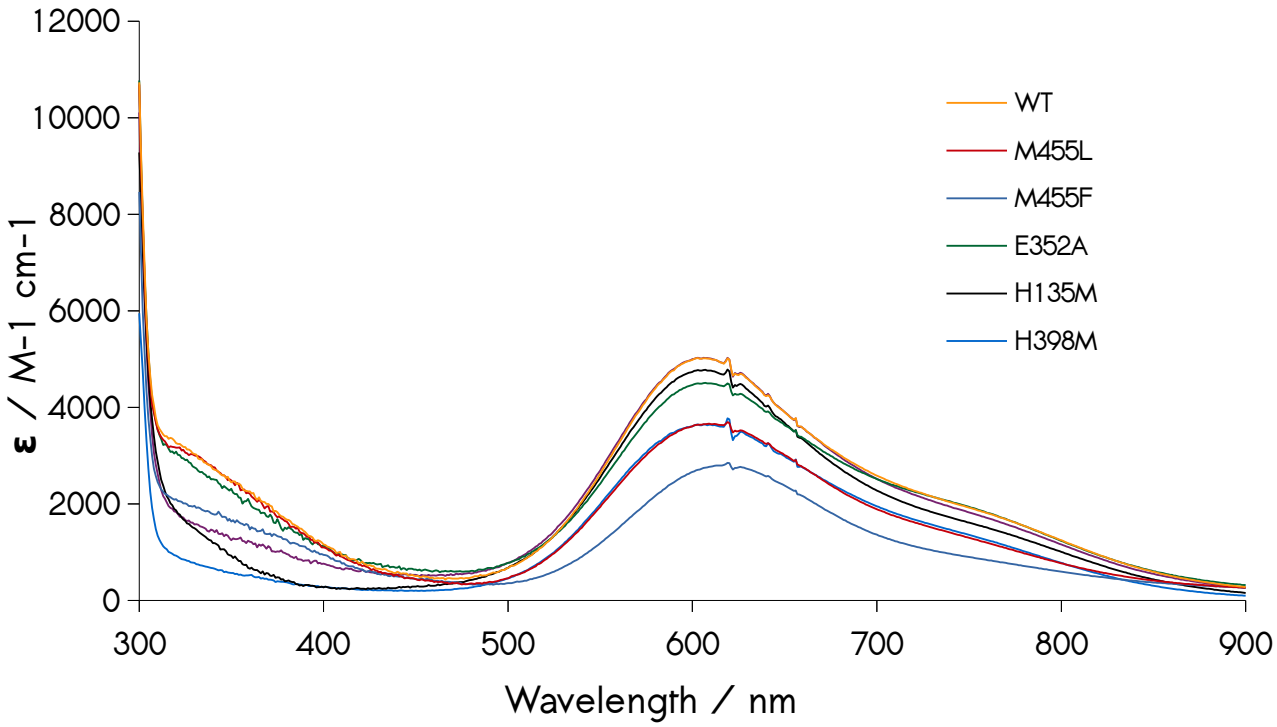

Figure 3-6
Absorption spectra of WT and mutant laccases.

form of *Thermus thermophilus* laccase exhibits these classic MCO traits, with the primary Zeeman transition occurring at $g_{\perp}$ = 1.95. No significant hyperfine coupling to the I = 3/2 nuclear spin of Cu is apparent in the main line transition for WT laccase. However, the typical MCO type 1 hyperfine coupling causing the 4-line splitting in the minor axial EPR resonance is observed for the wild-type ($A_{\parallel}$ = 8.4 mT, $g_{\parallel}$= 2.10). Intensities are lower for the resonances arising from type 2 copper in these enzymes, with most of the type 2 hyperfines being masked by the intense type 1 signal. However, the lowest-field type 2 hyperfine resonance can be resolved at ca. 2705 Gauss for the wild-type enzyme (Figure 3-10, top panel).

The inner-sphere type 1 mutants M455L and M455F show main line transitions occurring at $g_{\perp}$ = 1.96 and 1.97, respectively, values similar to the wild-type enzyme. Hyperfine interactions for these variants occur at $g_{\parallel}$ = 2.11 and 2.10, with coupling constants of $A_{\parallel}$ = 8.5 mT and 7.6 mT (M455L and M455F, respectively). Mutation of the methionine axial ligand to non-coordinating residues has the apparent effect of making one more of the type 2 hyperfines resolvable, allowing for observation of now two of the four type 2 hyperfines, located at 2687 and 2849 Gauss for M455L and 2674 and 2859 Gauss for M455F laccases, values shifted slightly downfield relative to wild-type. Magnified views of the EPR spectra of these mutants juxtaposed against the wild-type enzyme make resolution of this additional type 2 hyperfine more apparent (Figure 3-12). As the intensities for the type 2 signals were weak for these mutants, our reported values of the type 2 $A_{\parallel}$ (16 mT for M455L and 19 mT for M455F) are tentative. They are, however, consistent with literature values for type 2 MCO hyperfines.[1]

Structural perturbations to the type 1 secondary coordination sphere enforced by the E352A mutation show less pronounced changes in EPR relative to the native enzyme (Figure 3-11). Here, $g_{\parallel}$ and $g_{\perp}$ assume respective values of 2.11 and 1.96, with no appreciable value for $A_{\perp}$. Type 1 hyperfine couplings of 8.5 mT and one of the type 2 hyperfines at 2704 Gauss are observed, values similar to those of the wild-type.

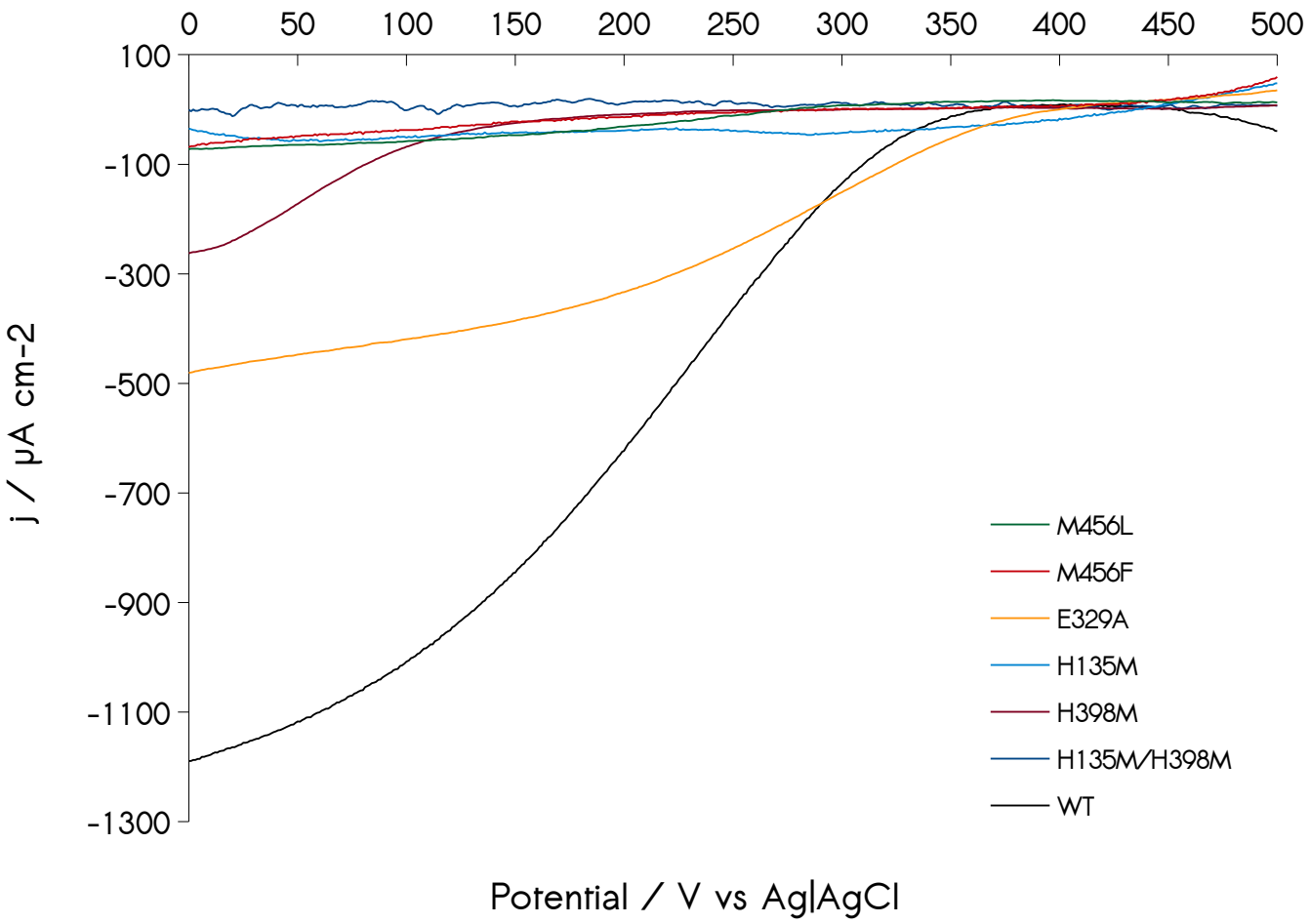

Figure 3-7

LSVs of mutant and wild-type laccases on PTFE / ketjen black electrodes. Electrode rotation is at 4000 rpm in pH 5.0 sodium acetate, 30 °C.

Mutations to the TNC show significant changes in EPR studies. The single, type 2 hyperfine generally seen is not found in the H135M or H398M T3 mutants, despite sufficient signal intensity (Figure 3-10). The type 1 hyperfines are observed at $g_{\parallel} = 2.11$ with coupling constants of 8.2 mT for both constructs. Unlike the wild type or type 1 mutants, a significant degree of hyperfine interaction along $A_{\perp}$ results from T3 ligand

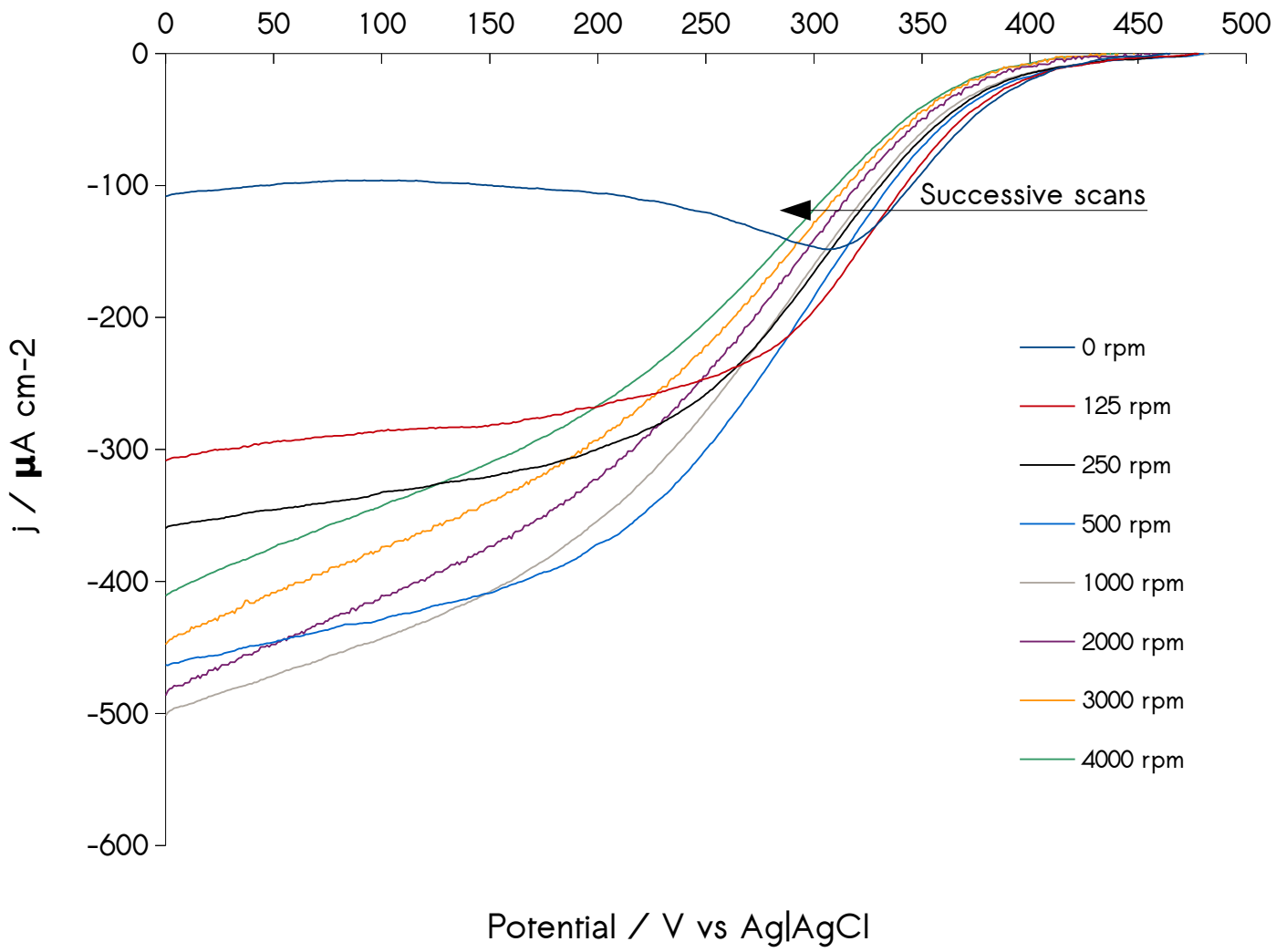

Figure 3-8

LSVs of E352A Laccase in pH 5.0 20 mM sodium acetate. With progressive scans, the onset potential drops. Drops in peak current with successive scans also result in non-ideal behavior when measuring rotational dependence of current for this enzyme. Note that after 1000 rpm, peak current begins to decrease.

modification, with observable hyperfine couplings of 0.6 mT for H398M and 0.9 mT for H135M (Figure 3-13).

Symmetric mutation to the T3 site to yield the H135M/H398M mutation results in a highly perturbed EPR spectrum. The main Zeeman interaction occurs at $g_{\perp}$ = 1.96, with evident coupling to Cu nuclei ($A_{\perp}$ = 0.8 mT) as

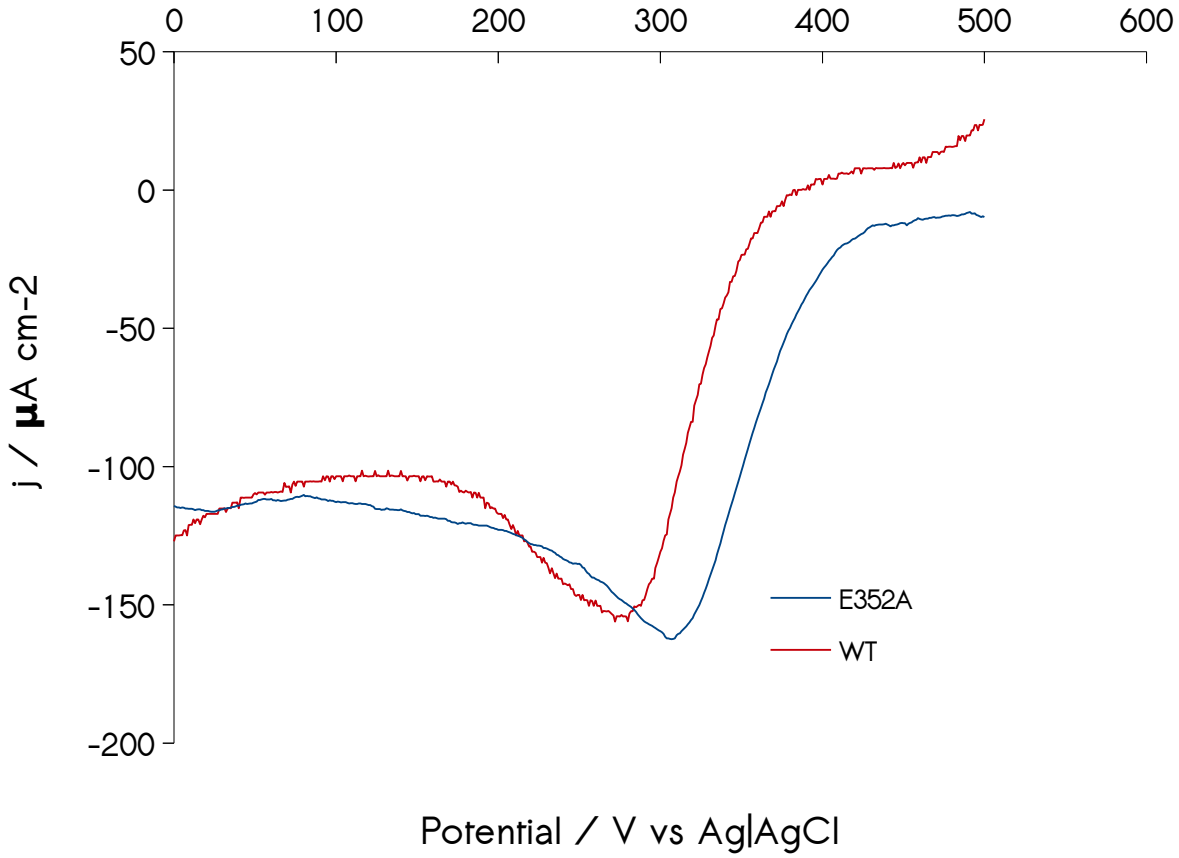

Figure 3-9

Comparison of WT and E352A laccases taken at 0 rpm, first scan.

observed in the asymmetric TNC mutants. Data suggest that the type 1 electronics in this mutant are not significantly perturbed by double mutation at the TNC, exhibiting $g_{\parallel}$ = 2.11 and $A_{\parallel}$ = 8.5 mT, values bearing close relation to the type 1 parameters of WT laccase. In H135M/H398M, multiple low-intensity resonances tentatively assigned to type 2 copper now appear at low field. Comparison with the wild-type EPR spectrum suggests that these additional resonances may result from a breakage in antiferromagnetic coupling at the T3 site (Figure 3-12). Such decoupling would yield paramagnetic Cu ions housed in the binuclear T3 ligand sphere that are EPR active with type 2 Cu signatures, consistent with our observed spectrum (Figure 3-13).

Cu Detection

Copper detection was carried out for all constructs examined here in order to discern whether or not changes to the absorption spectra, EPR and electrochemistry could be ascribed to electronic changes at the mutated active sites or if these differences were at least a partial function of incomplete metallation at the perturbed copper centers relative to wild-type laccase. Results of copper detection experiments are summarized in Table 3-1.

Table 3-1

	WT	E352A	M455L	M455F	H135M	H398M	H135M/H398M
Trial 1 / μM	226	162	159	134	111	167	66
Trial 2 / μM	187	164	116	159	122	110	69
Trial 3 / μM	296	162	119	-	133	113	76
Trial 4 / μM	225	159	-	-	-	107	-
Average / μM	233.5	161.8	131.3	146.5	122	124.3	70.3
Cu Content / Enzyme	**4.1**	**2.4**	**2.0**	**3.8**	**1.4**	**3.6**	**2.4**
σ	0.80	0.03	0.37	0.46	0.13	0.82	0.18

Discussion

Consolidation of the electrochemical, spectroscopic and biochemical assay data generated in this study provides some insight into why mutations of the type 1 center or TNC significantly reduce or completely inhibit dioxygen reductase activity in laccase. M455L/F mutation presumably raises the type 1 reduction potential relative to that of the TNC such that intramolecular ET from T1 to the TNC is significantly hampered, explaining the lack of any appreciable electrochemical activity by these mutants. The E352A mutant, which should be expected to raise the type 1 potential to a lesser degree than the inner-sphere mutants, does exhibit electrochemical activity (ca. 50 % that of the wild-type), while improving the onset potential for catalysis by merely ~ 50 mV. Copper assays suggest that metal incorporation is probably not the reason for lack of observed activity, as the M455F mutant demonstrates a level of metallation similar to that of the wild-type, while the M455L mutant incorporates Cu to a level on par with E352A. The notion of inner-sphere mutation inducing more dramatic

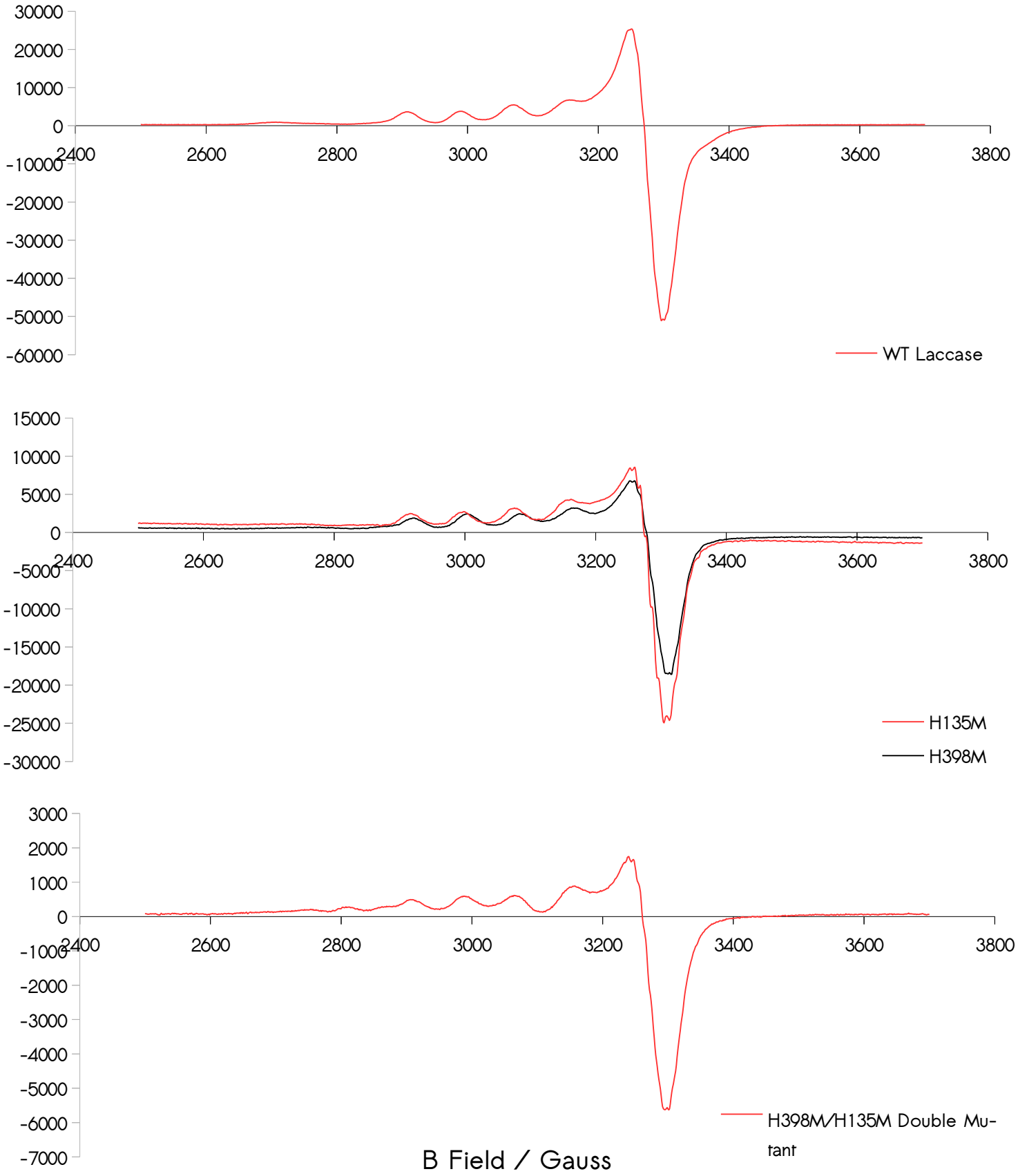

Figure 3-10

WT and trinuclear cluster mutant MCO EPR spectra.

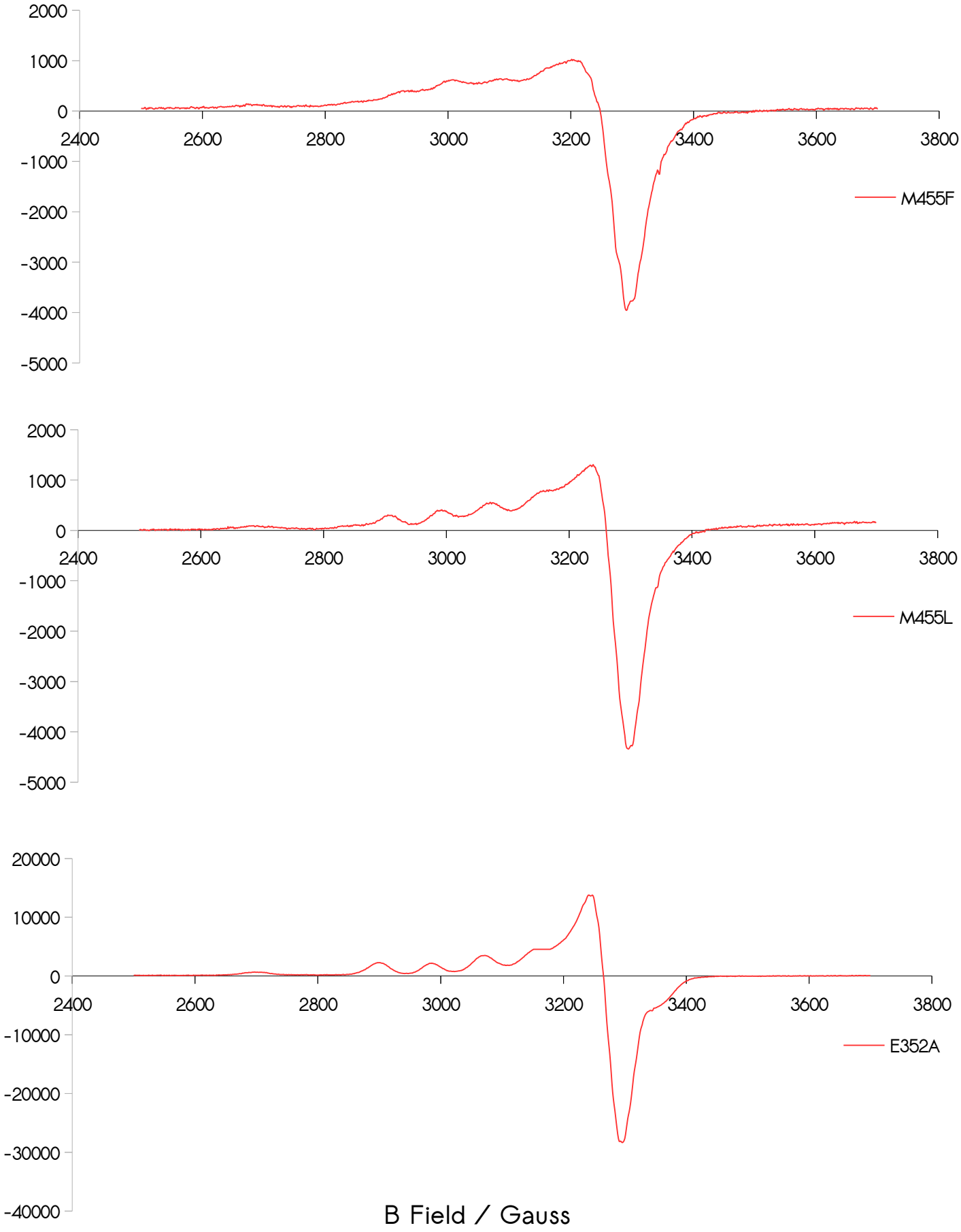

Figure 3-11

Type 1 mutant EPR spectra.

perturbations relative to outer-sphere changes is also supported by our absorption and EPR spectra, which show relatively minor electronic changes between the wild-type and E352A forms, but more drastic deviations from wild-type character when modifying the methionine axial ligand of the type 1 copper. However, none of these data can explain why the E352A mutant experiences a decay in activity with each subsequent turnover.

Marked changes to enzyme spectroscopy and metal content result from modification of the type 3 copper site. Mutants H135M, H398M and H135M/H398M show no electrochemical activity at all. In the case of H398M, insufficient copper incorporation does not seem a probable explanation for observed catalytic deactivation of the cluster, as Cu uptake for H398M approaches that of wild-type. Inspection of the absorption spectrum for this mutant also suggests that electronic effects are responsible for the change in catalytic activity, as the Cu detection assay indicates nearly complete metallation of the enzyme, but its absorption spectrum shows a significantly reduced trinuclear cluster absorption maxima at 330 nm. Similar arguments can be made for H135M/H398M, which, according to findings of the Cu assay, exhibits metallation behavior similar to that of the E352A mutant, which is still catalytically competent, albeit to a lesser degree than the native laccase. The presence of additional type 2 hyperfines in the double mutant EPR, which are not seen in the wild-type enzyme or any of the other mutants, suggests the possibility that loss of catalytic activity in the double mutant is caused by structural change at the TNC. Specifically, the resolution of additional type 2 hyperfines is most simply explained by the loss of antiferromagnetism at the T3 site. The clearest cause of such decoupling would be the loss of the -OH adduct that normally bridges the Cu ions of the T3 site. The drop in the absorbance at 330 nm for H398M and H135M/H398M also supports this interpretation, as this absorption band has been assigned to a μ-OH → Cu^{2+} charge transfer.[24]

Despite being an equivalent mutation to H398M on the other branch of the binuclear T3 site, H135M has the effect of both significantly reducing net copper incorporation while yielding significantly perturbed absorption and EPR spectra. Here, failure to see any electrochemical response could be the individual result of either electronic or structural changes or a

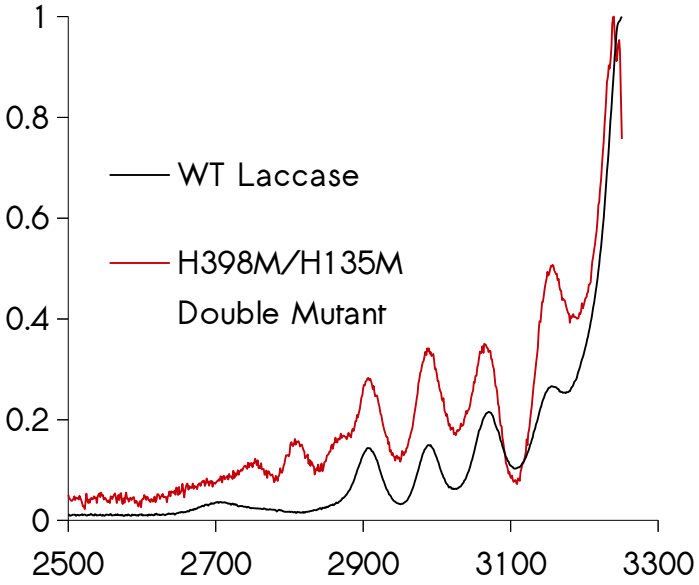

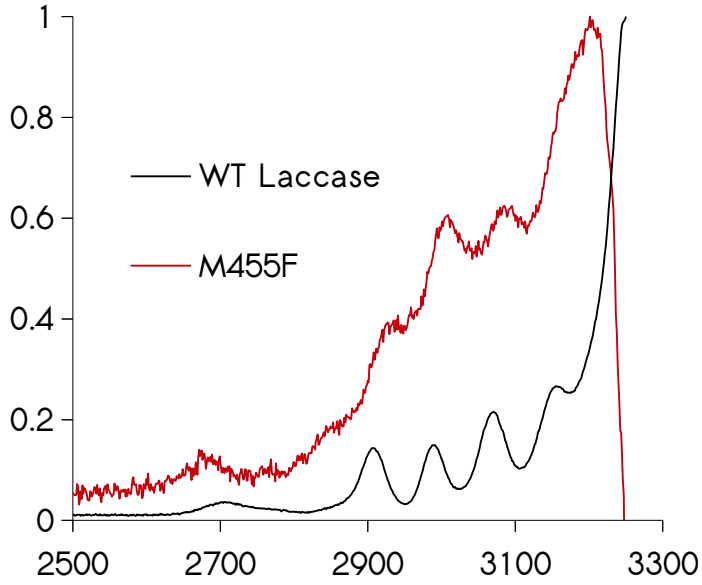

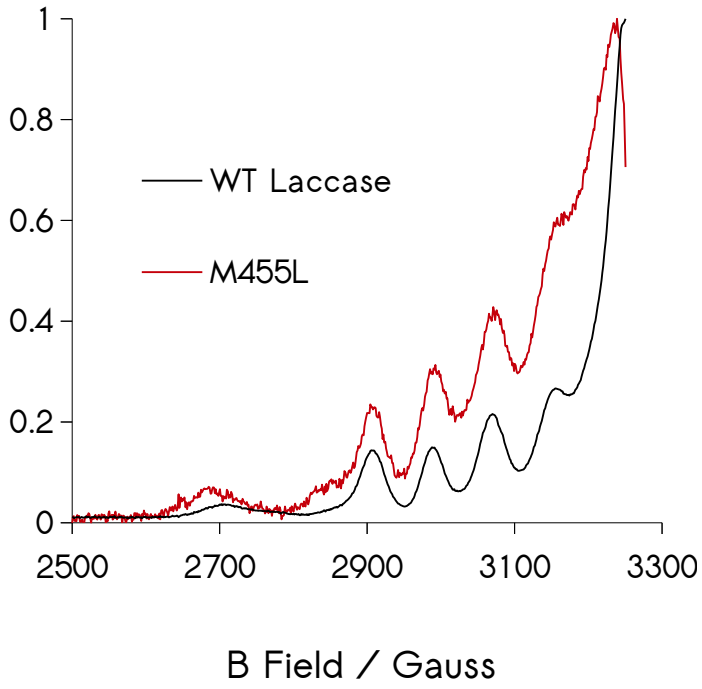

Figure 3-12

Magnified views of M455F/L and H135M/H398M laccase overlays with the wild-type enzyme in the low B field region. M455F/L show evidence of a partially obscured, type-2 hyperfine that is not resolvable in the wild-type enzyme at ca. 2850 Gauss. H135M/H398M shows evidence of two more type 2 hyperfines, likely arising from antiferromagnetic decoupling of the binuclear T3 site.

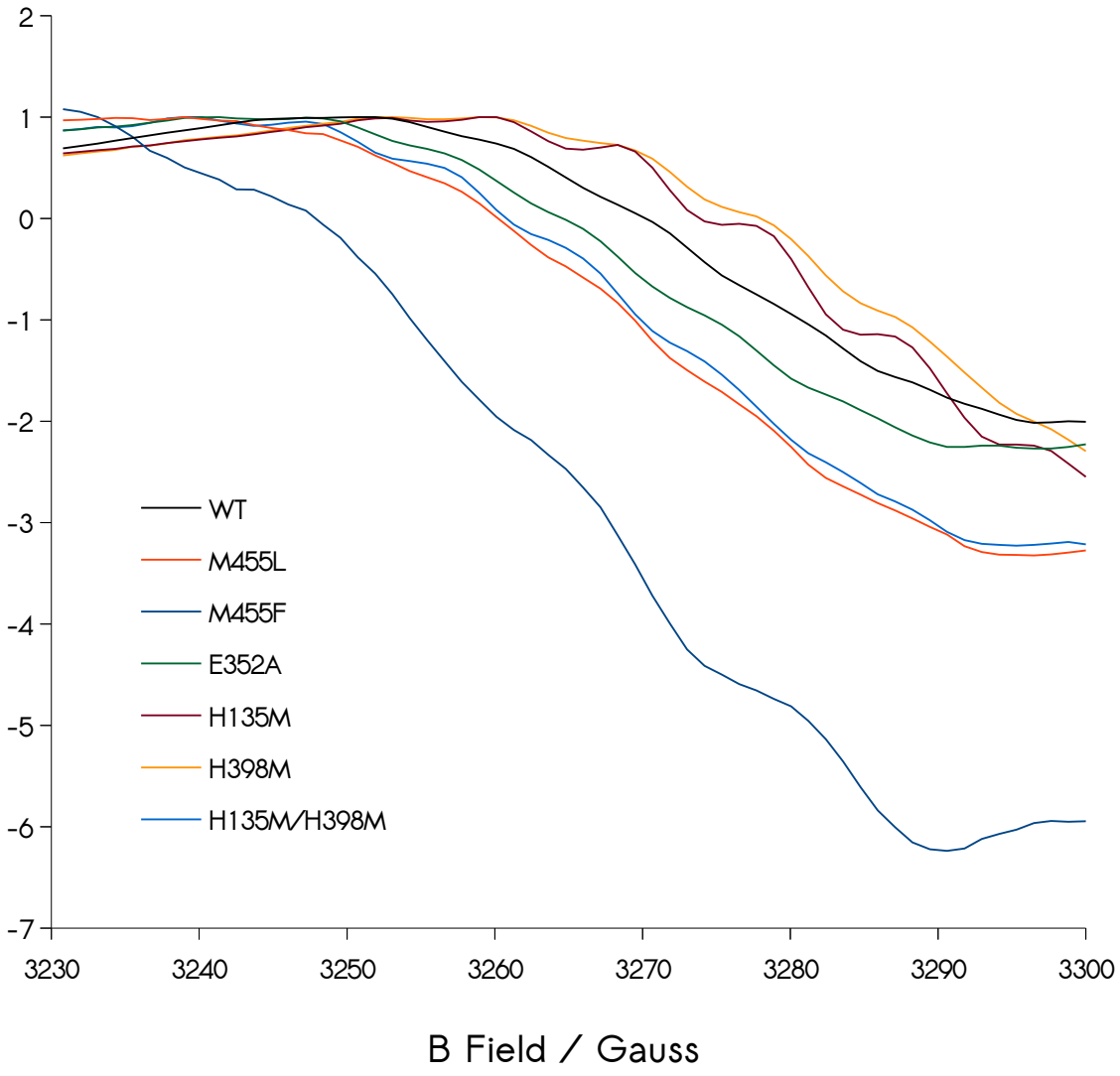

Figure 3-13

A magnified view of the main line (Zeeman) transition for wild-type and mutant laccases (data normalized). Hyperfine coupling is essentially absent for the native enzyme but pronounced in the H135M and H135M/H398M mutants. Evidence of weak hyperfine coupling in this region can be seen for M455F/L, E352A and H398M enzymes.

conflation of them. The marked differences between H135M and H398M has some precedent; Solomon and coworkers have shown that functional asymmetry does exist in the T3 active site of the MCO Fet-3p, where mutation of one branch of the T3 site still allows for reaction with O_2 but mutation to the ligands of the other T3-Cu does not.[25]

The presence of significant electronic coupling along $A_\perp$ in the TNC mutants also supports the the interpretation of catalytic arrest stemming from loss of the T3 hydroxide bridge, particularly for the H135M/H398M mutant. Increased coupling along $A_\perp$ implies increased localization of the unpaired d electron to the Cu nucleus, resulting in more intense hyperfine interactions. An increased localization of the electron to the Cu nucleus should be expected when the Cu ions are no longer covalently bound to an electron-withdrawing ligand such as the μ_2-hydroxide generally found in T3 sites. This description is consistent with our interpretation that catalytic deactivation in the TNC mutant constructs is caused primarily by a structural change to the type 3 Cu site which results in its adoption of type 2 copper character.

Conclusions

Mutations to the primary coordination sphere of the binuclear type 3 site are far too perturbing; any future efforts to modify the TNC redox potential should probably only be done through changes to the secondary coordination sphere, perhaps through the addition of more hydrophobic residues in this region to help raise the reduction potential of the cluster, rather than direct changes to T3 Cu ligands. Modifications to the type 1 center do allow for retention of some catalytic activity, particularly with outer-sphere mutation, as seen with the E352A construct. Mutation of the methionine axial ligand to non-coordination residues almost completely arrests catalysis, presumably by raising the type 1 potential above that of the trinuclear cluster, inhibiting intramolecular ET to from T1 to the TNC. Any construct featuring mutation to the type 1 primary coordination sphere will have to be accompanied by a compensating mutation to raise the TNC reduction potential by roughly the same amount. Our studies here suggest that attempting to do so through T3 ligand

modification will not be a viable route, at least in the MCO isoform examined here.

References

(1) Solomon, E. I.; Sundaram, U. M.; Machonkin, T. E. *Chem. Rev.* **1996**, *96*, 2563–2606.

(2) Solomon, E. I.; Augustine, A. J.; Yoon, J. *Dalton Trans.* **2008**, 3921–3932.

(3) Lau, C.; Adkins, E. R.; Ramasamy, R. P.; Luckarift, H. R.; Johnson, G. R.; Atanassov, P. *Adv. Energy Mater.* **2012**, *2*, 162–168.

(4) Blanford, C. F.; Foster, C. E.; Heath, R. S.; Armstrong, F. A. *Faraday Discuss.* **2008**, *140*, 319–335.

(5) Miura, Y.; Tsujimura, S.; Kurose, S.; Kamitaka, Y.; Kataoka, K.; Sakurai, T.; Kano, K. *Fuel Cells* **2009**, *9*, 70–78.

(6) Liu, X.; Gillespie, M.; Ozel, A. D.; Dikici, E.; Daunert, S.; Bachas, L. G. *Anal. Bioanal. Chem.* **2011**, *399*, 361–366.

(7) Tsujimura, S. *Electrochimica Acta* **2008**, *53*, 5716.

(8) Kataoka, K.; Sugiyama, R.; Hirota, S.; Inoue, M.; Urata, K.; Minagawa, Y.; Seo, D.; Sakurai, T. *J. Biol. Chem.* **2009**, *284*, 14405–14413.

(9) Tsujimura, S.; Asahi, M.; Goda-Tsutsumi, M.; Shirai, O.; Kano, K.; Miyazaki, K. *Phys. Chem. Chem. Phys.* **2013**.

(10) Thorum, M. S.; Anderson, C. A.; Hatch, J. J.; Campbell, A. S.; Marshall, N. M.; Zimmerman, S. C.; Lu, Y.; Gewirth, A. A. *J Phys Chem Lett* **2010**, *1*, 2251–2254.

(11) Blanford, C. F.; Foster, C. E.; Heath, R. S.; Armstrong, F. A. *Faraday Discuss.* **2008**, *140*, 319–335.

(12) Mano, N.; Kim, H.-H.; Heller, A. *J Phys Chem B* **2002**, *106*, 8842–8848.

(13) Mano, N.; Fernandez, J. L.; Kim, Y.; Shin, W.; Bard, A. J.; Heller, A. *J. Am. Chem. Soc.* **2003**, *125*, 15290–15291.

(14) Soukharev, V.; Mano, N.; Heller, A. *J Am Chem Soc* **2004**, *126*, 8368–8369.

(15) Udit, A. K.; Hill, M. G.; Gray, H. B. *Langmuir ACS J. Surf. Colloids* **2006**, *22*, 10854–10857.

(16) Udit, A. K.; Gray, H. B. *Biochem. Biophys. Res. Commun.* **2005**, *338*, 470–476.

(17)Lancaster, K. M.; George, S. D.; Yokoyama, K.; Richards, J. H.; Gray, H. B. *Nat. Chem.* **2009**, *1*, 711–715.

(18)Canters, G. W.; Kolczak, U.; Armstrong, F.; Jeuken, L. J. C.; Camba, R.; Sola, M. *Faraday Discuss.* **2000**, *116*, 205–220.

(19)Hwang, H. J.; Ang, M.; Lu, Y. *J. Biol. Inorg. Chem. JBIC Publ. Soc. Biol. Inorg. Chem.* **2004**, *9*, 489–494.

(20)Yokoyama, K.; Leigh, B. S.; Sheng, Y.; Niki, K.; Nakamura, N.; Ohno, H.; Winkler, J. R.; Gray, H. B.; Richards, J. H. *Inorganica Chim. Acta* **2008**, *361*, 1095–1099.

(21)Murphy, L. M.; Strange, R. W.; Karlsson, B. G.; Lundberg, L. G.; Pascher, T.; Reinhammar, B.; Hasnain, S. S. *Biochemistry (Mosc.)* **1993**, *32*, 1965–1975.

(22)Sakurai, T.; Kataoka, K. *Chem. Rec.* **2007**, *7*, 220–229.

(23)Xu, F.; Palmer, A. E.; Yaver, D. S.; Berka, R. M.; Gambetta, G. A.; Brown, S. H.; Solomon, E. I. *J. Biol. Chem.* **1999**, *274*, 12372–12375.

(24)Quintanar, L.; Yoon, J.; Aznar, C. P.; Palmer, A. E.; Andersson, K. K.; Britt, R. D.; Solomon, E. I. *J Am Chem Soc* **2005**, *127*, 13832–13845.

(25)Augustine, A. J.; Kjaergaard, C.; Qayyum, M.; Ziegler, L.; Kosman, D. J.; Hodgson, K. O.; Hedman, B.; Solomon, E. I. *J. Am. Chem. Soc.* **2010**, *132*, 6057–6067.

IV. Future Directions: Possible Strategies for Fabricating Enhanced Multicopper Oxidase cathodes

Abstract

In this section we discuss possible future strategies and present early-phase work for fabricating multicopper oxidase (MCO) cathodes that display higher interfacial charge transfer rates. In particular, we consider the possibility of high-surface area, gold self-assembled monolayer (Au-SAM) electrodes, using small-molecule bioconjugates covalently linked to surface residues on a protein to facilitate surface binding and, finally, the possibility of using electric fields to orient an MCO on electrically conductive substrates.

Introduction

To date, work in the field of multcopper oxidase (MCO) electrochemistry has demonstrated electrocatalytic dioxygen turnover by the enzyme at current densities reaching only 10 mA cm^{-2} at standard temperature and 1 atmosphere of O_2, far below the 100 - 1000 mA cm^{-2} operating regime of most platinum fuel cell cathodes. As discussed in Chapters I and II, the low-overpotential current in *Thermus thermophilus* laccase cathodes is limited by the rate of interfacial electron transfer (k_{ET} = 1.0 ± 0.3 s^{-1} at zero overpotential) between the enzyme active site and the electrode substrate. Our data, coupled with successful measurement of the typical surface concentration of electrochemically active laccase enzymes comprising a biochemical cathode (1.56 ± .44x10^{14} enzymes cm^{-2} on Ketjen Black carbon), have enabled us to chart a path towards realizing a laccase electrode operating in the 100 mA cm^{-2} current regime. Each of the following strategies to increase interfacial electron transfer rates derives from Marcus theory, which describes the rate of charge transfer between a redox-active donor and acceptor as:

$$k_{ET} = \frac{4\pi^2}{h\sqrt{4\pi\lambda k_B T}} H_{AB}^2 \exp\left[\frac{-(\Delta G + \lambda)^2}{4\lambda k_B T}\right] \qquad \text{(eq. 4.1)},$$

where H_{AB} describes the strength of electronic coupling between a species A (an electron donor) and B (an electron acceptor). The interfacial electron transfer rate, k_{ET}, is proportional to the cathodic current density at low overpotential. In our cathodes, the electrode surface functions as the electron donor while a ligated copper ion (the type 1 active site) in laccase serves as the electron acceptor. Since our initial characterizations of laccase as discussed in Chapter I, we have been able to demonstrate that on porous carbon substrates using PTFE rather than PVDF binders, this laccase exhibits a maximal current density of 1.2 mA cm^{-2} at 30 °C (data and protocols in Appendix, A.8). While representing a doubling of the current observed in our initial study, this number still lies far from our 100 mA cm^{-2} target. As implied by equation (1), realizing current

densities on par with platinum catalysis partly requires that we improve the interfacial k_{ET} of our present cathodes by a factor of ca. 100 fold (assuming the enzyme coverages reported in this thesis). The clearest path to achieving this is through enhancement of the electronic coupling (H_{AB}) between the laccase active site and the electrode surface. Previous studies on self-assembled monolayers of alkanethiols on planar gold substrates (Au-SAMs) have demonstrated that modifying electrically conductive materials with uniform alkane monolayers permits fast electron tunneling between conductive substrates and bound redox cofactors via enhancement of H_{AB}.[1–3] Indeed, reported electron transfer rates between the type 1 active site in the non-catalytic blue-copper protein *Pseudomonas aeruginosa* azurin and Au-SAM electrodes range from 100 – 1000 s^{-1}.[1–3] Given the similar nature of the electron acceptors in azurin and laccase (each have type 1 copper sites), these findings suggest that incorporation of *Thermus thermophilus* laccase into SAM-inspired substrates may solve the problem of rate-limiting interfacial charge transfer (Figure 4-1). To allow for an increased enzyme

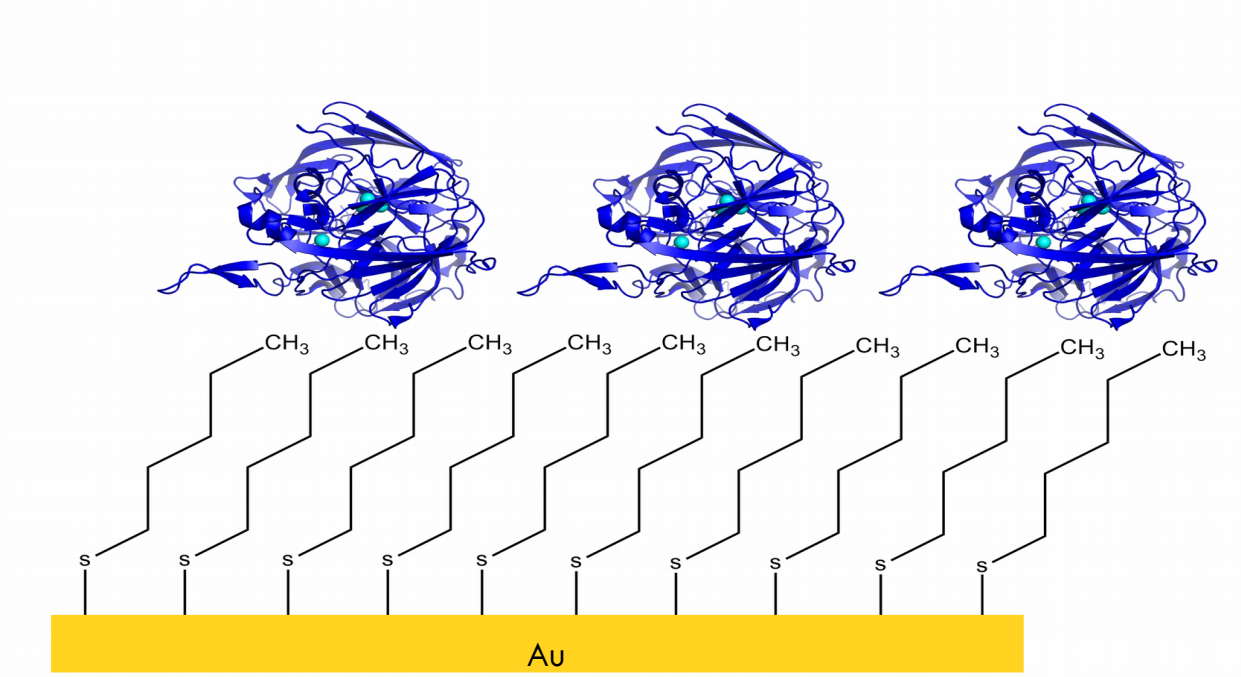

Figure 4-1
A depiction of *Thermus thermophilus* laccase adsorbed onto an Au-SAM made from coordination of 1-pentanethiol to gold substrate. Hydrophobic binding allows for strong adhesion of the enzyme to the alkane monolayer. Figure not to scale for illustrative purposes.

loading on the substrate, we propose using porous gold substrates produced by the etching of gold alloys upon which to establish SAMs. Here, we provide characterization via atomic force microscopy, scanning electron microscopy, and electron dispersive spectroscopy of nanoporous gold sheets as a prelude to possible future work for making laccase-SAM cathodes with this material.

In this chapter, we also consider the possibility of using molecular linkers to optimize interfacial electron transfer rates in these systems. Cysteine mutation at surface residues on a protein allows for the covalent attachment of commonly used small-molecule bioconjugates such as 1-(pyrene) iodoacetamide. The ability of the pyrene moiety to engage in strong π-stacking with basal planes of surfaces displaying aromaticity, such as graphene, single-walled carbon nanotubes, or highly-oriented pyrolytic graphite (HOPG), could possibly allow the selective positioning of an MCO on these conductive substrates which, unlike porous carbon and Au-SAMs, do not allow for the non-specific, hydrophobic adsorption of proteins. To this aim, we have synthesized a novel pyrene compound which can be coupled to proteins expressing a surface cysteine through a simple S_N2 displacement of a terminal halide by the deprotonated thiol of cysteineate at pH ~7.4. Respective studies by Udit[4,5] and Gorodetsky[6] have demonstrated the possibility of using pyrene-based compounds as successful immobilization strategies for cytochrome P450 DNA in studies of electron transfer at electrode-macromolecule interfaces.

Finally, we outline a possible method for controlling the surface orientation of MCOs using an electric field. Ideally, orientation would be performed on high-surface area substrates such as porous carbon; however, controlling orientation via molecular functionalization of a surface becomes impossible when the adsorbate of interest can bind non-specifically without the aid of a small-molecule linker, as in the case of MCOs on amorphous carbon powders and carbon nanotubes. A viable solution to this problem may lie in using the internal dipole moment of a protein to orient it on a surface. The property of dipoles to align themselves such that they oppose an external electric field should enable us to control the orientation of an MCO featuring a dipole moment. Furthermore, presence of a

net charge should allow for the controlled deposition of the protein on a surface using electrophoresis. Such a fabrication methodology, when properly implemented, would exclude the requirement for an organic linker, while allowing for the control over both the positioning of the protein (or any charged, macromolecular species) as well as the total number of catalytic centers immobilized on a substrate of interest. Only the former parameter may be controlled via assembly of proteins on surfaces through molecular linkers and neither of them is easily controlled using passive adsorption methods. It has been shown that electric fields can be used to orient lipid domains in vesicles within tens of seconds after applying an electric field.[7] Kuztenov et al. reported efforts to orient already-adsorbed cytochrome c on a surface using the electric field set up by the electrochemical double layer established at a glassy carbon electrode-electrolyte interface. However, they did not observe the anticipated enhancements in electron transfer between the iron heme of cytochrome c and the electrode.[8] Kanan et al. have reported that the employ of large electric fields may be used to direct substrates for enhanced selectivity in chemical catalysis.[9,10] We consider the possibility of using an electric field set up between two charged, parallel plates to control the orientation and translational motion of an MCO as it deposits on a conductive electrode surface, with the expectation that improved orientation of the type 1 site relative to the electrode surface will improve interfacial charge transfer kinetics. We derive and present the equations of motion describing the electrophoretic translation of an MCO modeled as a charged body in solution using classical electrodynamics and simple Newtonian force laws. Protein orientation is addressed through comparison of the MCO's dipole-electric field interaction to the energies of thermal vibrations giving rise to Brownian motion under ambient conditions.

i. Porous Au substrate fabrication and surface characterization

Methods & Materials

Gold alloy (49 % Au, 48% Ag) was purchased from SeppLeaf. To etch, pieces of the gold leaf were cut into approximately 2x2 cm squares with a razor and transferred to a nitric acid bath with a glass slide. Etch times of 30, 45, 60 and 120 minutes were tested to examine the effects of etch time on morphology of the resultant porous gold material. Following etching, samples were rinsed by pulling out the foil with a glass slide, forcing it to 'wick' up the slide, before being transferred to a water bath and then removed for drying by adsorbing the gold leaf onto a piece of weigh paper. For AFM studies, samples adsorbed to weigh paper were mounted on a metal puck (Bruker) for testing. Measurements were performed on a Nanoscope VII AFM (Bruker) in tapping mode. Measurements for each dealloying time were done in triplicate for all studies. AFM image processing was done in Gwyddion. All imaging data reported here, unless otherwise stated, are representatives of samples run in triplicate.

Scanning electron microscopy (SEM) measurements of the samples were performed on a Gemini SEM. Accelerating voltages of 10 kV were used for imaging and 15 kV were used for acquiring electron dispersive spectroscopy (EDS) data. Beam aperatures of 30 and 120 μm were used for SEM and EDS, respectively, with a sample working distance of 8 mm.

Results

AFM data of etched samples is shown in Figures 4-2,3. Within 30 minutes, extensive corrugation of the orginally smooth surface of the Au alloy results from the dissolution of the less noble metals of the alloy in HNO_3. Surface features appear their smallest around 45 minutes of etching in nitric acid, before broadening into wider surface corrugations again. This has been ascribed to the over-etching of the material at longer times, resulting in the gradual re-smoothening of the surface.[11]

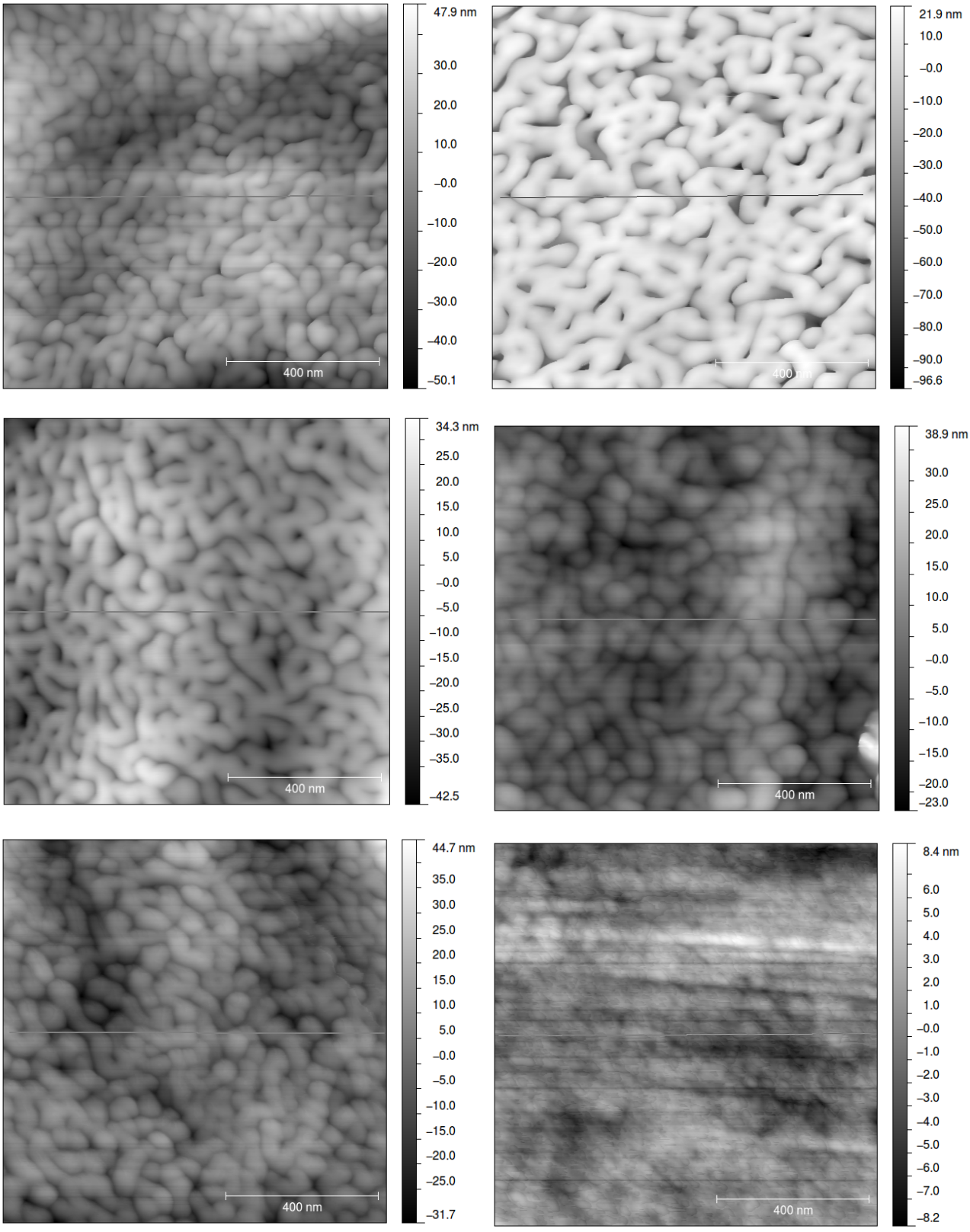

Figure 4-2a

Representative AFM images of gold-alloy leaf etched for (left to right)
Top row: 30, 45 minutes
Middle row: 1, 2 hours
Bottom row: 17 hours and a no-etch control. Horizontal lines through each image denote regions taken as sections for roughness calculations.

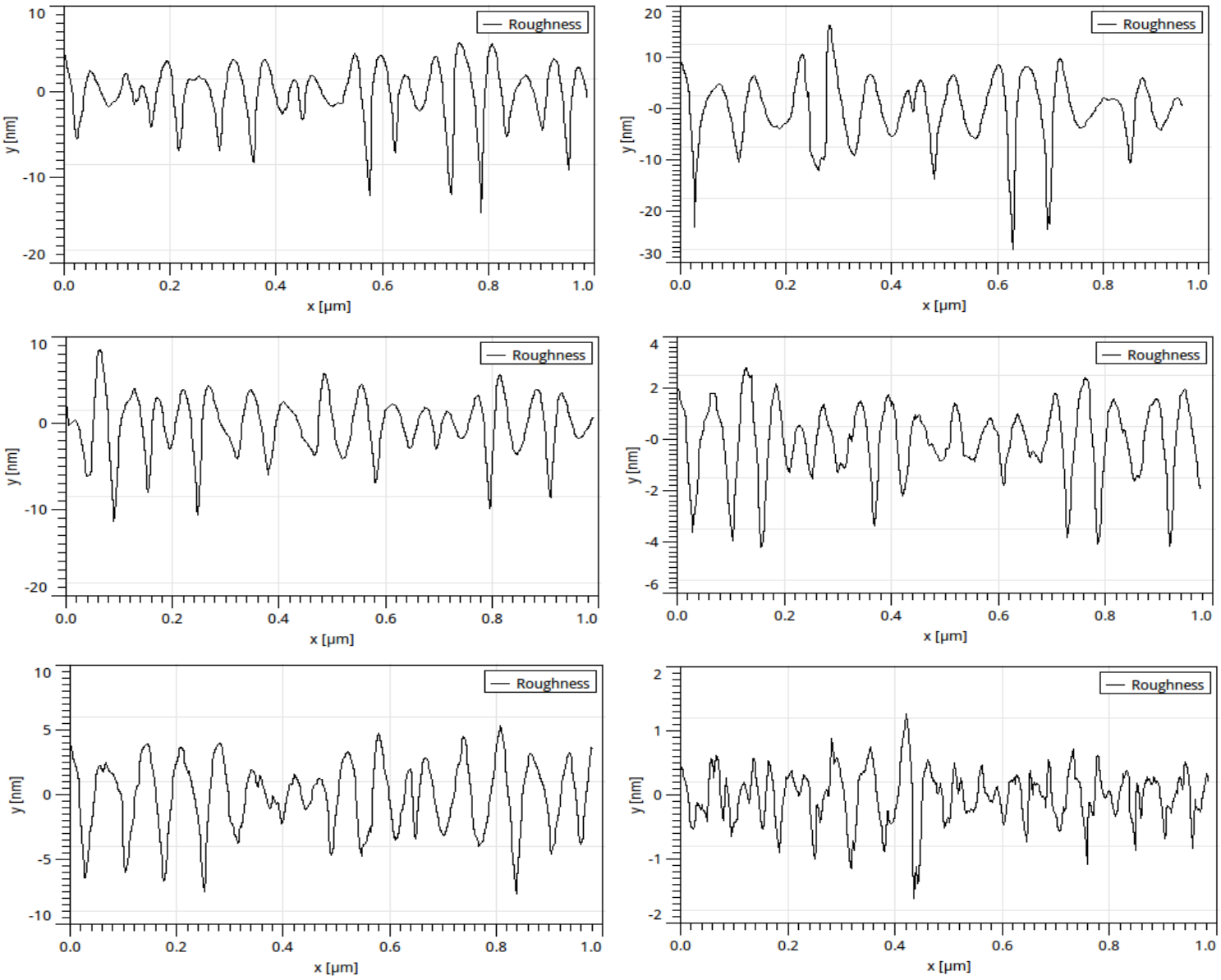

Figure 4-2b

Roughness sections of preceding images.
Top row: 30, 45 minutes
Middle row: 1, 2 hours
Bottom row: 17 hours and a no-etch control. Horizontal lines through each image denote regions taken for sections for roughness calculations.

Sample	Trial 1	Trial 2	Trial 3	Mean roughness (nm)	Std. Deviation
30 minutes	1.95	2.61	2.51	2.36	0.36
45 minutes	4.9	2.08	3.37	3.45	1.41
60 minutes	3.61	2.71	1.66	2.66	0.98
120 minutes	1.14	0.63	0.62	0.80	0.30
17 hours	2.03	2.26	3.00	2.43	0.51
No etch	0.36	0.70	-	0.53	0.24

Table 4-1

Compiled roughness data derived from AFM images for each etch time point.

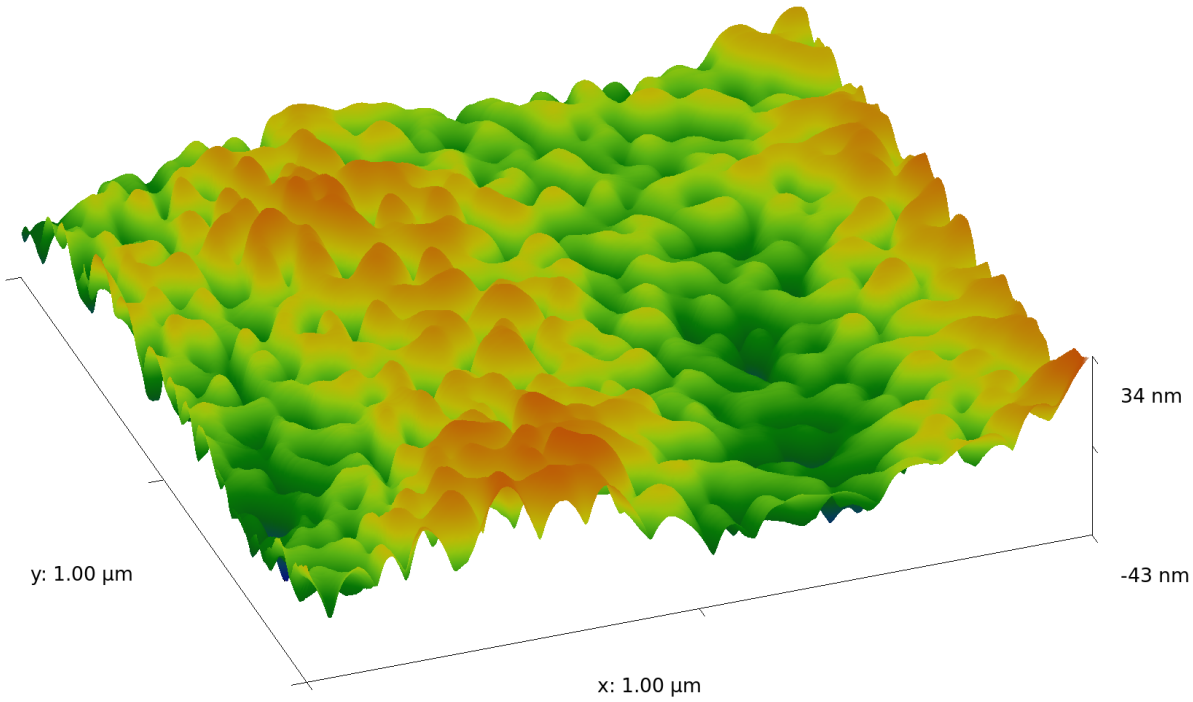

Figure 4-4

A 3-D AFM image of etched nanoporous gold.

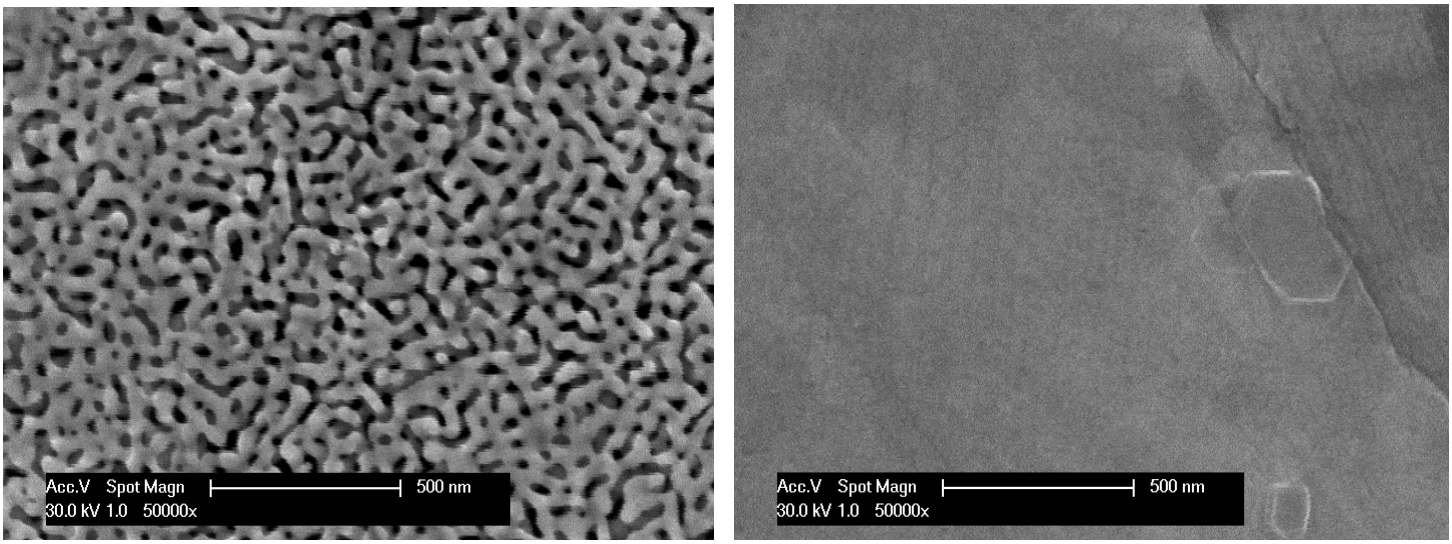

Figure 4-5
Representative SEM images of etched nanoporous gold leaf etched for 30 minutes (left) and a no-etch control (right). Images were acquired using a 30 kV accelerating voltage at 50000x magnification.

To provide more quantitative measures of the extent of dealloying, EDS was employed to determine whether or not trace metals persist in the etched gold leaf for various etch times (Figure 4-4). Within 30 minutes, samples show virtually no evidence of Ag or trace metals persisting in the leaf (elemental analysis using EDS reports a composition of 95.6% Au and 4.36% O). Carbon peaks in the spectrum are due to the presence of adventitious carbon which appeared in all samples measured. These results suggest that etching at later times is due primarily to the removal/surface diffusion of gold atoms, rather than the removal of less noble metals in the starting alloy.[12–15]

The high aspect ratios of these materials (BET analyses showing area increases exceeding 14,000 fold[12,16] have been reported for nanoporous gold sheets) suggest that successfully fabricating cathodes consisting of MCOs adsorbed to SAMs on nanoporous gold could offer significant enhancements in electrochemical dioxygen reduction activity of enzymatic cathodes. Furthermore, reported interfacial ET rates for SAM-azurin electodes show that reduction of type 1 copper centers in proteins can occur at rates in the regime of 10^3 s^{-1}, far higher than the rates currently observed on porous carbon electrodes.[2,17]

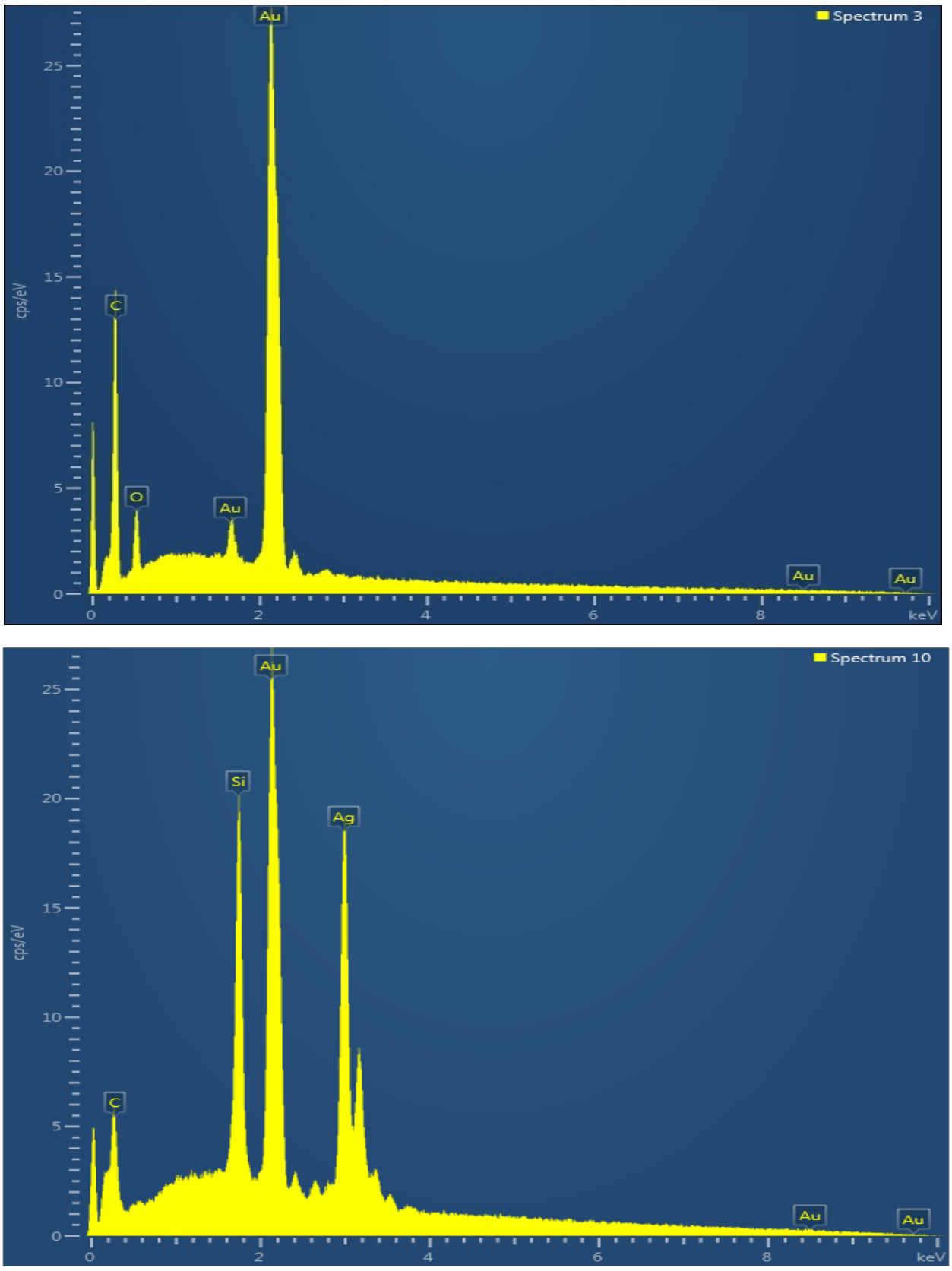

Figure 4-6

Electron dispersive spectra of gold leaf. Top: 30 minute etch (sample mounted on filter paper). Bottom: no etch control (note: here, sample was mounted on Si wafer, resulting in a background Si peak).

ii. Synthesis of a Pyrene-based Molecular Linker to control surface orientation of MCOs

In this section, we describe the synthesis of a novel, small-molecule bioconjugate intended to facilitate adsorption of a protein to graphite basal planes of HOPG through pi-stacking interactions with pyrene functional groups. The molecule of interest, N-(7-(3-iodopropanamido)-9*H*-fluoren-2-yl)-4-(pyren-1-yl)butanamide, is referred to as compound **A** from hereon. For use of this molecule, we have also constructed the G439C mutant of *Thermus thermophilus* laccase. Mutation at this position allows for covalent linkage of compound A at position 439 on laccase (primers and mass spec data in Appendix). This mutation was chosen because it both places the linker near the enzymes terminal electron acceptor, the type 1 active site. Furthermore, position 439 should allow for covalent through-bond tunneling to the type 1 center, as position 439 and the H443 ligand of the type 1 copper ion are on the same beta strand (G439C mass spec data in appendix).

While commercial bioconjugate pyrene compounds are available, these compounds generally feature linkers that are too short to allow reasonable degrees of freedom between the protein and the pyrene adsorbate. For example, in the case of 1-(pyrene) maleimide, the linker and pyrene are co-planar, a configuration that places considerable steric constraint between any protein featuring this linker and a surface on which we are trying to adsorb it using the pyrene group. This motivated our

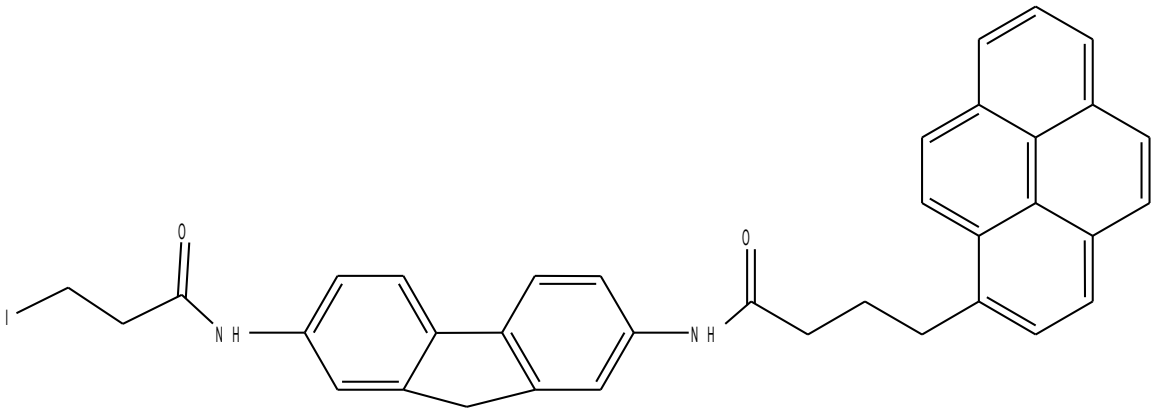

N-(7-(3-iodopropanamido)-9*H*-fluoren-2-yl)-4-(pyren-1-yl)butanamide

(A)

consideration of pyrene compounds featuring linkers long enough to allow reasonable amounts of torsional freedom between the protein and pyrene functionality.

In addition to these concerns, rationale for the incorporation of fluorene in the linker of compound A is founded on studies by Wenger and others, which have demonstrated the role of co-planarity of pi orbitals in facilitating fast ET rates in between model compounds featuring covalently linked donor and acceptor sites.[18–21] The co-planarity of pi-orbitals in adjacent phenyl groups is reinforced by the rigidity of the flourene structure, as opposed to dibenzyl substituents, where a single bond between benzene rings allows for rotation of the benzene rings relative to one another, allowing for thermal disruption of pi-pi overlap.[18,20] As a result, measured electronic couplings are greater in the case of molecular linkers featuring fluorene as opposed to those featuring alkyl-only or dibenzyl linkers.[18,21] Our intent is to exploit the property of forced co-planarity in fluorene and its derivatives to produce a linker that is more likely to facilitate fast ET between the protein active site and the electrode surface.

Methods & Materials

Synthesis

Pyrene butyric acid, pyrene butanoate succinimidyl ester, 2,7 diamino-flourene, 3-iodopropionic acid and N-(2 aminoethyl)-maleimide were all purchased from Sigma-Aldrich.

Compounds were made according to the following routes:

Compound A, method 1:

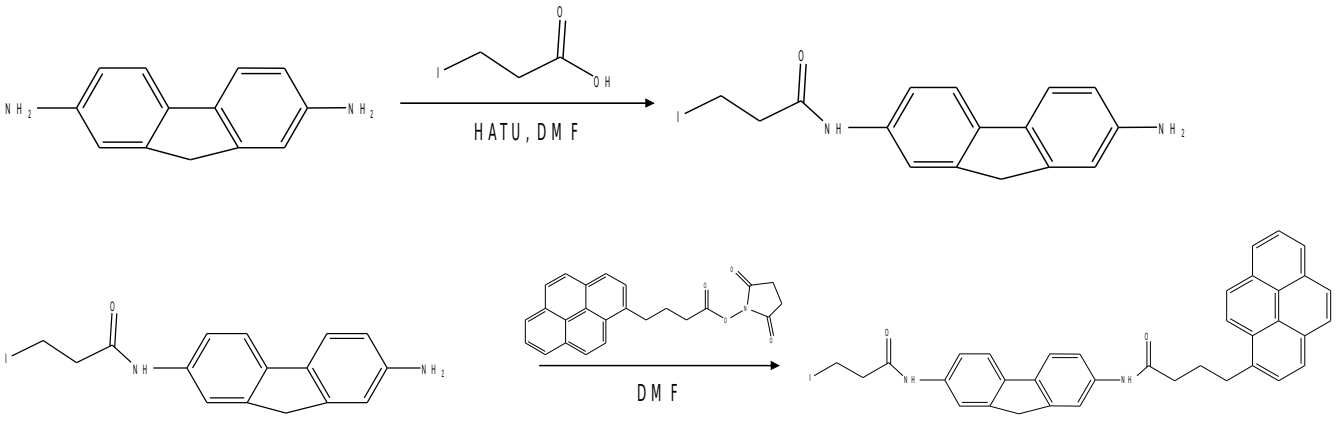

Compound A, method 2:

In practice, method 1 was found to be the best route for making compound A, as amide couplings using the succinimidyl ester of pyrene butyrate were found to yield much cleaner products than HATU couplings between pyrene butyric acid and terminal amines.

Synthesis of compound A according to method 1 was performed by dissolving 208 mg of 3-iodopropionic acid into 10-20 ml of dry DMF and stirring for 10 minutes in a round-bottom flask. Afterwards, 214 mg of 2,7 diamino fluorene and 390 mg of HATU were added to the solution and mixed for an additional 20 minutes. 82 μl of pyridine were then added to the reaction, which was then allowed to mix for 12 hours at room temperature. Product was isolated by adding cold water or saturated sodium chloride to the flask. The resulting solid (dark green) was then filtered over vaccum. Removal of residual starting carboxylic acid and amines were removed by washing the solid in saturated sodium bicarb. A final wash in a 3:1 methanol:water mixture followed by drying over vaccum yielded 2-iodopropylamide-7-amino fluorene, as confirmed by NMR. After extraction and cleaning, yield of this intermediate product was found to be 41% .The 2-iodopropylamide-7-amino fluorene intermediate was then dissolved in 3.0 ml DMF (70 mg) along with 71 mg of pyrene butyrate succinimidyl ester. The reaction was mixed for 16 hours at room temperature before extracting the product (brown) with 15 ml of saturated sodium chloride. The reaction was then filtered over a vaccum and cleaned in a mixture of diethyl ether and acetone. Additional cleans in methanol were found to improve purity

substantially. An 86% yield was found for this step.

UV-Vis

Measurements of molar absorptivitiy were performed by dissolving known masses of A in DMSO and forming ranges of dilutions that were in adherence to Beer's Law for all transitions of interest. Absorbance of each dilution was measured in a quartz cuvette, following blanking of the UV-vis spectrometer with a DMSO sample. Plots of species concentration vs. absorbance were then used to determine epsilon values of each molecule at each wavelength.

Results

2-iodopropylamide-7-aminofluorene

Dark Green Solid, ^{1}H NMR (300 Mhz, DMSO); δ 3.43 (t, 3H, alkyl), δ 3.70 (s, 2H, fluorene), δ 5.13 (s, 2H, amine), δ 6.52 (d, 1H, fluorene), δ 6.72 (s, 1H, fluorene), δ 7.40 (d, 2H, fluorene), δ 7.50 (d, 2H, fluorene), δ 7.76 (s, 1H, fluorene), δ 9.96 (s, 1H, amide). Residual Impurities and solvent give rise to resonances at δ 1.07 (q, diethyl ether), δ 2.07(s, acetone), δ 2.48 (s, DMSO), δ 2.98 (q, methanol OH), δ 3.31 (s, H_2O) and δ 3.87 (s, methanol CH_3). (Figure 4-4). Mass spectra (appendix) reveal a prominent peak for the molecular ion of this compound at m/z = 379.0 (expected: 378.2).

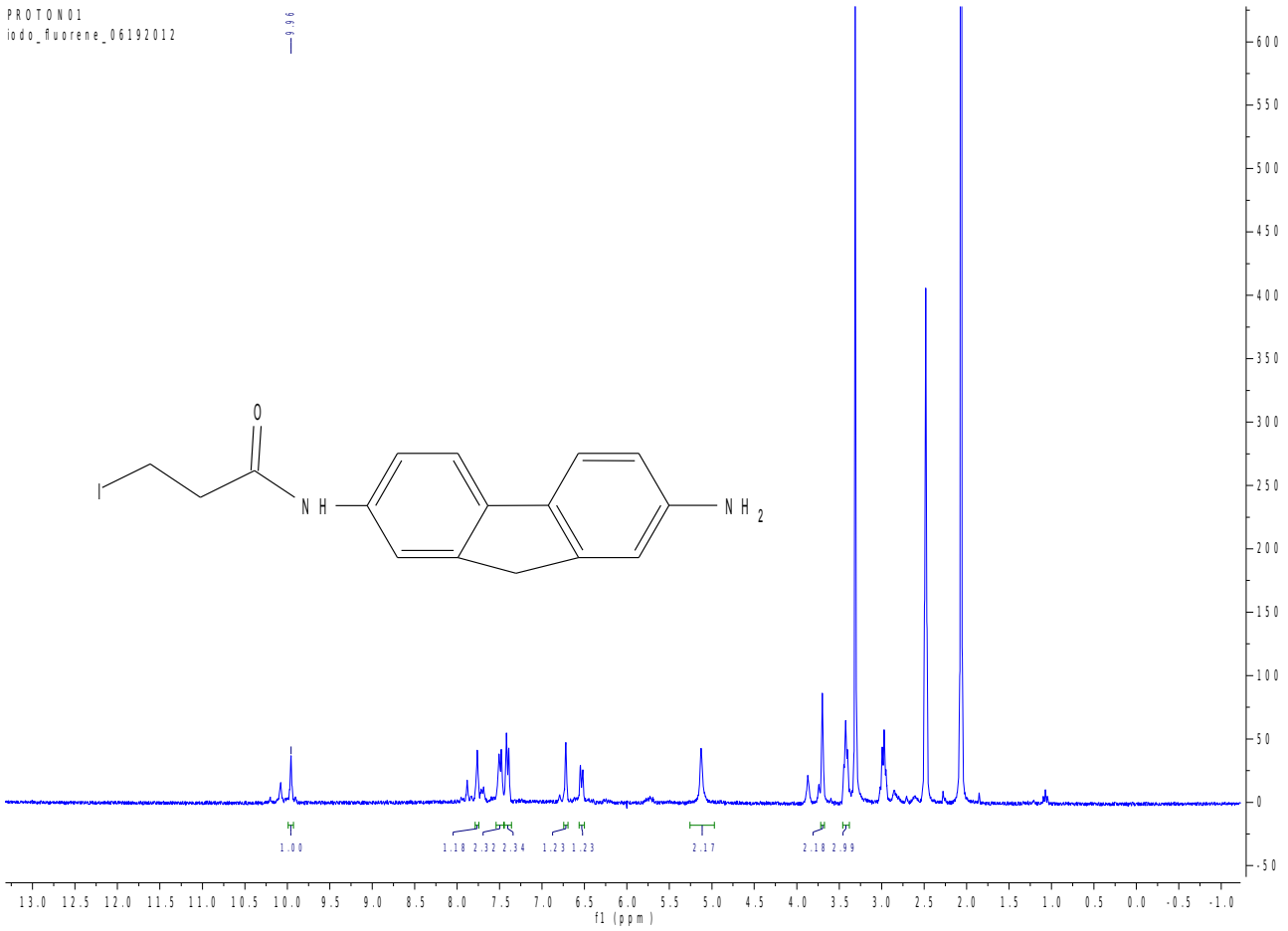

Figure 4-7

^{1}H NMR of 2-iodopropylamide-7-aminofluorene intermediate

Compound A

Brown Solid, ^{1}H NMR (300 Mhz, DMSO); δ 9.96 (s, amide), δ 8.15 ppm (m, 16H pyrene and fluorene), δ 7.68 (d, 1H, pyrene), δ 7.49 (d, 1H, fluorene), δ 3.40 (m, alkyl) and δ 2.83 ppm (s, 2 H fluorene). Lower peaks in the upfield region were not possible to assign due to obscuring solvent peaks (water, δ 3.33 and DMSO, δ 2.48). Mass spectroscopy in DMSO (Appendix) confirm synthesis of this compound, with peaks occurring at 649.1 (molecular ion + H; expected 648.13) and at 727.17 for the DMSO adduct of this molecule (expected mass for A+DMSO: 726.78).

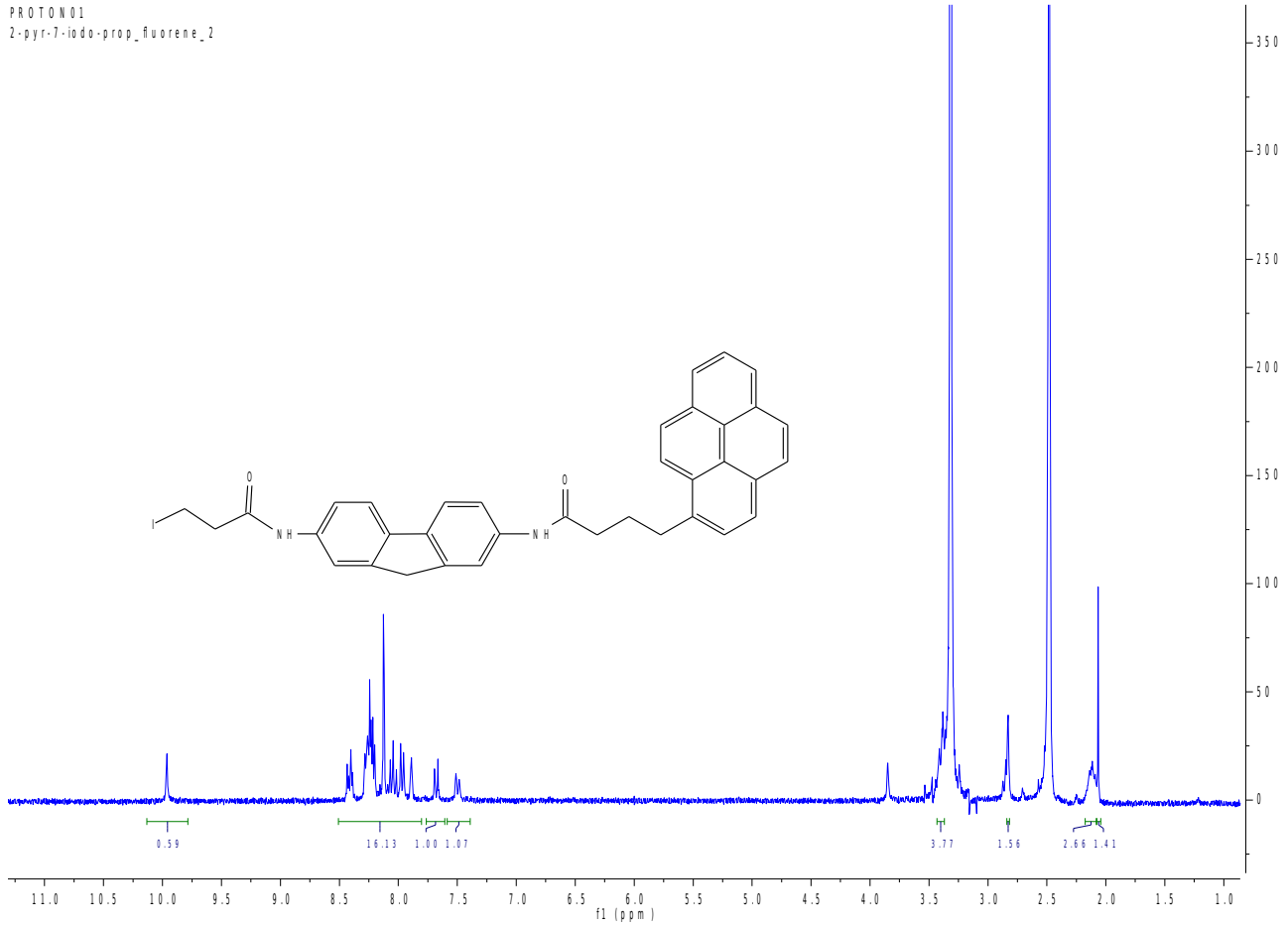

Figure 4-8

^{1}H NMR of compound A.

UV-vis absorption spectroscopy

Characterization via UV-vis reveals compound A to have an absorption spectrum that is readily described as a composite of characterstic flourene and pyrene spectra. The characterisitic intense transitions of pyrene occur at 330 and 345 nm. As expected, molar absorptivites of these transitions are similar to those of pyrene (ε_{330} = 43,00 M^{-1} cm^{-1}, ε_{345} = 46,000 M^{-1} cm^{-1}).

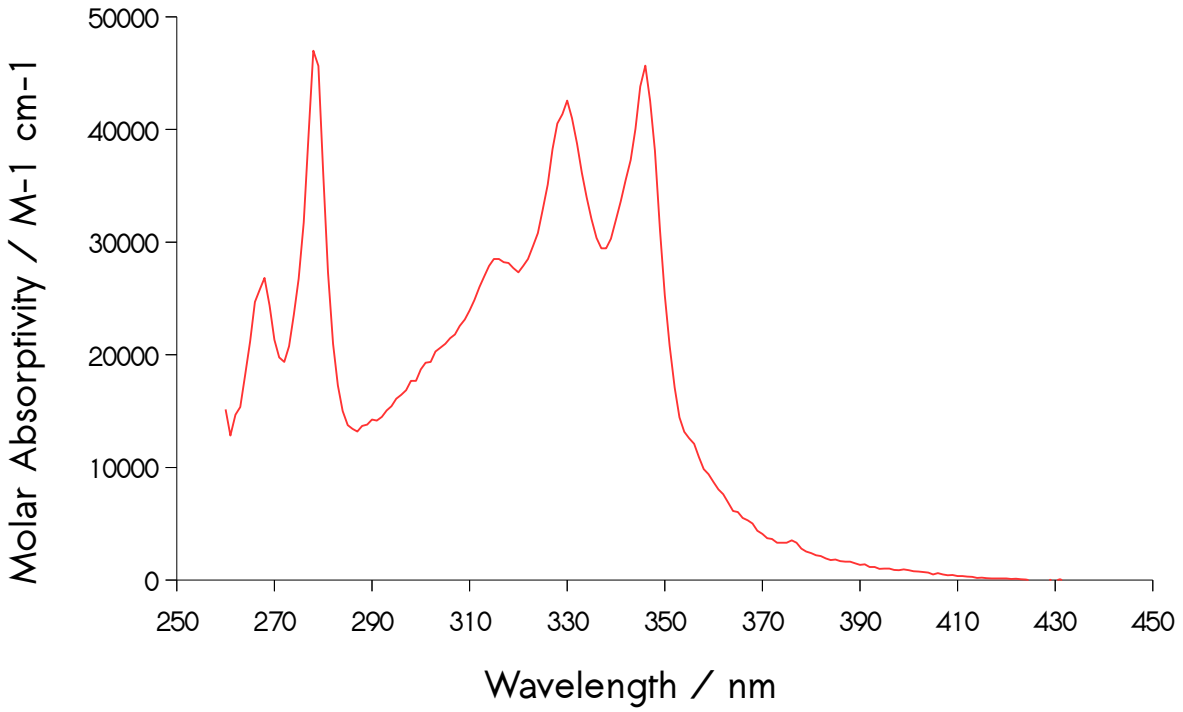

Figure 4-9
Absorption spectrum of compound A.

iii. Controlling MCO Surface Orientation with an Electric Field

Special Considerations

For our proposed scheme involving the orientation of an MCO in an electric field, we have identified the following requirements: (1) the protein must be charged, (2) the protein must have a net dipole, (3) the net dipole must lie along or near an axis that intersects the region of the protein that we wish to preferentially orient near an electrode surface (Figure 4-10) and (4) the dipole-field interaction energy must be above the threshold energy that results in the protein assuming random orientations under typical conditions in zero applied field. We suggest that this threshold should be determined by the average energy of molecular motions in solution under ambient conditions, which we approximate simply as ~ $0.5k_BT$, as given by the equipartition theorem for the case of 1 degree of translation motion. We only consider the 1-D case as the electric field only influences the protein along one translational coordinate. We make the reasonable assumption that a protein in solution, in the absence of any electric field, will exhibit no directional bias in its 3-D motion; that is, its time-averaged velocity will be zero at time-scales relevant to our study. This is supported by the fact that while particle *speed* induced by Brownian solvent fluctuations can be very fast (approximately 7.0 m/s for a 50 kda MCO in solution), the mean free path before collision is very short (only about 1 Å for a protein), with translational motion being dampened in roughly 10^{-13} s.[22] As our experiments will clearly be operating at timescales far longer than the sub-picosecond regime, we feel comfortable with our assumption of zero directional bias in no applied field.

Additionally, it is required that (5) the pH at which the protein exhibits a net charge must be the same pH at which it exhibits a net dipole. Furthermore, there must be agreement between the dipole direction and net charge to ensure that during application of the electric field, the result will be a protein that is translated toward a surface for deposition with an appropriate torque acting on the dipole that aligns our active site in the *same direction* as the enzyme's translational motion. For example, it is possible that under some conditions, the protein will have both a net

charge and a net dipole, but the dipole aligns the protein with the active site facing away from the surface intended for deposition. In principle, such a scenario would result in the surface and active site being positioned on opposite sides of the protein, with the consequent hampering or total inhibition of interfacial electron transfer to the active site during electrode catalysis. Between the two multicopper oxidases investigated by our group, the protein Copper Efflux Oxidase (CueO) satisfies all these requirements. Calculation of the CueO dipole using the Protein Dipole Moments Server (The Weizmann Institute) results in a net dipole of 639 debye and a net charge of -10 (-1.6×10^{-18} C) at pH 7.0. Examination of the protein structure for the calculated dipole reveals a dipole axis roughly intersecting the location of the type 1 copper active site, with the negative pole closest to the type 1 site. The calculated total charge and charge distribution are such that, in an applied electric field of sufficient intensity, these coulombic interactions should result in both a force that moves the protein towards a positively charged electrode and a torque on the CueO dipole that orients the type 1 active site with the same approximate directionality as the protein's translational vector, satisfying requirement (5).

The Protein Dipole Moments algorithm used for determining the CueO dipole does not account for the effects that the protein's bound copper ions have on electrostatics. However, we should expect that using a conservative assumption of no charge screening by residues in the protein, net charge would, at most, be reduced to -6 (-9.6×10^{-18} C) at pH 7.0. Furthermore, the trinuclear cluster, comprised of three copper ions, lies near the positively polarized region of the dipole. As a result, we should expect that factoring in the presence of the copper ions would, in fact, result in a slight *increase* of the calculated dipole moment in CueO. We can determine the electric field strength required to orient the protein dipole by subjecting our analysis to the constraint that $E_{dipole} \sim 0.5\ k_B T$. For a dipole of 639 debye (2.13×10^{-27} C m), the electric field strength must then be at least 6.3×10^{5} V m^{-1} in order to observe a field-dipole interaction equal to the energies of solvent thermal vibrations at room temperature. These high field strengths place stringent demands on the design of the

cell to be used for electrophoretic protein orientation and deposition; such device specifications are outlined in the following section.

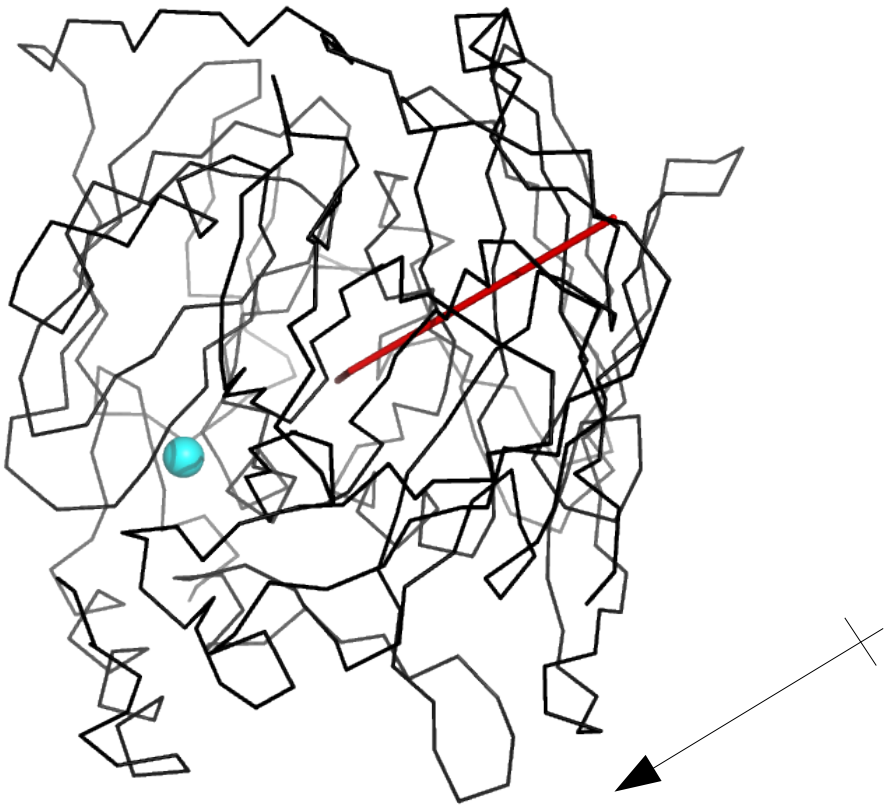

Figure 4-10

The crystal structure of Copper Efflux Oxidase (PDB: 1kv7). Shown is the type 1 electron acceptor (cyan) and the calculated net dipole moment for the protein at pH 7.0 (red line). Note that the dipole axis almost directly intersects the T1 copper ion. The arrow indicates the dipole orientation, with the arrowhead denoting the direction of negative polarization.

Proposed Methods

Deposition Cell design

Since electrochemical water oxidation is generally observed between 1.2-1.8 V (depending on the electrode material), we cannot establish an electric field of necessary strength with our electrodes resting inside a deposition cell of macroscopic dimensions (> 1 mm), as in the case of cells

used for DNA / protein gel electrophoresis. As a result, the cell for enzyme deposition will consist of two copper plate electrodes of identical geometry (1 cm^2 square electrodes, or 1 cm diameter circular electrodes) pressed flush against the outside of a 1 cm wide quartz cell (Starna Cells) which will contain a dilute (~1 μm) solution of CueO in pH 7.0, 5.0 mM sodium acetate buffer. A third electrode, featuring a porous carbon substrate, is to serve as our deposition surface and will be immersed in the enzyme solution, in a region between the copper plates, just before deposition is started. Note that this electrode is not to be electrically wired to the high voltage circuit. We have chosen a quartz holding cell because of its high tolerance for intense electric fields before exhibiting signs of dielectric breakdown, which occurs at fields as high as 10^7 – 10^9 V m^{-1} for this material.[23] In addition, our experiment may be conducted in ambient atmospheres, as our applied field strength (6.25×10^5 V m^{-1}) is less than the reported value for dielectric breakdown of air (3×10^6 V m^{-1}).[24] A 500 kV DC power supply (Spellman High Voltage Electronics Corp.) should allow us to achieve the needed field strength easily. As a result, we anticipate that the possibility of electrical shorting or arcing of the proposed device, stemming from dielectric breakdown of either the cell components or air itself, would not be an issue. Following deposition, the electrode serving as the deposition surface can be removed and have its electrochemical activity tested using the methods and techniques outlined in Chapter I.

We have derived equations of motion describing the expected behavior of CueO under conditions of electrophoretic deposition (Appendix, A.11). Using these, we show via simulation (Figures 4-11,12) that for proteins treated as a charged particles in solution under the influence of both the accelerating forces of an applied electric field and drag forces from surrounding solvent, the number of species depositing on a surface after some time, t, can be modeled by:

$$n(t) = N_A M \pi r^2 \frac{qE_0}{\delta \kappa}\left[t + RC\left(1 + \frac{m}{mRC - \delta}\right)\exp\left(-t/RC\right)\right] \quad \text{(eq. 4-2)},$$

for circular electrodes. For a cell using square electrodes, n(t) is calculated using:

$$n(t) = N_A M s^2 \frac{qE_0}{\delta \kappa}[t + RC\left(1 + \frac{m}{mRC - \delta}\right)\exp\left(-t/RC\right)] \qquad \text{(eq. 4-3)}.$$

Here, *M* is the enzyme concentration (molar), while *r* and *s* are electrode radii and side lengths for the respective cases of circular and square electrodes. E_o, the equilibrium field strength, is given by $E_o = V_o / d$, where V_o is the applied voltage and *d* is the electrode separation distance (here, dictated by the cuvette's width). The electric field strength in solution is attenuated by the solvent dielectric constant, κ, which is 80 for water. The '*m*' term denotes a protein mass in kg, while *q* is the net charge on the protein in coulombs and *t* is the deposition time in seconds.

The parameter δ gives the solution drag coefficient with units of N sec m^{-1}.[22] For our simulations, we use a value of 10^{-10} N sec m^{-1}, a typical value of the solvent drag coefficient for a protein the size of CueO.[22] The term δ is defined by Stokes' equation for fluid drag force:

$$F_{drag} = \delta V = \pi \mu d V \qquad \text{(eq 4-4)},$$

where μ is the dynamic viscosity of water, V is the particle velocity and d is the particle diameter. The Stokes' equation assumes laminar, rather than turbulent, fluid flow. We can check for whether our system satisfies this requirement at *all* timescales by determining the value of the Reynold's number, N_R, in the upper limit of the protein's velocity during deposition. If the condition for laminar flow, $N_R < 1$, is satisfied by our proposed experimental conditions, the assumptions under which we derived the deposition function are valid. We can perform this check readily by calculating the upper limit of the protein's velocity (i.e., determining the highest possible value of N_R). This will occur for t >> RC, where the function describing the protein's velocity:

$$v(t)=\frac{E_0 q}{\delta\kappa}[1-\exp(-t/RC)-\frac{m}{\delta RC-m}\exp(-t/RC)] \quad \text{(eq. 4-5)}$$

converges to the quantity $E_0 q\ \delta^{-1}\kappa^{-1}$, the maximum velocity assumed by the protein moving under the influence of an electric field. Under our stated conditions, v(t) reaches a limiting value of 0.013 cm s^{-1}. Using this value, we then solve for N_R according to eq. 4-6:

$$N_R=\frac{\rho V d}{\mu} \quad \text{(eq. 4-6),}$$

where, again, ρ is the density of water (1.0 kg m^{-3}), d is the enzyme diameter (~ 6 x 10^{-9} m) and μ is the dynamic viscosity of water (.001 kg m^{-1} s^{-1}). The resulting value of the Reynolds number (1 x 10^{-9}) falls far below the threshold for turbulent flow, so we conclude that application of the Stokes' law for describing fluid drag in our system is appropriate.

Appearance of the quantity *RC* stems from the time-dependence of the electric field intensity when charging a parallel-plate capacitor:

$$E(t)=E_0[1-\exp(-t/RC)] \quad \text{(eq. 4-7).}$$

As a result of the finite amount of time it takes to charge a capacitor (a property dictated by its time constant, RC), during the charging process (before E(t) = E_o), enzymes undergo non-linear acceleration due to the changing value of the electric field. Only when the equilibrium field strength is reached does the force exerted on the protein by the electric field become constant. This time-dependent field complicates the problem of determining the number of enzymes deposited and the time it takes for them to deposit on some surface. However, our model captures this extra degree of complexity and should allow for improved control over the number of deposited enzymes relative to naïve descriptions which assume a perfectly uniform electric field profile at all time scales (i.e., the limit of infinitely fast capacitive charging). Note that at long timescales (t >> RC), n(t) converges to a function exhibiting a purely linear dependence on the time allowed for deposition. This result agrees

well with empirical observations in the literature, which show linear scaling between time allowed in electrophoresis and the extent of ion migration.

The RC time constant can be measured through charging the cell to its equilibrium voltage and then discharging, monitoring of the discharge current over time. The resulting plot should give a mono-exponential decay given by:

$$i(t)=i_0\exp(-t/RC) \qquad \text{(eq. 4-8)}.$$

Fitting the data to this decay expression allows for extraction of a characteristic rate constant for capacitive current decay in our device, the reciprocal of which is the cell's RC time constant.

Discussion

Using our derived equations for the motion of our protein in the presence of an external electric field, we have been able to simulate how CueO should deposit on an electrode surface. Figures 4-11 and 4-12 highlight the two important limiting cases of deposition behavior of CueO, which occur when t ~ RC and t >> RC. From these data, we have been able to determine that for the device configuration we've described here, it should be possible to modify an electrode with ~ 10^{13} oriented enzymes per square centimeter after a mere 100 seconds of deposition. This compares very favorably with our current in-house methods, where saturating the surface with approximately 10^{13} enzymes takes two hours with passive adsorption. This method also has the benefit of allowing us to use much lower concentrations of enzyme to produce catalytically active electrodes. Currently, 1 μM represents a lower limit when fabricating these cathodes via passive adsorption. However, eqs. 4-2 and 4-3 indicate that if we wish to deposit for longer times, we have the option of achieving similar degrees of surface coverage while using significantly lower concentrations of CueO.

The torque applied on the CueO dipole should result in enzyme layers that have more specific orientations than in the case of randomly adsorbed

enzyme populations. With the experiment as designed here, electric field application should result in the type 1 copper site in CueO being oriented near the surface on which we are depositing. Therefore, we expect that testing the electrode for catalytic activity will exhibit enhanced catalytic activity relative to electrodes where CueO has been randomly adsorbed, as a result of an increased average value of the electronic coupling (H_{AB}) between the type 1 site and the electrode surface. The exact magnitude of this enhancement is difficult to predict. However, we can try and gain rough approximations for the coupling enhancement by first applying the properties of a uniform (maximum entropy) distribution to our system, as done in Chapter II. The expectation value of any continuously varying quantity is given by:

$$<x>=\int xP(x)dx \qquad \text{(eq. 4-9)},$$

where the definition of expectation value is mathematically isomorphic to the average value of x. For a uniform distribution,

$$P(x)=\frac{1}{x_{max}-x_{min}} \qquad \text{(eq. 4-10)}.$$

Applying this probability distribution to eq. 4-9 results in the expectation value for a uniform distribution being defined as simply the average of two distances:

$$<x>=\int_{x_{min}}^{x_{max}} x\frac{1}{x_{max}-x_{min}}dx \;=\; \frac{x_{max}^{\,2}-x_{min}^{\,2}}{2(x_{max}-x_{min})} \;=\; \frac{1}{2}(x_{max}+x_{min}) \qquad \text{(eq. 4-11)}.$$

Using the CueO crystal structure (PDB: 1KV7), the closest distance between the type 1 site and the protein surface is 10 angstroms. This value represents an ideal scenario where our deposition method results in a perfectly oriented system, with the type 1 site lying only 10 angstroms from the electrode surface (r_{min} = 10 angstroms). The longest path between the type 1 center and the protein surface is about 60 angstroms, according

to the crystal structure. From eq. 4-11, we then obtain an average value of 35 angstroms for the distance of the type 1 site in the case where enzymes are randomly oriented on an electrode. We now consider the situation where our strategy succeeds, with field orientation yielding a reduced average distance between the type 1 site in CueO and the electrode surface. For the sake of rigor and realism, we assume that our ability to orient the protein deviates far from ideality, with the electric field only reducing the average type 1-electrode distance to 3 x r_{min} = 30 angstroms. Even with such a conservative estimate, the resulting electronic coupling enhancement is dramatic. Using eq. 4-12, which provides the relation of the electronic coupling strength between an electron (or hole) donor (A) and acceptor (B):

$$H_{AB} = H^{0}_{AB} \exp\left(-\frac{1}{2}\beta(r - r_0)\right) \qquad \text{(eq. 4-12)},$$

where $r_{min} = r_0$. It can be readily shown that the degree of enhancement for the case we've outlined will be:

$$\frac{H_{AB}(r = 30A)}{H_{AB}(r = 35A)} = \exp(2.5\beta) \quad .$$

The decay constant, β, has been experimentally determined to be 1.1 A^{-1} for beta-sheet proteins such as members of the MCO family.[25–27] Evaluating the above expression with this value of the decay constant yields a total H_{AB} enhancement of 16 fold. Equation eq. 4-1 states that the rate of interfacial electron transfer will scale proportionally with H_{AB}^2. From this, our estimates, which assume that an applied electric field can only reduce the average donor-acceptor distance by a mere 5 angstroms, rather than the 25 angstrom reduction for an ideal case, still produces an enhancement of 245 fold for interfacial electron transfer rates. It should be appreciated that this factor of 245 is on par with our target rate enhancement of two orders of magnitude. The implication of this exercise estimating the potential coupling enhancement is significant, as it suggests electric field orientation only needs to achieve marginal

reductions in the average donor-acceptor distance for the observation of appreciable enhancements in interfacial electron transfer.

It should be emphasized that this model only calculates the number of charged species that will be *arriving* at a surface located at some position, l, after some time given for deposition. It does not predict the number of these species that will be retained on the surface once they reach it. Whether or not a CueO molecule will successfully adhere to the deposition surface once it has been reached is a function of the adsorption characteristics of the surface itself. If desired, it should be possible to combine our description of electrophoretic motion with a suitable adsorption isotherm, such as the Langmuir adsorption model. Doing so may allow for improved simulations that capture both phases of deposition — electrophoretic flux to the surface and subsequent surface adsorption processes — in order to gain more accurate predictions of enzyme surface coverage.

Conclusions

Porous gold SAMs and small molecule linkers may allow for the creation of multicopper oxidase cathodes exhibiting enhanced interfacial ET properties.

Furthermore, it may be possible to address the current problem of slow interfacial electron transfer rates which plague biochemical cathodes by making high-surface area SAMs or controlling their orientation on surfaces using molecular linkers or electric fields. Here, we have identified the enzyme CueO as a prime candidate for testing such a fabrication method. The intrinsic electrostatic properties of this protein should allow both its motion and orientation to be controlled by an electric field. In particular, the position of its internal dipole relative to the type 1 site in the protein, which has been shown to serve as the enzyme's electron acceptor when reducing oxygen electrocatalytically, should enable us to orient this site proximal to an electrode surface for enhanced electronic coupling. As a complement to this qualitative concept, we have outlined a quantitative model that should provide a reasonable description of CueO's translational motion under the influence of an

electric field. The model incorporates the extra dimension of the non-linear, time-dependent electric field which exists in a charging capacitor at short timescales, enabling finer control over enzyme deposition behavior, relative to models assuming a constant electric field at all times. Finally, we've managed to vet this strategy by providing reasonable estimates for the extent of electronic coupling and consequent rate enhancement that may be expected from our deposition methodology.

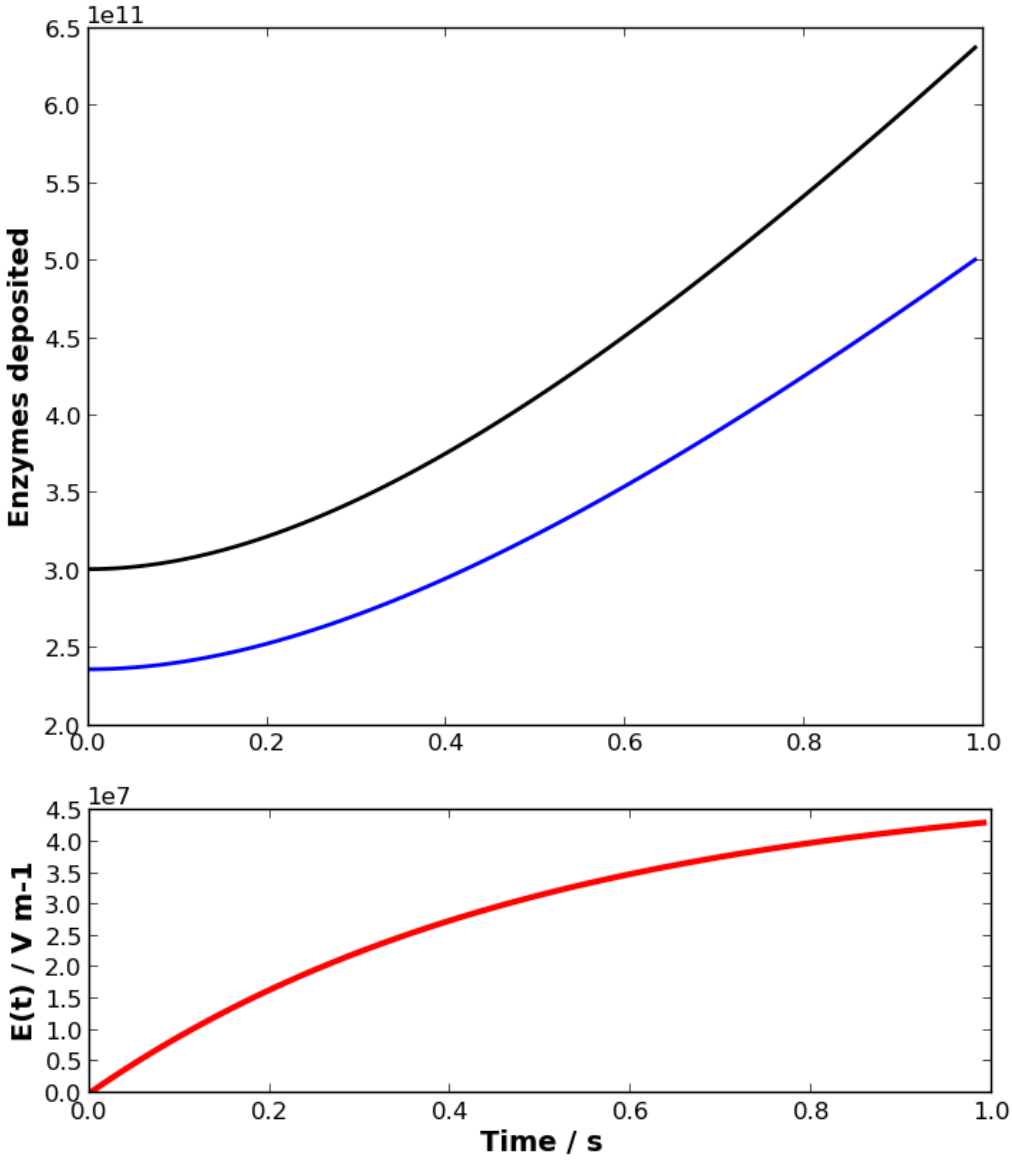

Figure 4-11

A simulation of CueO enzymes depositing on a surface for electric fields applied at short timescales (calculated using eqs. 4-2,3). As implied by the lower subplot showing the time-evolution of the electric field, the number of enzymes reaching the surface displays a non-linear time dependence at times on the order of RC. Black = square electrodes, blue = circular electrodes. *Simulation parameters:* ([CueO] = 1 μM, electrode diameter = 0.5 cm, electrode spacing = 1 cm, protein mass = 8.9×10^{-23} kg, protein charge = 1.6×10^{-18} C, $E_o = 6.25 \times 10^5$ V m^{-1}, RC = 0.5 s)

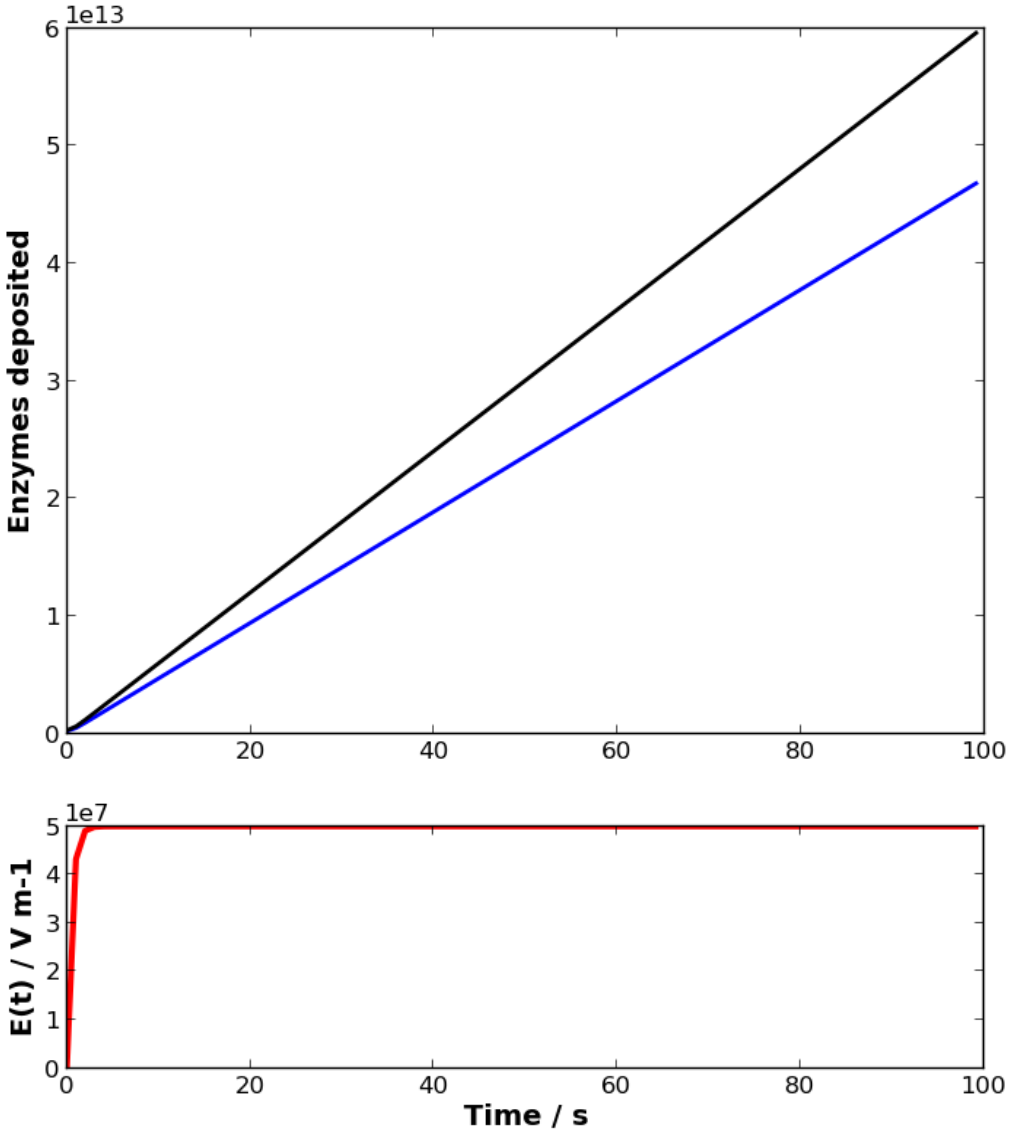

Figure 4-12

A simulation of CueO enzymes depositing on a surface during electric field application at longer times. The linearity now observed in the deposition function's time dependence is a result of the constant value assumed by the electric field when t >> RC (subplot). Black = square electrodes, blue = circular electrodes.

Simulation parameters:

([CueO] = 1 μM, electrode diameter = 0.5 cm, electrode spacing = 1 cm, protein mass = 8.9×10^{-23} kg, protein charge = 1.6×10^{-18} C, E_o = 6.25×10^{5} V m^{-1}, RC = 0.5 s)

References

(1) Finklea, H. O.; Hanshew, D. D. *J. Am. Chem. Soc.* **1992**, *114*, 3173–3181.

(2) Khoshtariya, D. E.; Dolidze, T. D.; Shushanyan, M.; Davis, K. L.; Waldeck, D. H.; Eldik, R. van *PNAS* **2010**, *107*, 2757–2762.

(3) Fujita, K.; Nakamura, N.; Ohno, H.; Leigh, B. S.; Niki, K.; Gray, H. B.; Richards, J. H. *J. Am. Chem. Soc.* **2004**, *126*, 13954–13961.

(4) Udit, A. K.; Hill, M. G.; Bittner, V. G.; Arnold, F. H.; Gray, H. B. *J. Am. Chem. Soc.* **2004**, *126*, 10218–10219.

(5) Van der Felt, C.; Hindoyan, K.; Choi, K.; Javdan, N.; Goldman, P.; Bustos, R.; Star, A. G.; Hunter, B. M.; Hill, M. G.; Nersissian, A.; Udit, A. K. *Journal of Inorganic Biochemistry* **2011**, *105*, 1350–1353.

(6) Gorodetsky, A. A.; Barton, J. K. *Langmuir* **2006**, *22*, 7917–7922.

(7) Zendejas, F. J.; Meagher, R. J.; Stachowiak, J. C.; Hayden, C. C.; Sasaki, D. Y. *Chem. Commun.* **2011**, *47*, 7320–7322.

(8) Kuznetsov, B. A.; Byzova, N. A.; Shumakovich, G. P. *Journal of Electroanalytical Chemistry* **1994**, *371*, 85–92.

(9) Gorin, C. F.; Beh, E. S.; Kanan, M. W. *J. Am. Chem. Soc.* **2012**, *134*, 186–189.

(10) Gorin, C. F.; Beh, E. S.; Bui, Q. M.; Dick, G. R.; Kanan, M. W. *J. Am. Chem. Soc.* **2013**, *135*, 11257–11265.

(11) Ding, Y.; Kim, Y.-J.; Erlebacher, J. *Advanced Materials* **2004**, *16*, 1897–1900.

(12) Scanlon, M. D.; Salaj-Kosla, U.; Belochapkine, S.; MacAodha, D.; Leech, D.; Ding, Y.; Magner, E. *Langmuir* **2012**, *28*, 2251–2261.

(13) Jia, F.; Yu, C.; Ai, Z.; Zhang, L. *Chem. Mater.* **2007**, *19*, 3648–3653.

(14) Ciesielski, P. N.; Scott, A. M.; Faulkner, C. J.; Berron, B. J.; Cliffel, D. E.; Jennings, G. K. *ACS Nano* **2008**, *2*, 2465–2472.

(15) Shulga, O. V.; Jefferson, K.; Khan, A. R.; D'Souza, V. T.; Liu, J.; Demchenko, A. V.; Stine, K. J. *Chem Mater* **2007**, *19*, 3902–3911.

(16) Hodge, A. M.; Hayes, J. R.; Caro, J. A.; Biener, J.; Hamza, A. V. *Advanced Engineering Materials* **2006**, *8*, 853–857.

(17) Yokoyama, K.; Leigh, B. S.; Sheng, Y.; Niki, K.; Nakamura, N.; Ohno, H.; Winkler, J. R.; Gray, H. B.; Richards, J. H. *Inorganica Chim Acta* **2008**, *361*, 1095–1099.

(18) Wenger, O. S. *Chem. Soc. Rev.* **2011**, *40*, 3538–3550.

(19) Wenger, O. S. *Acc. Chem. Res.* **2010**, *44*, 25–35.

(20) Walther, M. E.; Wenger, O. S. *Inorg. Chem.* **2011**, *50*, 10901–10907.

(21) Wenger, O. S. *Inorganica Chimica Acta* **2011**, *374*, 3–9.

(22) Fall, C. P.; Marland, E. S.; Wagner, J. M.; Tyson, J. J. *Computational Cell Biology*; Springer, 2002.

(23) Serway, R. A.; Vuille, C.; Faughn, J. S. *College Physics*; Cengage Learning, 2008.

(24) Tipler, P. A. *College Physics*; Worth Publishers, 1987.

(25) Gray, H. B.; Winkler, J. R. *Chemical Physics Letters* **2009**, *483*, 1–9.

(26) Edwards, P. P.; Gray, H. B.; Lodge, M. T. J.; Williams, R. J. P. *Angewandte Chemie International Edition* **2008**, *47*, 6758–6765.

(27) Onuchic, J. N.; Beratan, D. N.; Winkler, J. R.; Gray, H. B. *Annual Review of Biophysics and Biomolecular Structure* **1992**, *21*, 349–377.

Appendix

A.1 Mass Spectra (MALDI-TOF) of Proteins

WT *Thermus thermophilus* strain HB27 Laccase

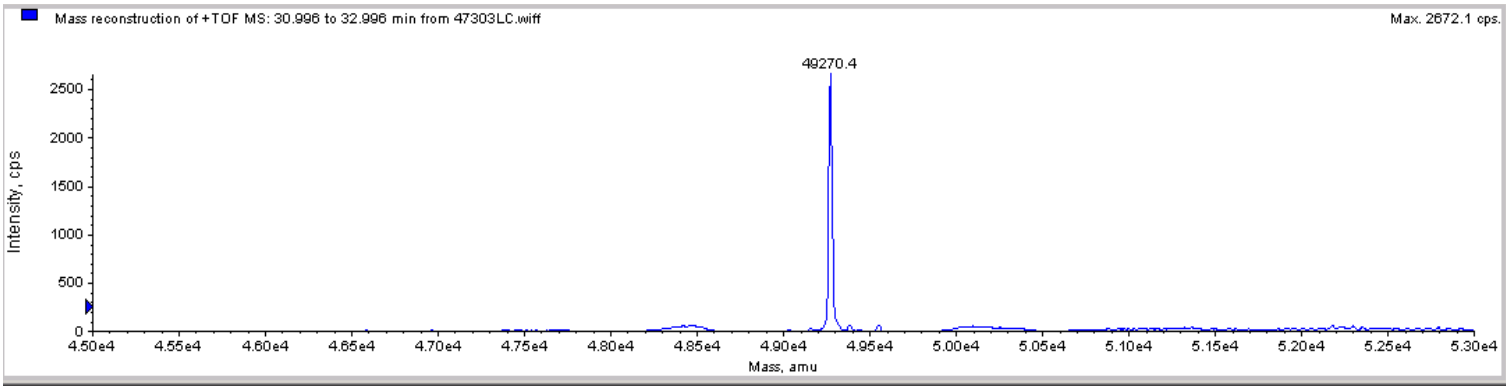

M455F

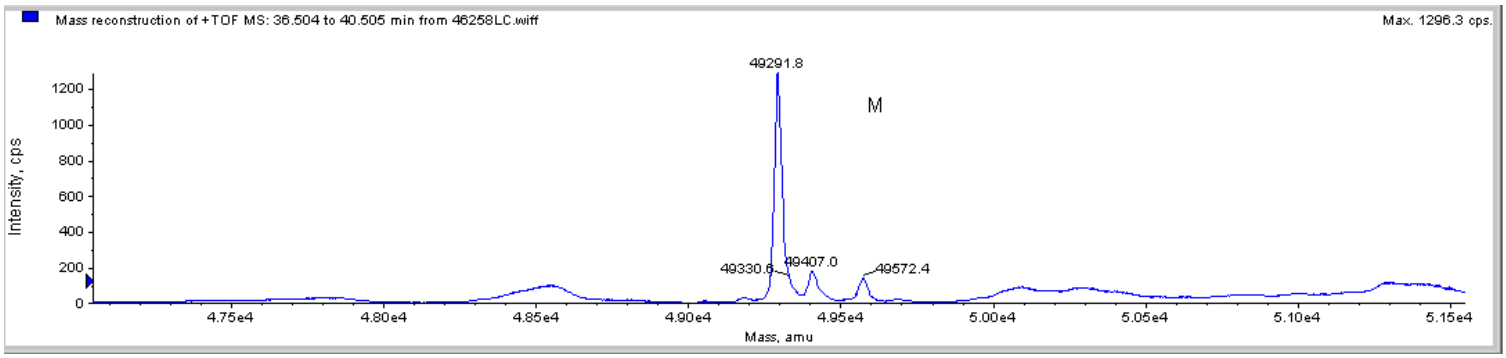

M455L

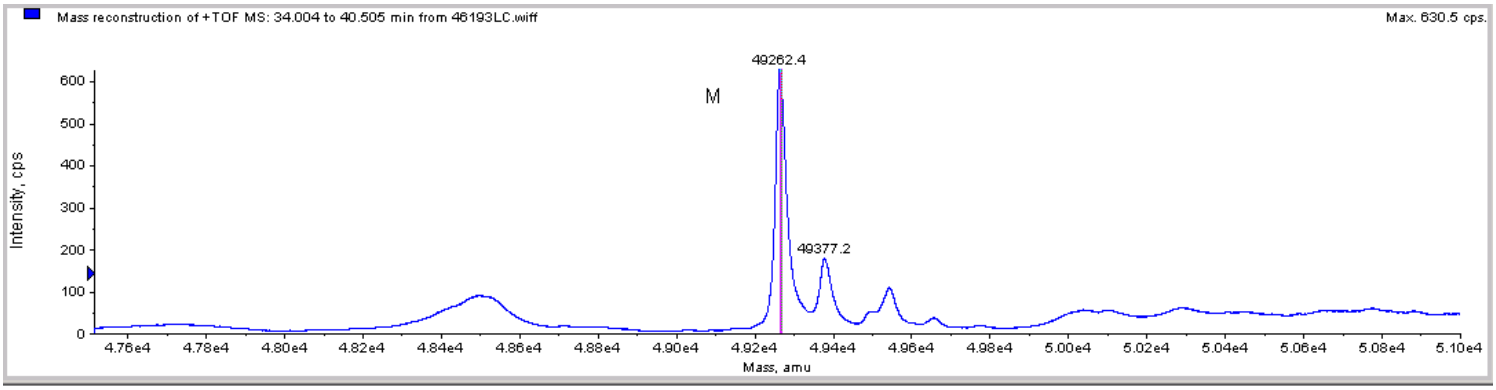

E352A

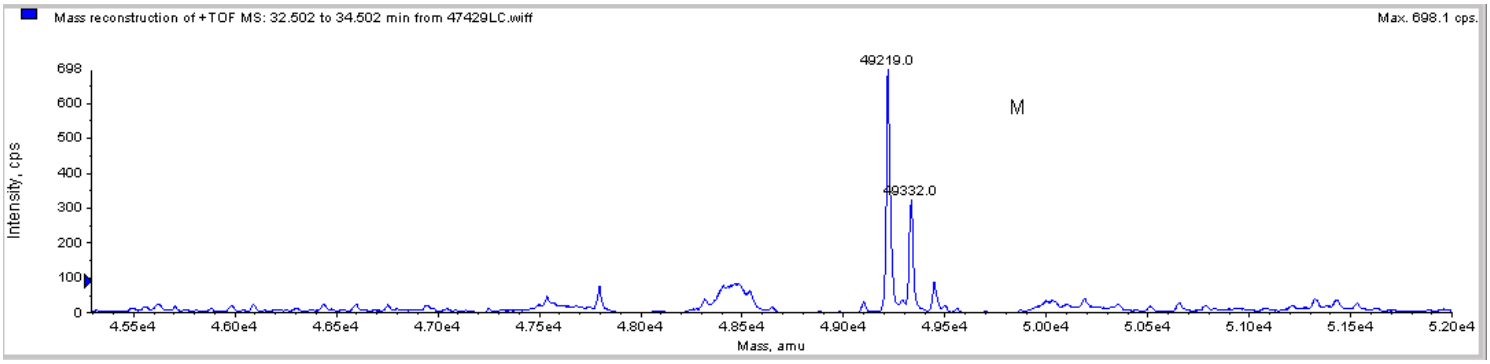

H398M

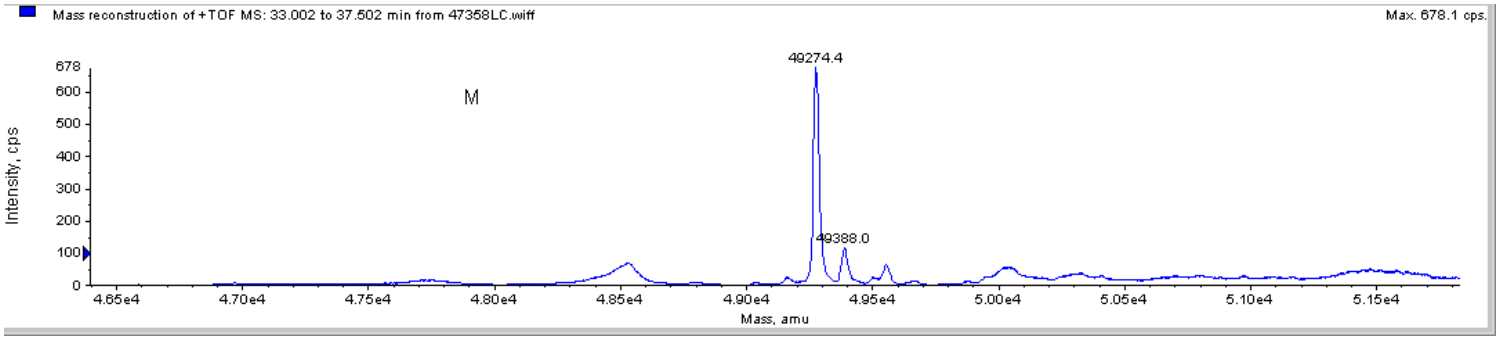

H135M

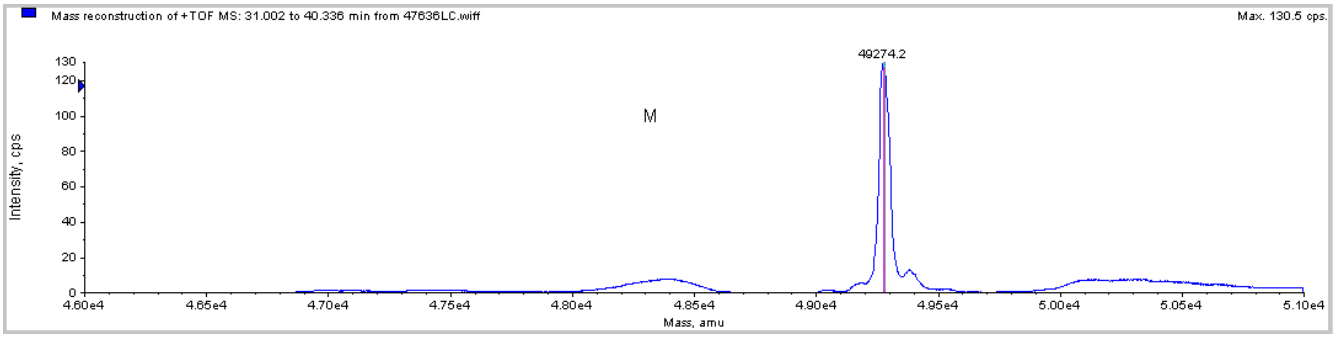

H398M/H135M

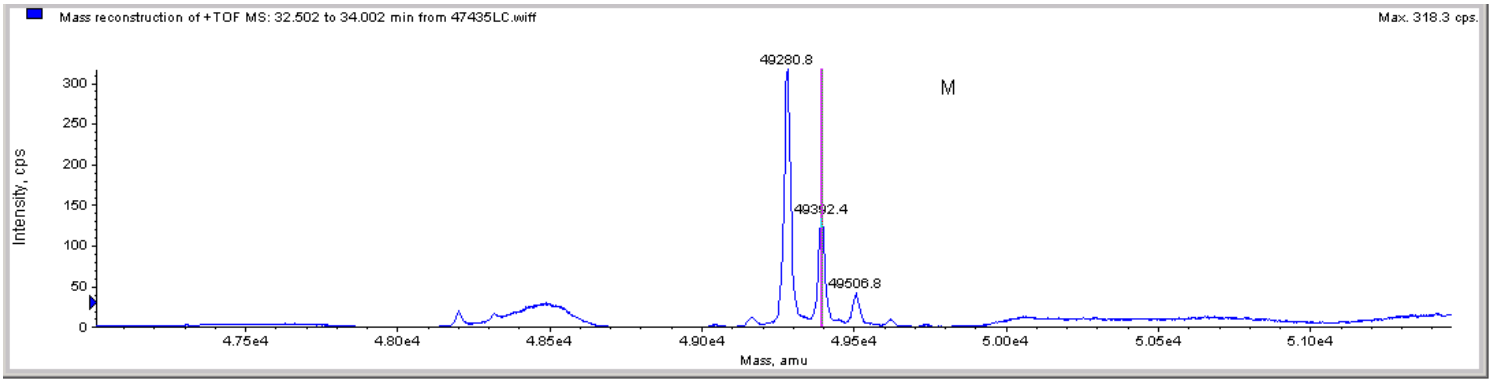

G439C

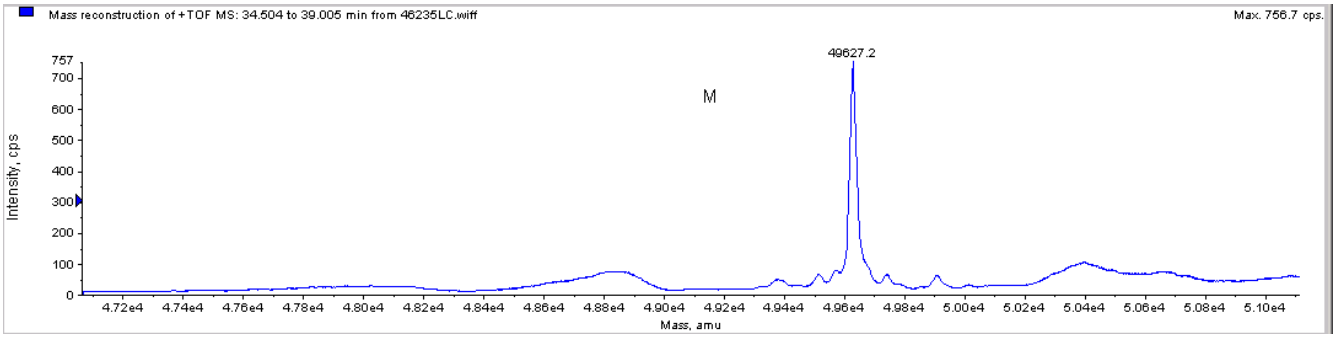

The minor higher molecular weight peaks in the spectra for M455L, M455F, G439C, E352A and H398M laccases represent mature forms of these enzymes where post-translational modification of the N-terminus results in minor products that are 1 and 2 amino acids longer than the main peak.

A.2 DNA Mutagenesis & Cloning Primer Sets

Note: primers used for creation of the G439C construct assume the laccase gene is in the pET-22b (+) vector (Novagen). For other vectors, the G439C reverse primer must be re-designed.

WT (cloning):

EcoR1
Fwd (5' → 3'): GGATCC G ATG CTG GCG CGC AGG AGC TTT CTC CAA (34 bp)

Bam H1
Rev (5' → 3'): C GAA TTC CTA ACC CAC CTC GAG GAC TCC CAT CAT CCC (34 bp)

M455F * *
Fwd (5' → 3'): CAC GAG GAC CGG GGG TTT ATG GGA GTC CTC GAG (33 bp)
H E D R G F M G V L E

Rev (5' → 3'): CTC GAG GAC TCC CAT AAA CCC CCG GTC CTC GTG (33 bp)

M455L *
Fwd (5' → 3'): CAC GAG GAC CGG GGG CTG ATG GGA GTC CTC GAG (33 bp)
H E D R G L M G V L E

Rev (5' → 3'): CTC GAG GAC TCC CAT CAG CCC CCG GTC CTC GTG (33 bp)

E352A *
Fwd (5' → 3'): CGC CTG GTC CTC ACC GCG GAC ATG ATG GCC GCC (33 bp)
R L V L T A D M M A A

Rev (5' → 3'): GGC GGC CAT CAT GTC CGC GGT GAG GAC CAG GCG (33 bp)

M195P *
Fwd (5' → 3'): G CAC ACC CCC ATG GAC TGG CCG AAC GGG AAG GAG GGC (37 bp)
H T P M D W P N G K E G

Rev (5' → 3'): GCC CTC CTT CCC GTT CGG CCA GTC CAT GGG GGT GTG C (37 bp)

H135M * * *
Fwd (5' → 3'): GGT ACC TTC TGG TAC ATG CCC CAC CTG CAC (30 bp)
G T F W Y M P H L H

Rev (5' → 3'): GTG CAG GTG GGG CAT GTA CCA GAA GGT ACC (30 bp)

H398M * * *
Fwd (5' → 3'): CCC TTC CAC CTC ATG GTC CAC CCC TTC (27 bp)
P F H L M V H P F

Rev (5' → 3'): GAA GGG GTG GAC CAT GAG GTG GAA GGG (27 bp)

G439C * *

Fwd (5'->3'): GGA GTC CTC GAG GTG TGC TAG GAA TTC GAG CTC CGT CGA C (40 bp)

G V L E V C stop E F E L R R

Rev (5'->3'): G TCG ACG GAG CTC GAA TTC CTA GCA CAC CTC GAG GAC TCC (40 bp)

A.3 The Gene of WT *Thermus thermophilus* laccase

The gene presented here was used for all studies and mutagenesis work in this thesis. The codon usage of this particular gene is *not* the *E. coli* K12 codon-optimized form of the laccase ORF.

ATGCTGGCGCGCAGGAGCTTTCTCCAAGCGGCGGCGGGCAGTCTGGTCCTGGGCCTG
GCCCGGGCCCAAGGCCCTTCCTTCCCCGAGCCCAAGGTGGTGCGGAGCCAGGGCGGC
CTCCTCTCCCTGAAGCTTTCTGCCACCCCCACCCCGCTTGCCCTGGCGGGGCAAAGGG
CCACCCTCCTCACCTACGGGGGGAGCTTTCCCGGGCCCACCCTCCGGGTCCGCCCCAG
GGACACGGTGCGCCTCACCCTGGAAAACCGCCTTCCCGAGCCCACCAACCTCCACTGG
CACGGCCTGCCCATCTCCCCTAAGGTGGACGACCCCTTCCTGGAGATCCCCCCGGGGG
AGAGCTGGACCTACGAGTTCACCGTTCCCAAGGAGCTGGCAGGTACCTTCTGGTACCAC
CCCCACCTGCACGGCCGGGTAGCCCCCCAGCTCTTTGCCGGCCTCCTGGGAGCCCTCG
TGGTGGAAAGCTCCCTGGACGCCATCCCCGAGCTCAGGGAGGCGGAGGAGCACCTCCT
CGTCCTGAAGGACCTGGCCCTCCAGGGCGGGCGCCCGGCGCCGCACACCCCCATGGA
CTGGATGAACGGGAAGGAGGGCGACCTGGTCCTGGTGAACGGGGCCCTGCGGCCCAC
CCTGGTGGCCCAGAAGGCCACCCTGAGGCTTCGCCTCCTCAACGCCTCCAACGCCCGC
TACTACCGCCTGGCCCTGCAGGACCACCCCCTTTACCTCATCGCCGCCGATGGGGGCTT
CCTGGAAGAGCCCCTGGAGGTGTCCGAGCTCCTCCTGGCCCCAGGAGAGCGGGCCGA
GGTCCTGGTGCGCTTGCGGAAAGAGGGCCGCTTCCTCCTCCAGGCCCTGCCCTACGAC
CGCGGGGCCATGGGCATGATGGACATGGGGGGCATGGCCCACGCCATGCCCCAAGGGC
CAAGCCGGCCCGAAACCCTTCTTTACCTCATCGCCCCCAAGAACCCCAAGCCCTTACCC
CTGCCCAAGGCCCTAAGCCCCTTCCCCACCCTGCCCGCCCCCGTGGTCACCCGCCGCC
TGGTCCTCACCGAGGACATGATGGCCGCCCGCTTCTTCATCAACGGCCAGGTCTTTGAC
CACAGGCGGGTGGACCTGAAGGGGCAGGCCCAGACGGTGGAGGTCTGGGAGGTGGAA
AACCAGGGGGACATGGACCACCCCTTCCACCTCCACGTCCACCCCTTCCAGGTCCTCTC
CGTGGGCGGGAGGCCTTTCCCCTACCGGGCCTGGAAGGATGTGGTCAACCTGAAGGCG
GGCGAGGTGGCCAGGCTTCTGGTTCCCTTGAGGGAAAAGGGCCGGACCGTTTTTCACT
GCCACATCGTGGAGCACGAGGACCGGGGGATGATGGGAGTCCTCGAGGTGGGT

A.4 A General Expression Protocol for *Thermus thermophilus* strain HB27 Laccases

Using this protocol, expression levels of 70 mg ml^{-1} are readily achieved for the wild-type enzyme. Still, the gene used for experiments and mutagenesis in this thesis does not represent a form that is codon-optimized for *E. coli* K12 strains, such as our BL21 Rosetta2 expression host.

Biochemical Reagents

- Lysis Buffer:
  300 mM Tris pH 8.1 (36.34 g / l of Tris),
  1 mM EDTA (341 mg / l; metal chelator)
  20% Sucrose (200 g / l)
- 100 mM Sodium Acetate pH 6.8
- 100 mM Sodium Acetate pH 6.8 + 500 mM NaCl
- 20 mM Sodium Acetate pH 6.5
- 20 mM Sodium Acetate pH 6.5 + 1M NaCl
- 1 M IPTG (1.5 g / 6 ml H_2O)
- 45 ml 10 mM $CuSO_4$
- 100 mg / ml Ampicillin
- 1 M PMSF in 1:9 Isopropyl Alcohol: DMSO
- Lysozyme: (as solid)
- DNAse (as solid)
- PhosStop Protease Inhibitor (Roche)
- Complete EDTA Free Protease Cocktail (Roche)

Collection of crude extracts

- Prep 6 liters of TB growth media: 50.8 g / l, autoclave 45 minutes. Allow the broth to cool to RT, then add 1-2 ml of 100 mg / ml ampicillin.
- Inoculate growth media with ~2 ml of *E. coli* DE3, Rosetta 2 strain cells grown on LB in 15 ml culture tubes. Incubate at 37 C for 16 hours, with shaking (180 rpm).
- Induce protein expression by adding IPTG to a final concentration of 1 mM for 4.5 hours.
- Following induction, centrifuge the cells at RT at 5000 rpm for 10 minutes. Discard the supernatant and add repeat centrifugation until all the cells have been spun down into a pellet.
- Pelleted cells may be stored at –20 C following this step, if a pause is needed in the protocol.
- Resuspend the pellets in the 20% Sucrose Buffer (pre-exposure to EDTA is a necessary for effective lysozyme activity).
- Equilibrate the cell suspension at RT for 1 hour.
- Spin cells at 7000x for 25 minutes. Decant supernatant, leaving a small amount of residual buffer (~ 3-5 ml).
- With spatula, mix the cells and residual buffer to form a thick

paste.

- After forming cell paste, add 80 ml of 20 mM sodium acetate, pH 6.0-7.0. Dissolve two tablets of Complete Protease Cocktail in 2 ml of water and add the solution to lysate. Repeat procedure for PhosStop tablets, using 4 tablets in 4 ml of water. Add a speck of lysozyme as solid to the lysate. Incubate for 30 minutes at RT. Also add a speck for DNAse to the lysates. Incubate on benchtop for 1 hour.
- Following chemical disrupting, perform ultrasonication to physically lyse the cells. Place the cell suspension in an ice-water bath and put in the sonication chamber. Dip the probe into the sample, but be careful to let the sonication probe touch the bottom of the container.
- Following physical lysis, spin down the supernatant at 4 C at 14,000 rpm for 1-2 hours. Discard the pellet and store supernatant. This may be stored overnight at ~4 C if needed.
- Metallate extracts by dropwise addition of 45 ml of 10 mM $CuSO_4$ to the extracts, with stirring. Following copper addition, set extracts to stir slowly in cold room for at least an hour.
- To remove proteins that precipitate during metallation, centrifuge extracts at 14,000 rpm for 2 hours.
- Collect extracts from centrifuge tubes and proceed with batch column purifcation. Equilibrate a column packed with CM Cepharose gel (cation exchanger, GE) with pH 6.8 100 mM sodium acetate. Load the lysate on column, allowing non-binding proteins to flow through.
- Elute protein in pH 6.8 100 mM sodium acetate +500 mM NaCl buffer. Protein should elute as a blue band from the column.
- Concentrate the protein elution using a 30,000 kda amicon filter. Note: to use the amicon properly, never touch the shiny surface of the membrane. Doing so will scratch the membrane and possibility allow cell matter even above the MWCO to run through the amicon. Run one volume of pure water through the membrane, followed by a volume of 0.1M NaOH (removes denaturants used to treat the membrane, and also denatures any bound extraneous protein), followed by another volume of water to prep the membrane for use.
- Following concentration of the protein, dialyze against pH 6.5 100 mM sodium acetate, 50 mM sodium acetate, 20 mM sodium acetate to reduce the ionic strength gradually to avoid precipitation of laccase. Amend the 20 mM buffer with 500 μM $CuSO_4$ and allow to dialyze for at least 24 hours to assure full metallation of all copper centers in the protein.

Chromatography

- Equilibrate two HiTrap Mono SP column linked in series with pH 6.5, 20 mM acetate (+ 1M NaCl). Ramp up to 50% buffer B over 30 minutes to elute.
- Load protein onto Sephadex 75 column equilibrated with pH 6.5 100 mM sodium aeetate. Run at 0.5-1.0 ml/minute. The eluted protein should be pure.

A.5 Mass Spectra of Small Molecules

2-Iodopropylamide-7-aminofluorene

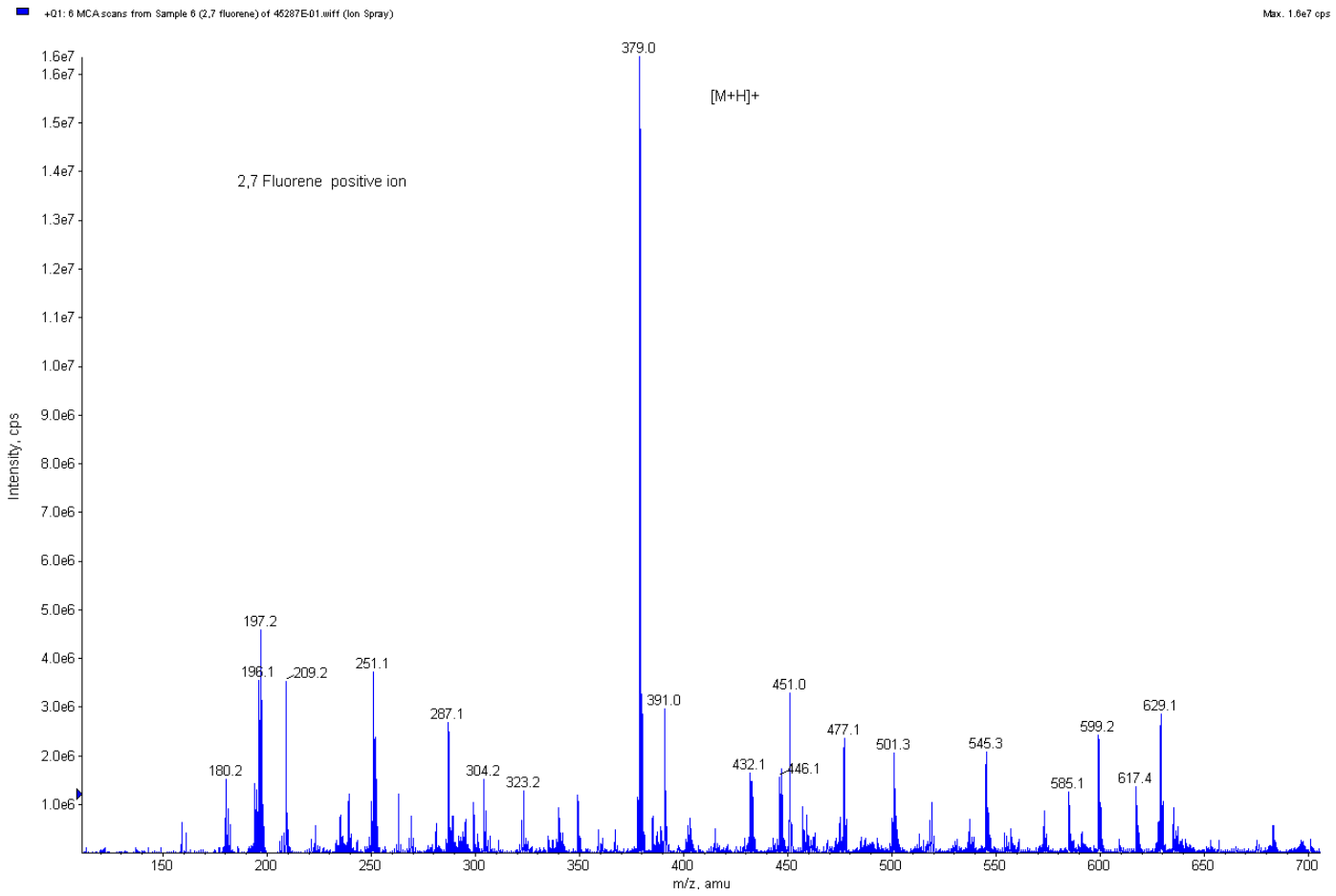

[Molecular ion + H] at m/z = 379.0 (expected: 378.2).

Compound A (in DMSO)

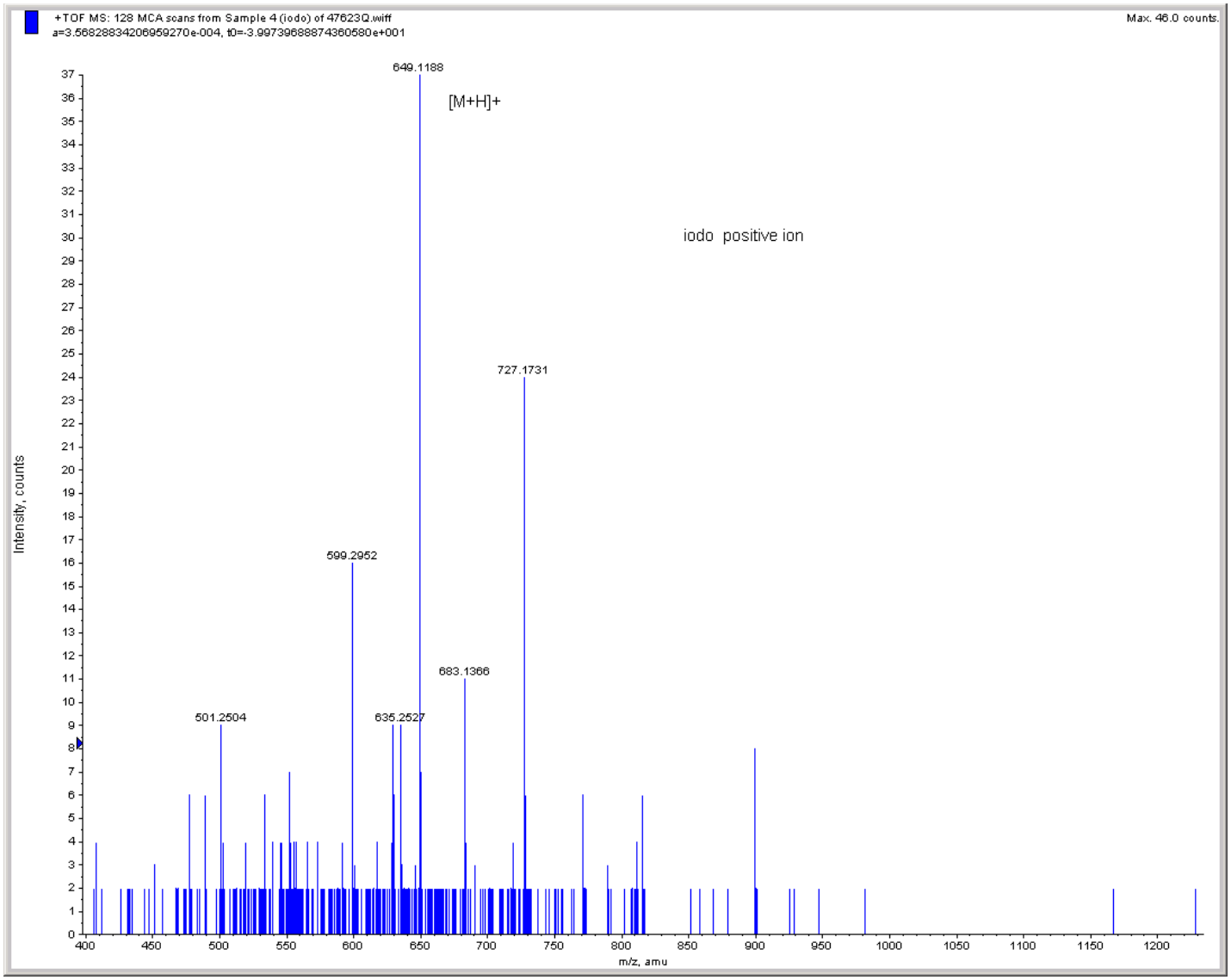

Molecular ion + H peak at m/z = 649.1; expected 648.1. DMSO forms an adduct with the molecular ion (m/z = 727.17; expected 726.7).

A.6 A surface integration script for AFM data (Python)

A general procedure used for determining surface areas given 2D arrays containing height data. Attempts were made to use this procedure to calculate surface area enhancements of etched gold sheets intended for electrode fabrication using AFM data arrays. However, the surface areas calculated give far smaller values than the reported BET values of these materials. Such underestimates are likely caused by the fact that many of the pores giving rise to N_2 adsorption isotherms in BET data of nanoporous gold are on size scales smaller than what are readily resolved by the AFM. Furthermore, imaging artifacts caused by the tapping or dragging of an AFM tip over a roughened surface can easily result in an underestimate of reported surface areas.

As a result, care should be taken when using this script for calculating surface area enhancements to ensure that any surface features are the same size or larger than that of the AFM tip and will not be obscured by any physical limitations of the tip.

```
import xlrd
def sint(filename, scanlines, scanwidth, excelsheet):
#scanlines = AFM scanning resolution, scanwidth in meters
#employ columns to determine line integral (ds)
    data = xlrd.open_workbook(filename)
    sheet = data.sheet_by_index(excelsheet)
    colcounter = 0
    columnA = sheet.col_values(colcounter)
    columnB = sheet.col_values(colcounter+1)
    rows = sheet.row_values(0)
    counter = 0 #tracks positions in y coordinate (column)
    ds = 0 # path integral counter
    dsa = 0 # differential surface area counter
    dl = scanwidth/scanlines #machine stepping resolution
    while colcounter+1 < len(rows):
        while counter+1 < len(columnA):
            ds += (dl**2 + (columnB[counter] - columnA[counter])**2)**0.5
            counter += 1
        counter = 0
        dsa += ds*dl
        colcounter += 1
    return 'Total surface area (um^2):',dsa*(1e12), counter, colcounter, 'surface enhancement:', dsa/
(0.5*scanwidth**2)
```

A.7 A line integrator script for Dektak profiler data analysis.

```
import xlrd; import matplotlib.pyplot as mt
#note: xdata is in um and y data are in nm. procedure converts both to meters.
def lint(filename, scanlength, scanwidth, col, format):
    data = xlrd.open_workbook(filename)
    sheet = data.sheet_by_index(0)
    counter = 0
    column1 = sheet.col_values(0)
    column2 = sheet.col_values(col)
    ds = 0
    while (counter + 1) < len(column1):
        dl = (column1[counter+1] - column1[counter])*1e-6
        ds += (dl**2 + (1e-9*(column2[counter+1] - column2[counter]))**2)**0.5
        counter += 1
    mt.plot(column1, column2, format)
    mt.xlabel(' micrometers')
    mt.ylabel('height / nanometers')
    mt.grid(True)
    mt.show()
    print 'enhancement =', ds/scanlength, 'differential area (um^2) =',  ds*scanwidth*1e12, counter
    return ['total line integral (um) = ', ds*1e6]

#computes average of all line integrals in a file
def average_data(filename, stop, scanlength, scanwidth):
    sum = 0
    counter = 1
    while counter <= stop:
        sum += lint(filename, scanlength, scanwidth, counter)[1]
    return sum/stop, counter

def graph(filename, col, format):
    #format -> give plot color and line type as a string.
    data = xlrd.open_workbook(filename)
    sheet = data.sheet_by_index(0)
    column1 = sheet.col_values(0)
    column2 = sheet.col_values(col)
    mt.plot(column1, column2, format)
    mt.xlabel('profile / micrometers')
    mt.ylabel('height / nanometers')
    mt.grid(True); mt.show()
```

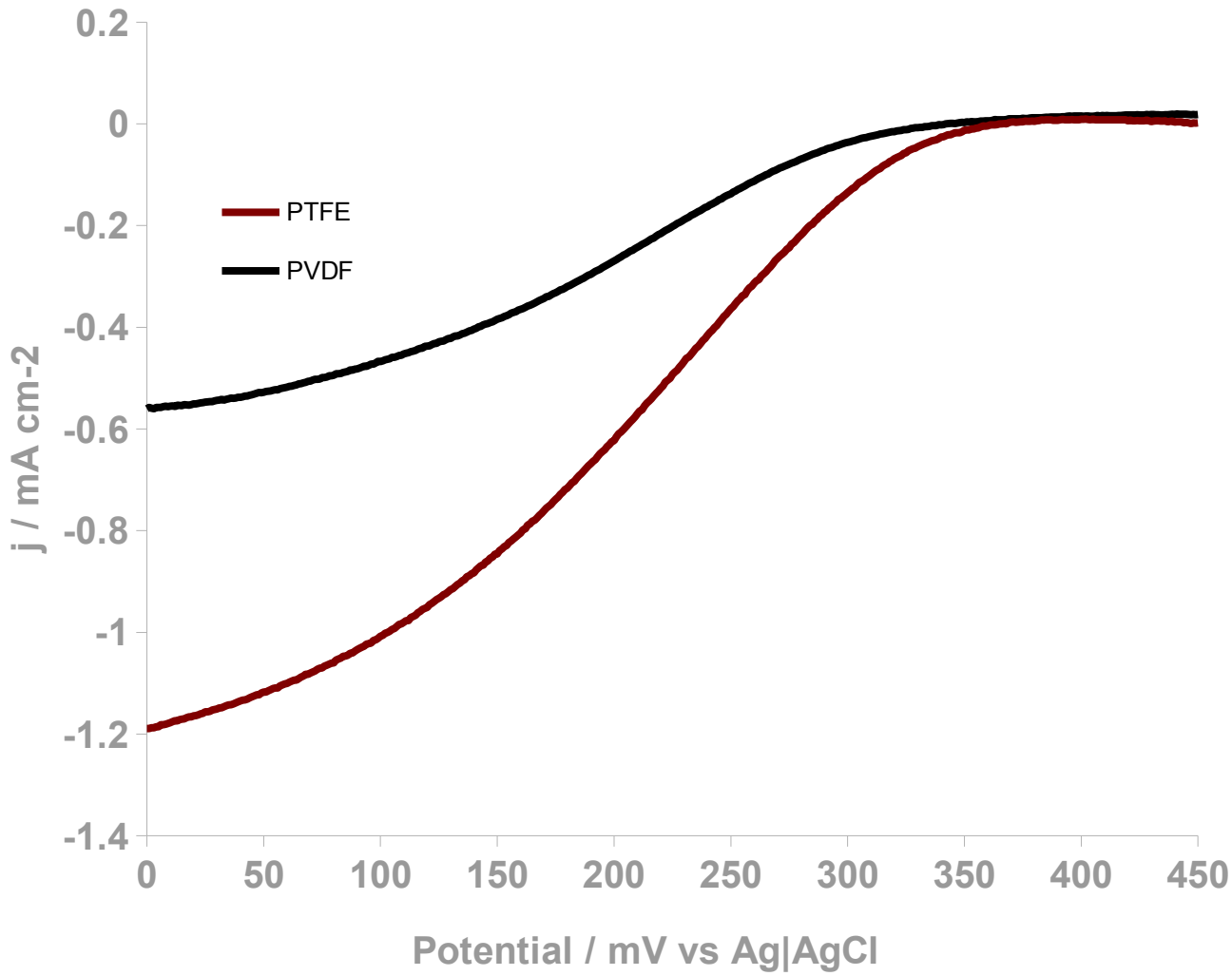

Figure A.1

Enhanced performance of laccase on ketjen black following improved metallation procedures and employ of PTFE as an electrode binder. Measurement conditions: pH 5.0 20 mM sodium acetate, 30 °C, 4000 rpm.

A.8 Improved cathode fabrication

Following the studies of Chapter I, improved metallation procedures (described in section A.4) and introduction of PTFE binders instead of PVDF for electrode fabrication led to improved cathode performance. Currently, our best performance of this particular laccase on carbon electrodes is 1.2 mA cm^{-2} at 0 V vs Ag|AgCl. While a considerable improvement, this still falls far below the highest reports for MCO cathodes in current literature, and even farther behind our ultimate goal of ~ 100 mA cm^{-2}. Electrode fabrication procedures are outlined below.

PTFE / Ketjen Black electrode substrate preparation

Prep a solution of 10 mg/ml PTFE (Sigma-Aldrich) in N-methyl-2-pyrrolidone (NMP, Sigma-Aldrich). Sonicate for an hour to homogenize. Measure out 40 mg of ketjen black (AkzoNobel) and add it to a scintillation vial. Add 1.5 ml of the polymer solution to the vial (this emulsion represents a PTFE/ketjen weight ratio of 37.5%, which we found gives the best electrochemical performance with laccase). Finally, add 2.0 ml of NMP to the vial. Shake vigorously to mix, and then place in sonicator to sonicate for at least 2 hours the first time the emulsion is made. During subsequent uses, it is sufficient to sonicate the slurry for 5-15 minutes before dropcasting.

After sonication, the emulsion should be pipetted up and down several times just before deposition onto the substrate (abraded HOPG in the studies here). To avoid clumping during the drying process, only about 32 μl slurry cm^{-2} of substrate area should be used to get an evenly deposited layer devoid of cracks or clumps. Curing of the surface to remove solvent is best done by incubation for at least three more hours at 65-80 °C. A well-formed dropcast carbon layer should have a dry, fuzzy appearance. If it appears flat and slick, the polymer ratio in the emulsion is probably too high; even if the slurry is prepped correctly, this can be caused simply by insufficient suspension of the carbon particles in the emulsion prior to use.

A.9 Methods for redox titration of wild-type *Thermus thermophilus* laccase

The perchlorate salt of the compound $Ru(NH_3)_5Py^{2+/3+}$ was prepared according to literature protocols for use as a reductant in laccase redox titrations.[1,2] This mediator has previously been used for determination of type 1 potentials in *Pseudomonas aeruginosa* azurin.[1] Stock solutions of this compound were prepared fresh before each redox titration experiment by measuring out approximately 1 mg of the compound and dissolving it in 50 μl DMSO and then adding 350 μl of milliq H_2O to the solution, which should be a bright yellow. To measure mediator stock concentration, an aliquot of this solution was diluted 50 fold and measured via UV-vis, using the ε_{407} (7762 M^{-1} cm^{-1})[1] to determine sample concentration. Solutions were adjusted either by further dilution in water or minor additions of the mediator solid in order to bring the sample concentration to 6.5 mM. Mediator stocks were then pipetted degassed on a schlenk line for at least 30 minutes under argon flow, with intermittent vacuum pumping. 900 μl solutions of ~ 70 μM wild-type laccase in pH 6.5 100 mM sodium acetate were also degassed on schlenk lines by stirring under argon flow for at least an hour.

Following sample deaeration, samples were transferred into a wetbox with an argon atmosphere contaning an ocean optics UV-vis and a Gamry potentiostat. A 1 ml quartz cuvette (Starna Cells) containing an Ag|AgCl reference electrode served as the cell for the redox titrations. Two platinum wires glued to the edge of the cell using 9460 Hysol epoxy served as counter electrodes and working electrodes. The cuvette was first blanked on sodium acetate buffer, emptied, and then filled with 800 μl of laccase. Leads to the potentiostat were attached to their respective electrodes. At the start of each experiment, open circuit voltages were measured until the cell OCV stabilized. Generally this took 1-2 hours. Following this initial equilibration, mediator was added to the laccase solution to total volumes of 4, 8, 12, 16, 20, 24, 28, 32, 40, 44, 48, and 52 μl. A Pasteur pipet was used to gently mix the solution, while taking care to avoid disturbing the electrodes and introduction of bubbles, each time mediator was added. Generally equilibration took 1-1.5 hours following an addition of mediator.

Following the conclusion of each equilibration, the UV-vis spectra were saved.

Plots of log[oxidized laccase]/[reduced laccase] vs. the open circuit voltage were then made and fit to the Nernst equation:

$$E = E^0 + \frac{RT}{nF} \ln \frac{[oxidized]}{[reduced]} \quad ,$$

with a slope of RT/nF and an intercept of E^0, which here, gives the type 1 redox potential in laccase.

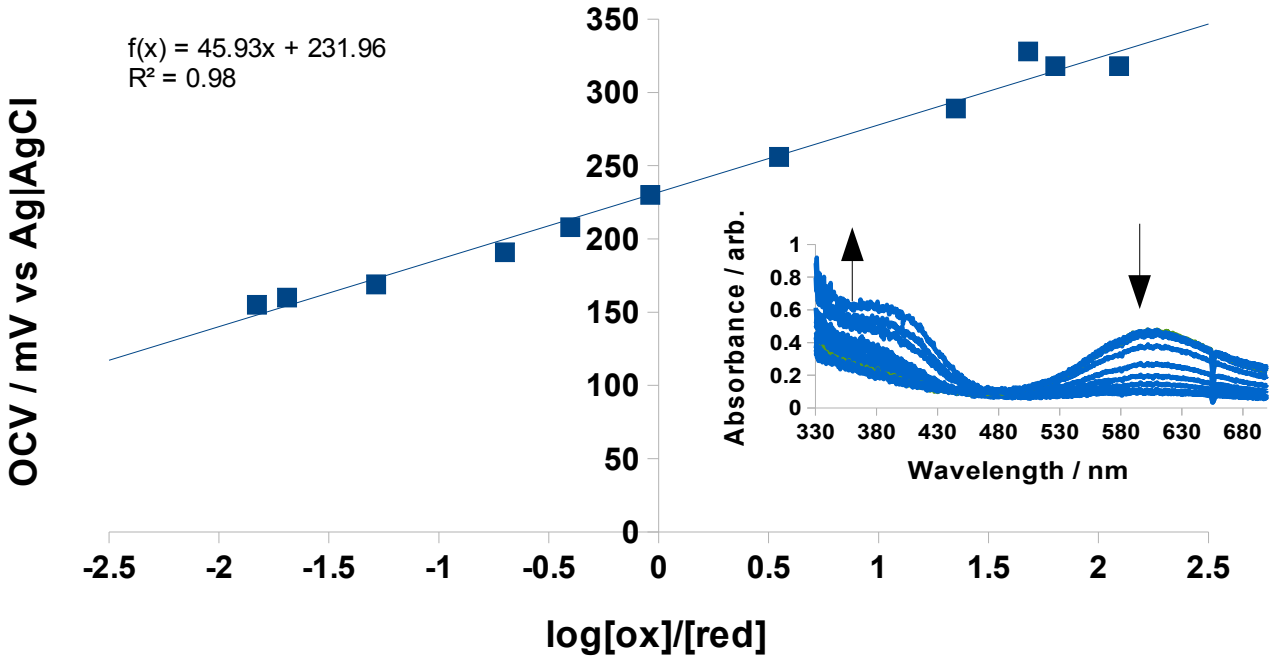

Figure A.2

Redox Titration of WT *Thermus thermophilus* laccase at pH 6.5 yields a value of 227 mV ± 6.4 mV for the type 1 active site of this enzyme. Using earlier pH titrations as a basis for conversion (57 ± 1 mV decade^{-1} has been found for this enzyme)[3] allows for estimation of the type 1 active site reduction potential at pH 5.0, for which we find a value of 313 ± 6.4 mV vs Ag|AgCl. This value lies close to our initial estimates of the type 1 redox potential of laccase when adsorbed on ketjen black electrodes.[3]

References

(1) Cummins, D.; Gray, H. B. *J. Am. Chem. Soc.* **1977**, *99*, 5158–5167.

(2) Ford, P. C.; Rudd, D. F. P.; Gaunder, R.; Taube, H. *J. Am. Chem. Soc.* **1968**, *90*, 1187–1194.

(3) Agbo, P.; Heath, J. R.; Gray, H. B. *J. Phys. Chem. B* **2013**, *117*, 527–534.

A.10 Atomic Force Microscopy data of Ketjen Black electrode substrates

Data and images reported below are for ketjen black surfaces established on HOPG substrates. Surfaces were generated through dropcasting of a ketjen black/PTFE emulsion made according to the methods described in section A.8.

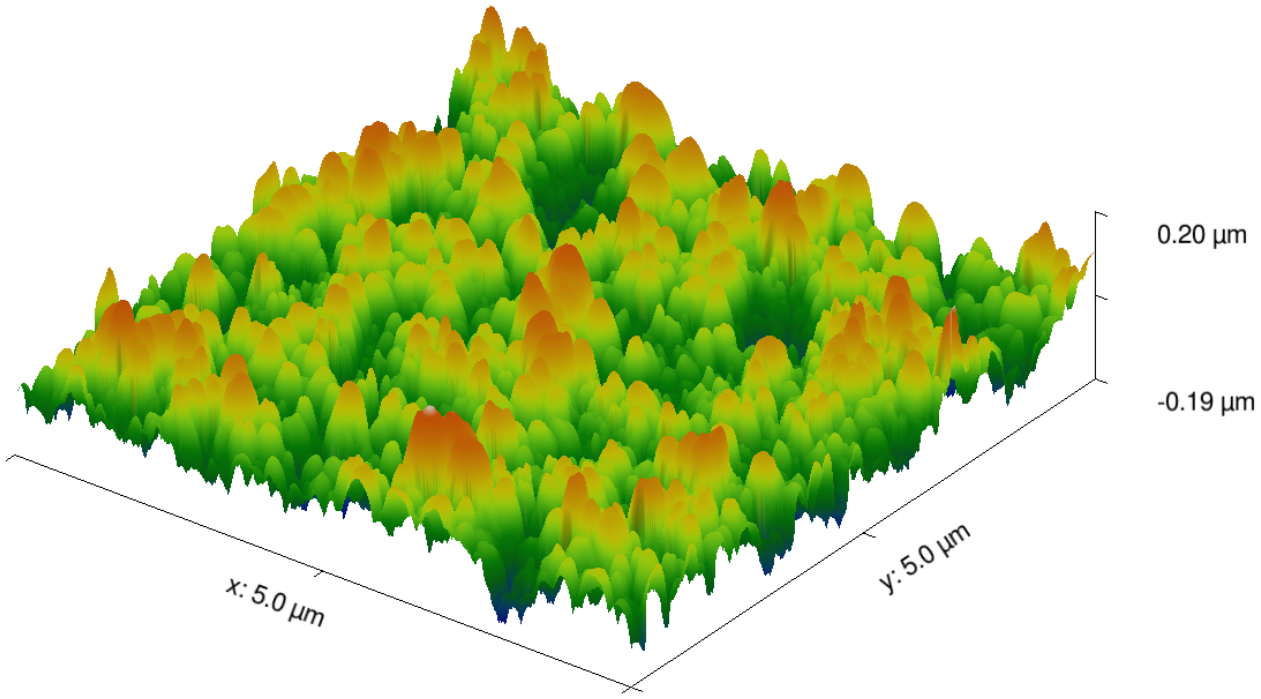

Figure A.3
An 3-D atomic force microscope image (AFM) of a ketjen black surface, highlighting the increased aspect ratio and surface heterogeneity of this material.

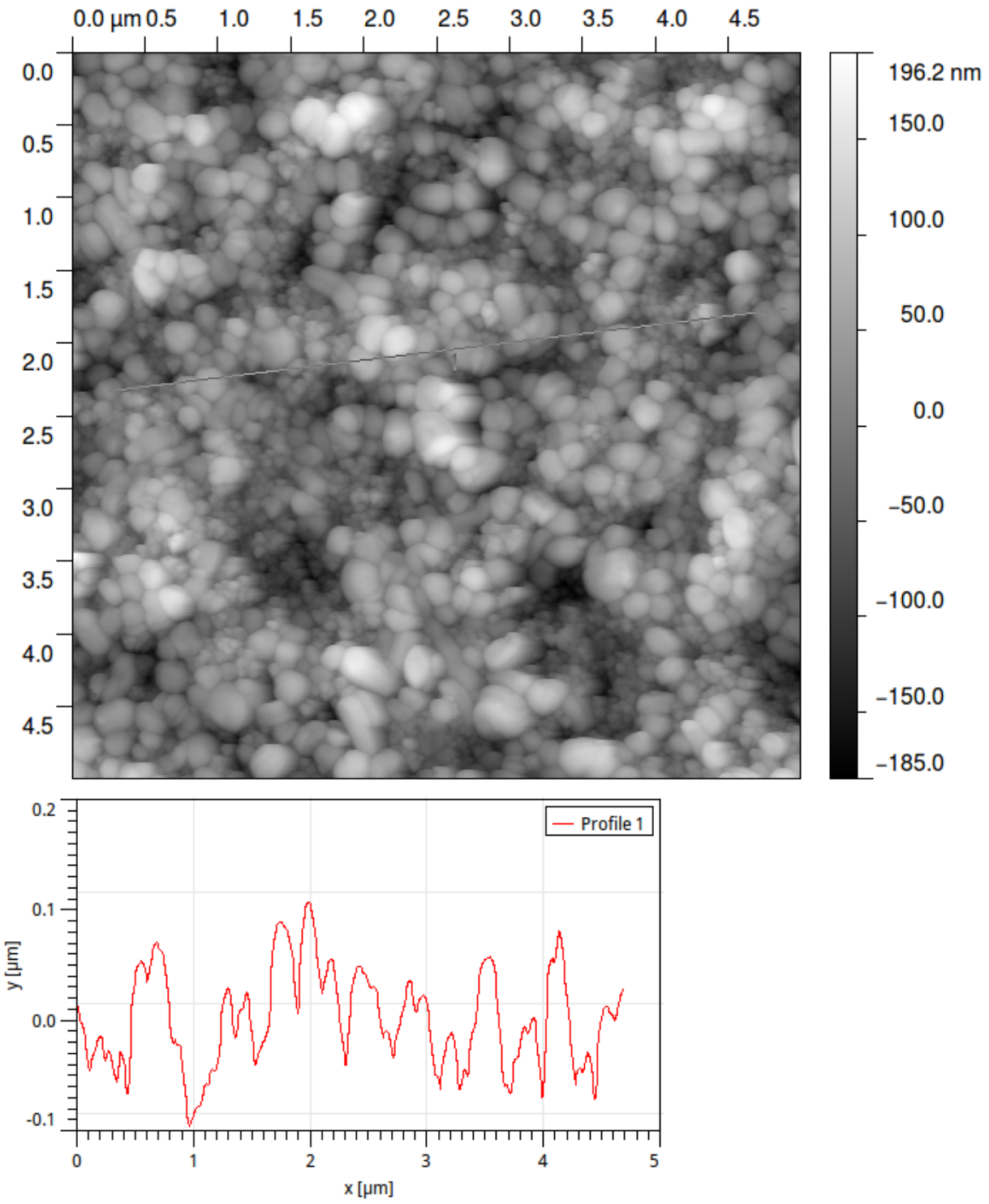

Figure A.4

Top: A 2-D AFM map of the same ketjen black surface. Bottom: extracted 1-D profile data of the ketjen black substrate. Note that corrugations are on the order of 20-100 nm (typical MCO diameter ~ 6 nm).

Representative Roughness Statistics of Ketjen Black surfaces

File: /media/pcagbo/Research/data/AFM/ketjen black/ketjen+ptfe-s3_plane+cubic_fit-000(5x5um).gwy
Data channel: Height

Selected line: (6, 249) to (507, 87) px
(0.063, 2.437) to (4.956, 0.854) μm

Amplitude

Roughness average (Ra):	14.4 nm
Root mean square roughness (Rq):	17.9 nm
Maximum height of the roughness (Rt):	103.4 nm
Maximum roughness valley depth (Rv):	61.3 nm
Maximum roughness peak height (Rp):	42.1 nm
Average maximum height of the roughness (Rtm):	82.6 nm
Average maximum roughness valley depth (Rvm):	48.7 nm
Average maximum roughness peak height (Rpm):	33.9 nm
Average third highest peak to third lowest valley height (R3z):	82.9 nm
Average third highest peak to third lowest valley height (R3z ISO):	44.4 nm
Average maximum height of the profile (Rz):	68.9 nm
Average maximum height of the roughness (Rz ISO):	82.6 nm
Skewness (Rsk):	-0.511
Kurtosis (Rku):	3.042
Waviness average (Wa):	32.9 nm
Root mean square waviness (Wq):	40.1 nm
Waviness maximum height (Wy=Wmax):	162.6 nm
Maximum height of the profile (Pt):	230.4 nm

Spatial

Average wavelength of the profile (λa):	0.180 μm
Root mean square (RMS) wavelength of the profile (λq):	620.641 μm

Hybrid

Average absolute slope (Δa):	0.5004
Root mean square (RMS) slope (Δq):	181.7 10^-6
Length (L):	5.152 μm
Developed profile length (L0):	6.011 μm
Profile length ratio (lr):	1.191

A.11 Model Derivation of MCO Electrokinetics

1 *Derivation of the general rate equation.*

The rate law for this process can be written as:

$r = k_2[B][O_2] - k_2'[C]$, where here the term [$O_2$] refers to the surface concentration (mol cm^{-2}) of O_2 following its adsorption onto, the electrode surface.

Surface concentrations of all intermediates can be expressed through the following set of equations:

$\frac{d[A]}{dt} = k_1'[B] - k_1[A] = 0$

$\frac{d[B]}{dt} = k_2'[C] + k_1[A] + k_4[D] - k_1'[B] - k_2[B][O_2] - k_4'[B] = 0$

$\frac{d[C]}{dt} = k_2[B][O_2] + k_3'[D] - k_2'[C] - k_3[C] = 0$

$\frac{d[D]}{dt} = k_3[C] + k_4'[B] - k_3'[D] - k_4[D] = 0$

Having applied the steady-state condition, we now solve for the surface concentration of the intermediate species:

$[C] = \frac{(k_3'+k_4)k_2[B][O_2]}{(k_3'+k_4)(k_2'+k_3)-k_3k_3'} = f[B]$. With this new definition for [C], we solve for [D]:

$[D] = \frac{[B](k_3f+k_4')}{k_3'+k_4}$

Knowing surface concentrations of intermediates C and D in terms of [B], we can determine [B] solely as a function of [A]:

$\frac{d[B]}{dt} = 0 = k_2'f[B] + k_1[A] + \frac{k_4[B](k_3f+k_4')}{k_3'+k_4} - k_4'[B] - k_1'[B] - k_2[B][O_2]$

$[B] = k_1[A](k_4' + k_1' + k_2[O_2] - k_2'f - \frac{k_4(k_3f+k_4')}{k_3'+k_4})^{-1} = \frac{k_1[A]}{G}$

Our rate law can now be expressed as:

$r = k_2[B][O_2] - k_2'f[B] = \frac{k_1[A]}{G}(k_2[O_2] - k_2'f)$

We must now address the problem of [A] showing up in the rate law. As the surface concentration of intermediates will be unknown during catalytic cycling, we must express [A] as a function of the total enzyme surface concentration, N_T, which can be measured:

$N_T = [A]+[B]+[C]+[D] = [A]+\frac{k_1[A]}{G}+f\frac{k_1[A]}{G}+\frac{k_1[A](k_3f+k_4')}{G(k_3'+k_4)} = [A](1+\frac{k_1}{G}(1+f+\frac{k_3f+k_4'}{k_3'+k_4}))$

$[A] = \frac{N_T}{(1+\frac{k_1}{G}(1+f+\frac{k_3f+k_4'}{k_3'+k_4}))}$.

Plugging the new definition for [A] into the rate law gives

$r = \frac{k_1N_T(k_2[O_2]-k_2'f)}{G(1+\frac{k_1}{G}(1+f+\frac{k_3f+k_4'}{k_3'+k_4}))}$, with units of mol cm^{-2} s^{-1}.

.

.

.

This equation represents turnover rates for oxygen reduction to water. We convert this to a current density, with units of mA cm^{-2}, by multiplying the rate by a factor of $\frac{eF}{N_A}$, where e is the number of electrons tranferred during a single turnover, F is Faraday's constant and $N_A$is avagadro's number. A negative sign is used to indicate a cathodic current:

$$j = -\frac{eFk_1N_T(k_2[O_2]-k_2'f)}{N_AG(1+\frac{k_1}{G}(1+f+\frac{k_3f+k_4'}{k_3'+k_4}))}.$$

1.1 Notes on conversion of oxygen concentration from a homogenous concentration to a heterogenous surface concentration.

Oxygen consumption by the electrode surface involves transport of O_2 through bulk (homogeneous process) to the electrode surface, where it is adsorbed prior to consumption by enzyme; i.e., the step B+O_2 <-> C can be decomposed into two steps: the diffusion of O_2through the bulk, followed by O_2 adsorption onto the electrode surface:
B + O_2 <->BO_2 <-> C, with respective forward and back rates of k_d, k_d' for the first intermediate step and k_2, k_2' for the second intermediate step.
Explicitly accounting for an oxygen adsorption step gives rise to an intermediate, BO_2. Assuming steady state conditions for [BO_2]:

$[BO_2] = \frac{k_d[B][O_2]+k_2'[C]}{k_2+k_{d'}}$, modifying the rate expression to:

$$r = k_d[B][O_2] - \frac{k_d'k_d[B][O_2]}{k_2+k_d'} - \frac{k_d'k_2'}{k_2+k_d'}[C]$$
$$= \frac{k_dk_2}{k_2+k_d'}[B][O_2] - \frac{k_d'k_2'}{k_2+k_d'}[C].$$

If we assume that rates of O_2 adsorption/desorption are large relative to k_2,

then k_d'>> k_2:

$$r = \frac{k_d}{k_d'}k_2[B][O_2] - k_2'[C] = K_{O_2}k_2[B][O_2] - k_2'[C].$$

Note that here, since we have explicitly accounted for O_2 diffusion and adsorption, we now use the homogeneous solution value for [O_2]; that is [O_2] is now in units of M rather than mol cm^{-2}(presence of the K_{O_2} term, which has units of M^{-1}, keeps our final rate expression in the proper units of mol cm^{-2} s^{-1}).

Treating adsorption as a separate step modifies the system of differential equations

slightly, where now, the term k_2[O_2][B] that arises in the definitions for

$\frac{d[B]}{dt}$ and $\frac{d[C]}{dt}$

is written as $K_{O_2}k_2$[O_2][B]. Solution of the resulting system proceeds as described above.

.
.
.
.

2 *Expressing interfacial charge transfer.*

Having found a possible rate law for dioxygen reduction by MCOs, we now address the problem of accounting for how charge is transferred between the electron acceptor in the enzyme and the electrode surface. That is, we now find a sufficient way to express the interfacial rate constants k_1, k_1', k_4, and k_4' of the model. The Butler-Volmer equation is a commonly used description of charge transfer at an electrode surface:

$$k(\eta) = k_0(e^{-nF\eta\alpha} + e^{nF\eta(1-\alpha)})^{\frac{1}{RT}},$$

where $k(\eta)$ is the rate of interfacial charge transfer as a function of the overpotential,η, defined as the displacement of the applied potential relative to the formal potential of a redox couple of interest. The exponential terms represent the forward and back electron transfer rates, respectively.

n = number of electrons transferred (1 in the case of interfacial reduction of Type 1 Cu)
F = Faraday's constant
α= symmetry factor
k_0 is the exchange rate, the rate of electron transfer in the forward and back reactions at zero overpotential.

When $\eta = 0$, $k_0 = k_f = k_b$.

The exchange current is itself a complex term which we should be able to express in terms of the Marcus equation, allowing for explicit description of the temperature dependence of the exchange current, its dependence on reorganization energy of the site in contact with the electrode surface and the coupling energy between the site and the electrode. As $k_0$is simply the rate of charge transfer at no applied potential, we should be able to express it as the Marcus equation in the case of zero driving force:

$k_0 = \frac{4\Pi^2}{h}|H_{AB}|^2\frac{1}{\sqrt{4\Pi\lambda k_b T}}e^{-\frac{\lambda}{4k_b T}}$. In the kinetic scheme for MCOs, rates k_1 and k_4 represent cases of charge from the electrode surface reducing the Type 1 copper site, and so are described using the forward (cathodic) terms of the B.V. equation:

$$k_1 = k_4 = \frac{4\Pi^2}{h}|H_{AB}|^2\frac{1}{\sqrt{4\Pi\lambda k_b T}}e^{-\frac{\lambda}{4k_b T}}e^{\frac{-nF\eta\alpha}{RT}}$$

Similarly, the reverse rates for interfacial electron transfer, k_1', k_4', are written:

$$k_1' = k_4' = \frac{4\Pi^2}{h}|H_{AB}|^2\frac{1}{\sqrt{4\Pi\lambda k_b T}}e^{-\frac{\lambda}{4k_b T}}e^{\frac{nF\eta(1-\alpha)}{RT}}$$

.
.
.
.
.
.
.
.
.
.
.
.
.

2.1 Limiting case: Infinite Overpotential

In the high overpotential limit ($\eta \to -\infty$), the current should converge to a constant value as mass transport of oxygen becomes rate-limiting to current production. In the limit $\eta \to -\infty$, terms k_1 and k_4 will diverge, while terms k_1' and k_4' will converge to zero. First, we evaluate the limit of the complex term f:

$$\frac{lim}{\eta \to ^{-}\infty} f(\eta) = \frac{lim}{\eta \to ^{-}\infty} \frac{k_2[O_2](k_3'+k_4)}{(k_3'+k_4)(k_2'+k_3)-k_3k_3'} = \frac{k_2[O_2]k_4}{k_4(k_2'+k_3)} = \frac{k_2[O_2]}{k_2'+k_3}$$

We can now evaluate the rate law in the limit $\eta \to -\infty$:

$$\frac{lim}{\eta \to ^{-}\infty} j(\eta) = \frac{lim}{\eta \to ^{-}\infty} \frac{-eFk_1N_T(k_2[O_2]-k_2'f)}{N_AG(1+\frac{k_1}{G}(1+f+\frac{k_3f+k_4'}{k_3'+k_4}))} = \frac{lim}{\eta \to ^{-}\infty} \frac{-eFN_T(k_2[O_2]-k_2'f)}{N_A(1+f+\frac{k_3f+k_4'}{k_3'+k_4})}$$

$$= -\frac{eFN_Tk_2[O_2](1-\frac{k_2'}{k_2'+k_3})}{N_A(1+\frac{k_2[O_2]}{k_2'+k_3})}.$$

For the system under study, $k_2' << k_3$. We can then approximate the limit of j as:

$$-\frac{eFN_Tk_2[O_2](1-\frac{k_2'}{k_3})}{N_A(1+\frac{k_2[O_2]}{k_3})}.$$

Note that for the rates used in modeling in this study, this limiting case can be approximated as:

$$j = -\frac{eFN_Tk_2[O_2](1-0)}{N_A(1+5.1/350)} = -\frac{eFN_Tk_2[O_2]}{N_A(1.01)} \approx -\frac{eFN_Tk_2[O_2]}{N_A}.$$

Written as a rate, this is simply $r = N_Tk_2[O_2]$, the classic limiting case of the Michaelis-Menten equation.

A.12 Equations of Motion for Electrophoretic Deposition

1 Determining the equations of motion for CueO.

$F_{net} = F_{electric} - F_{drag}$

$m\frac{dv}{dt} = qE - \delta v$; $\frac{dv}{dt} + \frac{\delta v}{m} = \frac{qE}{m}$, where m= protein mass, v = velocity, δ = drag coefficient,

E = electric field. It must be appreciated that establishing a uniform electric field between two parallel electrodes takes a finite amount of time; that is, some time is required before the equilibrium electric field strength is reached in a parallel plate capacitor (this characteristic time is defined by the device's RC time constant):

$E(t) = E_0(1 - e^{-t/RC})$,

where t is the amount of time allowed for charging, and E_0 is the electric field at equilibrium (capacitor fully charged). As a result of the time-dependence of the electric field, our force equation now becomes:

$\frac{dv}{dt} + \frac{\delta v}{m} = \frac{qE_0}{m}(1 - e{-}^{t/RC})$.

We solve the resultant differential equation for the velocity by first considering the case of no electric field:

$m\frac{dv}{dt} + \delta v = 0; \int \frac{dv}{v} = -\int \frac{\delta}{m}dt$; $v = e^{-\frac{\delta}{m}t}e^c = Ae^{-\frac{\delta}{m}t}$; $A = ve^{\frac{\delta}{m}t}$.

Differentiation of A then gives us an expression equal to the R.H.S. of our original force equation multiplied by a factor of $e^{\frac{\delta}{m}t}$:

$\frac{d}{dt}(ve^{\frac{\delta}{m}t}) = \frac{dv}{dt}e^{\frac{\delta}{m}t} + v\frac{\delta}{m}e^{\frac{\delta}{m}t} = e^{\frac{\delta}{m}t}(\frac{qE_0}{m}(1 - e{-}^{t/RC}))$; $v = \frac{qE_0}{m}e^{-\frac{\delta}{m}t}\int e^{\frac{\delta}{m}t}(1 - e^{-t/RC})dt$.

We now solve the resulting integral to find the analytical solution for v(t):

$u = 1 - e^{-t/RC}$
$du = \frac{1}{RC}e^{-t/RC}dt$
$dz = e^{\frac{\delta}{m}t}dt$
$z = \frac{m}{\delta}e^{\frac{\delta}{m}t}$

$\int udz = (1 - e^{-t/RC})\frac{m}{\delta}e^{\frac{\delta}{m}t} - \int \frac{1}{RC}\frac{m}{\delta}e^{\frac{\delta}{m}t}e^{-t/RC}dt = [(1 - e^{-t/RC})\frac{m}{\delta}e^{\frac{\delta}{m}t} - \frac{m}{\delta RC - m}e^{\frac{\delta RC - m}{mRC}t}]$

$v = \frac{E_0 q}{m}(e^{-\frac{\delta}{m}t})[(1 - e^{-t/RC})\frac{m}{\delta}e^{\frac{\delta}{m}t} - \frac{m}{\delta RC - m}e^{\frac{\delta RC - m}{mRC}t}]$

$\mathbf{v(t)} = \frac{\mathbf{E_0 q}}{\delta}[(\mathbf{1} - \mathbf{e^{-t/RC}}) - \frac{\mathbf{m}}{\delta\mathbf{RC - m}}\mathbf{e^{-t/RC}}]$.

This is the velocity equation for a charged particle in
an electric field subject to solution drag forces. From this, we now derive the other equations of motion.

Particle Acceleration:

$\mathbf{a(t)} = \frac{\mathbf{dv}}{\mathbf{dt}} = \frac{\mathbf{E_0 q}}{\delta\mathbf{RC}}[\mathbf{e^{-t/RC}} + \frac{\mathbf{m}}{\delta\mathbf{RC - m}}\mathbf{e^{-t/RC}}] = \frac{\mathbf{E_0 q}}{\delta\mathbf{RC}}[\mathbf{e^{-t/RC}}(\mathbf{1} + \frac{\mathbf{m}}{\delta\mathbf{RC - m}})]$

.
.
.
.
.
.

Particle position:

$\Delta x(t) = v\Delta t = \int_0^t v(t)dt$, for an accelerating body.

$\Delta x(t) = \frac{E_0 q}{\delta}\int_0^t[(1-e^{-t/RC}) - \frac{m}{\delta RC - m}e^{-t/RC}]dt = \mathbf{\frac{E_0 q}{\delta}[t + RC(1 + \frac{m}{\delta RC - m})e^{-t/RC}]}$

2 Calculating the number of deposited CueO enzymes at time t.

We can now express the time dependence for the number of enzymes that will be deposited on a surface located at some position $\Delta x = l$. In the case of an electric field established between circular parallel plates, enzymes are bounded by a cylindrical volume element. Assuming the enzymes in solution between the plates are evenly distributed (a homogenous, well-mixed solution), the total number of enzymes is then given by:

$n = N_A M\pi r^2 \Delta x$,

where N_A is Avogadro's number, r is the electrode radii, and M is the enzyme concentration. From this, we get the time-dependence for the number of deposited enyzmes on our surface located at some distance, l :

$\mathbf{n(t) = N_A M\pi r^2 \frac{E_0 q}{\delta}[t + RC(1 + \frac{m}{\delta RC - m})e^{-t/RC}]}$.

For an electric field established between square parallel plates, n(t) becomes:

$\mathbf{n(t) = N_A M s^2 \frac{E_0 q}{\delta}[t + RC(1 + \frac{m}{\delta RC - m})e^{-t/RC}]}$,

where s is the length of a side of an electrode. To account for the effects of dielectric screening of solvent, a dielectric constant term, κ, is used to adjust the electric field strength such that $E_{effective} = \frac{E_0}{\kappa}$.

A.13 Tafel Fitting Method for Curved Plots

1 General Methodology.

The fitting of curved tafel plots suffers from the problem of choosing the correct interval range of overpotential values for performing linear fits in order to extract tafel parameters. To perform a linear fit, we can use the condition

$\frac{dj}{d\eta} = \frac{j_0 F}{RT}$ (eq. 1)

to fit our data. This is done through collection of J / V curves and tafel data for any given electrode under identical conditions. If the proper range of overpotentials are chosen for tafel fitting, eq. 1 implies that the R.H.S. of the above equality should then equal the quantity dj/dη calculated for the same range of overpotentials (we can get the L.H.S. from a linear sweep voltammagram; the j_0 term of the R.H.S. we get from a tafel plot).We now outline the derivation for eq. 1.

2 Derivation of Equation 1.

We start with the Butler-Volmer (B.V.) equation for electrode kinetics:

$j(\eta) = j_0[exp(\frac{nF\eta\alpha}{RT}) - exp(-\frac{nF\eta(1-\alpha)}{RT})]$ (eq. 2).

Taylor expansion of the above equation proceeds through the Taylor series definition for e^x:

$e^x = \sum \frac{x^n}{n!}$, for n = 0, 1, 2...

Subsequent expansion of the B.V. equation, followed by retention of the 0th and 1st order terms yields:

$j(\eta) = j_0[(1 + \frac{nF\eta\alpha}{RT}) - (1 - \frac{nF\eta(1-\alpha)}{RT})] = j_0\frac{nF\eta}{RT}$ (eq. 3).

Following differentiation of equation 3 with respect to the overpotential, η, eq. 1 results:

$\frac{dj}{d\eta} = \frac{j_0 nF}{RT}$.